UNIVERSITY OF OKLAHOMA

GRADUATE COLLEGE

DESIGN AND SYNTHESIS OF NIR BODIPY DYES: APPLICATION FOR IN VIVO FLUORESCENCE IMAGING AND PHOTODYNAMIC THERAPY

A DISSERTATION

SUBMITTED TO THE GRADUATE FACULTY

in partial fulfillment of the requirement for the

Degree of

DOCTOR OF PHILOSOPHY

By

SAMUEL G. AWUAH
Norman, Oklahoma
2012

DESIGN AND SYNTHESIS OF NIR BODIPY DYES: APPLICATION FOR IN VIVO FLUORESCENCE IMAGING AND PHOTODYNAMIC THERAPY

A DISSERTATION APPROVED FOR THE
DEPARTMENT OF CHEMISTRY AND BIOCHEMISTRY

BY

_____
Dr. Kenneth Nicholas, Chair

_____
Dr. Youngjae You

_____
Dr. Daniel Glatzhofer

_____
Dr. George Richter-Addo

_____
Dr. Roger Harrison

To:

Mum Joana, Millicent G. Awuah, CCR Prayerline and Siblings

Acknowledgement

The development of NIR BODIPY probes for fluorescence and PDT describes my dissertation undertaken at the Biophotonics and Medicinal Chemistry Laboratory of the Department of Pharmaceutical Sciences at the University of Oklahoma Health Sciences Center.

Sincere appreciation goes to Prof. Youngjae You for the enormous scientific direction, mentoring and the opportunity he offered me to join his research team to do a PhD. Over the years, moving from South Dakota State University to the University of Oklahoma my work would have been much misguided without Prof. You's astute scientific knowledge, encouragement and confidence. I am also thankful for his availability for frequent discussions and the liberty to pursue my ideas at my pace.

The Department of Chemistry and Biochemistry at the University of Oklahoma deserves thanks for accepting me to the Organic Chemistry Division under the tutelage of Prof Ken Nicholas. Prof. Nicholas' direction and chairing my advisory committee has made the PhD road a mission possible. Special thanks go to all members of the Advisory committee for their invaluable input.

Funding of this work by the South Dakota Board of Regents, Department of Pharmaceutical sciences, OUHSC and Oklahoma Center for

the Advancement of Science and Technology (OCAST) is priceless and made this PhD attainable.

Special thanks go to Dr. Susan Nimmo, Dr. Seth Darling and all my lab mates who offered useful insights, support and encouragement to make the work feasible. I thank Dr. Doug Powell for determining the x-ray structure and the National Science Foundation (grant CHE-0130835) and the University of Oklahoma for funds to purchase the x-ray instrument. Sincere thanks also goes to Dr. Alice Bergaman for mass spectrometry data obtained at the University of Buffalo Chemistry Instrumentation Center, Buffalo, NY with instrumentation acquired with NSF Award CHE0091977.

Thanks to my beloved mother and family for their sacrifices and support to propel me to this pedestal. I thank my lovely wife whose love, prayers, sacrifices and encouragement have been unrivaled throughout the period of this work. Big Thanks to all friends and well wishers.

[Awuah, S.G. & You, Y. Boron dipyrromethene (BODIPY)-based photosensitizers for photodynamic therapy. *RSC Adv.* **2**, 11169-11183 (2012)] – Reproduced by permission of The Royal Society of Chemistry.

Chapter 2 was reprinted (adapted) with permission from Awuah, S.G., Polreis, J., Biradar, V. & You, Y. Singlet Oxygen Generation by Novel NIR BODIPY Dyes. *Org. Lett.* **13**, 3884-3887 (2011). Copyright © 2011, American Chemical Society.

Table of Contents

List of Abbreviations

$^1O_2$:	Singlet oxygen
^{1}PS:	Singlet state photosensitizer
$^3O_2$:	Molecular oxygen
^{3}PS:	Triplet state photosensitizer
BODIPY:	4,4-difluoro-4-bora-3a,4a-diaza-s-indacene
BDP:	BODIPY
$CDCl_3$:	Deuterated chloroform
CD_2Cl_2:	Deuterated methylene chloride
CMP:	Core-modified porphyrin (dithiaporphyrin)
DPBF:	1,3-diphenylisobenzofuran
DCM:	Dichloromethane
DMSO-d_6:	Deuterated dimethyl sulfoxide
DNA:	Deoxyribonucleic acid
D-π-A:	Donor-pi-acceptor
EtOH:	Ethanol
FDA:	Food and drugs administration
HCl:	Hydrochloric acid
HOMO:	Highest occupied molecular orbital
HPLC:	High pressure liquid chromatography
HPD:	Haemotoporphyrin derivative
IP:	Intraperitoneal

ISC:	Inter-system crossing
ICG:	Indocyanine green
LUMO:	Lowest unoccupied molecular orbital
MeOH:	Methanol
mTHPC:	meta-tetrahydroxyphenylchlorin
mTHPBC:	meta-tetrahydroxyphenylbacteriochlorin
NMR:	Nuclear magnetic resonance
NIR:	Near infrared
PDD:	Photodynamic diagnosis
PDT:	Photodynamic therapy
PP:	Phototoxic power
PS:	Photosensitizer
PBS:	Phosphate buffer solution
RT:	Room temperature
SBDP:	Sulfur BODIPY
TEA:	Triethylamine
TFA:	Trifluoroacetic acid
THF:	Tetrahydrofuran
TLC:	Thin layer chromatography
TTF:	Tetrathiafulvalene
TCNQ:	Tetracyano-p-quinodimethane
UV:	Ultra-violet

List of Tables

List of Figures

List of Reaction Schemes

List of ^{1}H-NMR Spectra

Abstract

DESIGN AND SYNTHESIS OF NIR BODIPY DYES: APPLICATION FOR *IN VIVO* FLUORESCENCE IMAGING AND PHOTODYNAMIC THERAPY

SAMUEL G. AWUAH

2012

Photodynamic therapy (PDT) and fluorescence imaging are non-invasive modalities for disease treatment and diagnosis respectively. Both modalities require the use of a dye (light harvesting material) and light or source of excitation. In the case of PDT a sensitizer is needed while a fluorophore is used in the case of fluorescence imaging. PDT in addition to a sensitizer and light thrives on oxygen to generate a key cytotoxic species known as singlet oxygen. PDT has shown promise in the clinic for the treatment of surface cancers and age-macular degeneration. Fluorescence imaging on the other hand has a long history for in vitro use but a growing interest for in vivo preclinical and clinical use for diagnosis, particularly in malignancies, angiography and neurobiology. Fluorescence imaging due to its sensitivity, relatively low cost and less toxicity makes it reliable. The need to improve PDT and imaging heavily relies on the effectiveness of the sensitizer or imaging probe/fluorophore. Near infra-red (NIR) sensitizer/probes with a potential to target specific sites of interest could change the paradigm in the non-invasive modalities.

In this dissertation, the design and synthesis of NIR BODIPY for use as photosensitizers and fluorescent probes was explored. We followed a synthetic strategy of incorporating heavy atoms in the BODIPY chromophore to obtain effective singlet oxygen generating BODIPY without compromising on their optical and photophysical properties with an added advantage of red-shifting to the NIR region. We further developed a robust but versatile strategy for building fluorescent molecular probes spanning the entire therapeutic window with potential for optical imaging. We then explored the capacity to functionalize these NIR dyes for potential targeting to vectors such as peptides, antibodies, etc. We also investigated the ability of representative dyes to induce photodynamic response and to serve as optical contrast agents.

Chapter 1

General Introduction

1.0. Introduction

An enhanced clinical approach of disease diagnostics and treatment is of great interest due to its implication for healthy living. The search for novel non-invasive regimen/agents using tissue penetrable light (600 – 900 nm) to improve disease prognosis and therapy is expanding among the scientific (clinical and preclinical) community due to its advantages of reduced toxicity by avoiding non-ionized species, relatively low cost and real time monitoring. The development of fluorescent probes for optical imaging and photosensitizers (PSs) originating from organic, inorganic and material science (especially nanomaterials) has been explored to produce diverse probes for various outcomes. In general, near infra-red (NIR) fluorescent probes and PSs for photodynamic diagnosis and therapy (PDD/PDT) respectively, are more effective than visible ones in the clinic due to deeper tissue penetration due to reduced absorption by cells/tissues and water, light scattering and autofluorescence.[1, 2]

Currently, indocyanine green (ICG) as a fluorescent probe and a few PSs such as Photofrin, Visudyne, Foscan are used in the clinic. However, since those are not ideal for optical imaging or PDT, better probes/PSs

should be developed. Organic based dyes are relatively cheap, offer flexibility in tuning properties and show good biocompatibility. Frequently used dyes have been cyanines, squarines, porphyrins and boron dipyrromethene (BODIPY). BODIPY is noted for high photostability, unique optical properties evidenced in sharp absorption and emission bands, high extinction coefficient and high fluorescence quantum yields as well as flexible synthesis and tunability. The central theme of my dissertation is focused on the development of NIR BODIPY structural variants for fluorescence imaging and PDT. The work: 1) developed NIR PSs from the low triplet state BODIPY via the heavy atom effect. 2) established a robust but versatile synthetic platform for fluorescent probes across the NIR therapeutic window (650 – 800 nm), and 3) developed functionalization strategies and dual functioning NIR BODIPY agent for PDT and fluorescence imaging.

1.1. PDT

The operation of PDT follows a tripartite modality involving light, PS and oxygen. A PS is administered and then the treatment site (e.g. tumor) is subjected to light irradiation to generate reactive oxygen species, especially singlet oxygen from oxygen, to damage target diseases. When a PS is irradiated, it is converted to the triplet state via intersystem crossing from the singlet state (Fig. 3).[3] In what is known as the type II process, the triplet state PS transfers its energy to molecular oxygen to produce singlet

oxygen. In a type I process, a chemical reaction of the excited PS with a substrate occurs, initiating an electron or proton transfer leading to the formation of radicals which react with molecular oxygen to produce reactive oxygen species such as superoxide, hydrogen peroxide, and hydroxyl ion.[4]

1.1.1. Light

Optical technology has aided the groundbreaking evolution of the use of light in PDT from the use of sunlight to very sophisticated light sources and light delivery tools.[5-7] Light for PDT is generally classified into laser and non-laser light sources. The effectiveness of lasers is higher than the other light sources offering advantages such as delivering high intensity with monochromaticity, no thermal effect, and easy adaptability with fiber optic delivery tools. Attenuation of incident light by biological tissue requires relatively high fluence rates or light doses for the treatment of bulky targets. The property of monochromaticity of lasers makes the dosimetry relatively more accurate than non-monochromatic light at least at the surface of the target tissue. In a classic PDT example, the FDA approved Photofrin® and Visudyne® work in combination with laser irradiation (630 and 689 nm, respectively). Diode lasers have become more popular in the PDT community due to their comparatively cheap but effective application. Alternatively, non-coherent light sources offer some advantages over lasers such as relatively low cost, ability to excite a wide range of spectra, compact size, easier handling, and less regulation. In instances where less

accurate dosimetric control is acceptable like dermatologic diseases, non-coherent light sources are advantageous. The use of a narrow banded fluorescence light source (BLU-U®, 400-450 nm) with absorption in the UV-visible region has been used for the treatment of acne keratosis with Levulan®. Another type of non-coherent light source available for preclinical application is the Lumacare®, where special fibers are used to make narrow band outputs covering a wide range of spectrum. Recently, the portable, non-coherent but adjustable light emitting diodes (LEDs) have become readily available for PDT application. The availability of good quality light, high power, low cost, and desirable delivery fibers has in part popularized PDT.[1]

1.1.2. Singlet Oxygen, $^1O_2$ ($^1\Delta_g$)

Among reactive oxygen species (ROS), O_2 ($^1\Delta_g$) proved to be the main cytotoxic agent of PDT to cause biological effects.[3, 8-11] The quenching of the lowest electronically excited singlet (S_1) and triplet (T_1) states of substances with the possibility of transferred energy higher than 158 kJ/mol produces electronically excited two singlet oxygen states [$^1\sum^+_g$ (158 kJ/mol) and $^1\Delta_g$ (94 kJ/mol)] above the triplet state oxygen.[12, 13] The metastable but reactive O_2 ($^1\Delta_g$) can be generated by the deactivation of O_2 ($^1\sum^+_g$) through electronic and vibrational energy transfer.[12, 13] Moreover, the longer lifetime of T_1 than S_1, supports that singlet oxygen ($^1\Delta_g$) is generated by energy transfer from T_1 to triplet oxygen (Fig. 3). In assessing the biological effects

of singlet oxygen in PDT, three factors come into play. First, the concentration of oxygen and the source of singlet oxygen impact the capacity of singlet oxygen generation and consequently biological activity. The concentration of oxygen at atmospheric pressure in aqueous and organic media are different: for example, 0.27 mM (water) vs 2.40 ($CHCl_3$), respectively.[14] This affects the oxygen distribution at the tissue level. For a solid tumors known for its hypoxic property[15] a reduction of oxygen concentration from 5 % to 1 %, results in 50 % decrease in PDT activity.[9] Second, the lifetime of singlet oxygen is short in aqueous media and thus its diffusion is limited to a short distance (10-300 nm).[16-18] Singlet oxygen generated in a cell can only damage the cell conferring some degree of selectivity for PDT in targeted cells over normal cells. Third, singlet oxygen quantum yield (Φ_Δ) which is the quantitative expression of a PS's potential to generate singlet oxygen[19, 20] has been a useful characteristic in the assessment of PS efficacy in PDT, at least in solutions and in mono-layer cell culture models. A more useful term to predict PS efficiency may be "phototoxic power (PP)" where $PP = \Phi_\Delta \times \boldsymbol{\varepsilon}$, accounting for singlet oxygen quantum yield and extinction coefficient of the PS[1] for in vivo systems where light will be one of the limiting factors due to tissue attenuation.

1.1.3. PSs

Over the past century, PSs evolved in terms of its chemical and photophysical properties and biological applications. A PS is a dye that generates ROS for cellular/tissue damage after light irradiation. In 1903 a report by Jesionek and Von Tappeiner on the effect of the topical treatment of tumors with eosin exposed to white light marked one of the notable advances in photodynamic events (Fig. 3).[21, 22] Photodynamic activity was extended by Polycarp in 1924 by using porphyrins to treat tumors.[23] The rise of photodynamic activity received a major boost in 1960 when Richard Lipson and co-workers developed the "Haematoporphyrin derivative" (HPD) after the observation of fluorescence upon localization in tumors.[24-28] In fact, a number of mouse model experiments buttressed the localization of haematoporphyrin and its analogues in tumors.[29] Dougherty and his colleagues took PDT a step further by treating mammary tumors in vivo with HPD and red light.[30] Subsequently, Kelly and Snell examined the first human treatment with HPD for bladder cancer.[31, 32] Successful preclinical and clinical trials of HPD led to the approval of its purified form under the trade name Photofrin for PDT treatment of Barrett's oesophagus, cervical cancer, endobroncheal cancer, oesaphageal cancer, gastric cancer and papillary bladder cancer in a number of countries.[33]

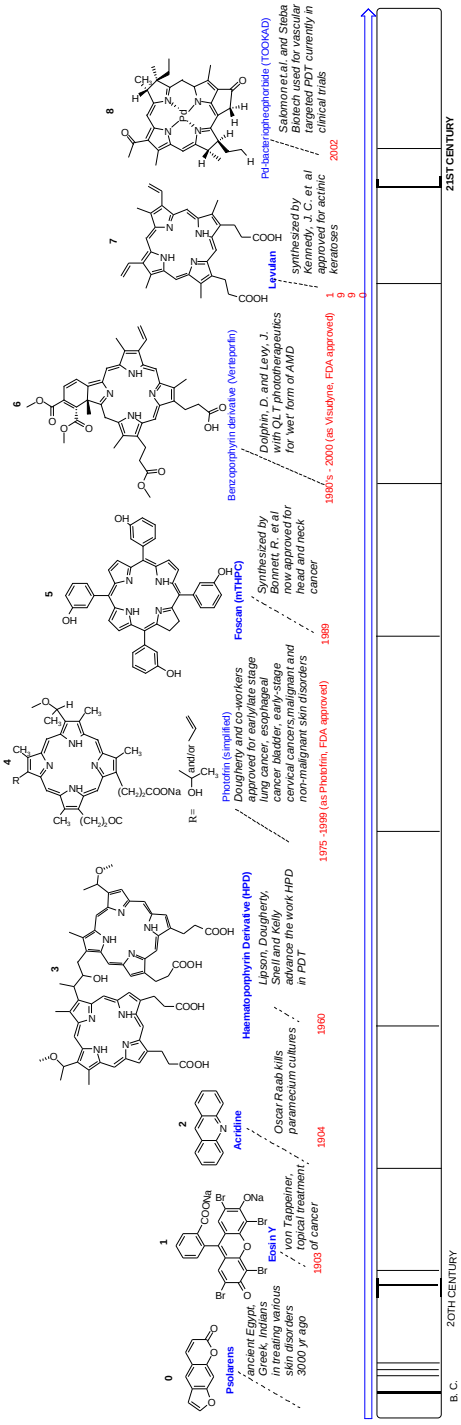

Figure 1. Milestones of PS development

1.2. Fluorescence Imaging

In biological research fluorescence imaging proved useful in vitro and in vivo preclinical and clinical applications. Optical imaging generally offers high sensitivity and frame rate, low cost and portability, lack of radiation exposure and an ability to multiplex several colors simultaneously.[34]

The sensitivity of fluorescence imaging in molecular biology, in vivo and clinical diagnostics accompanied with other numerous advantages has attracted great research attention. Fluorescent probes have been used to detect and quantify total DNA, RNA and protein. Using multicolor fluorescence detection, a time and cost effective strategy could be employed to resolve multiple targets. Fluorescent labeled biomolecules tend to be relatively stable in comparison to their radioisotope labeled counterparts. In addition, fluorophores are easier to transport and dispose, influencing their low cost. In vivo fluorescence imaging has been useful for cancer diagnostics (early stage), tumor boundary identification, assessment and visualization of blood and lymph vessels, fluorescence guided tumor resection etc. It is noteworthy that fluorescent probes can be characterized on the property of their brightness ($BT=\varepsilon \times \Phi_{f,}$ where ε: extinction coefficient, Φ_f: fluorescence quantum yield), which is dependent on its excitation coefficient and quantum yield of fluorescence.

Fluorochromes such as cyanines, rhodamine, fluorescein, BODIPY, and etc. (Fig. 4) have been used as imaging probes and their improved versions have been developed. In current clinical practice, indocyanine green and fluorescein are the only two fluorescent probes approved by the Food and Drug Administration (FDA) for retinal angiography.[35]

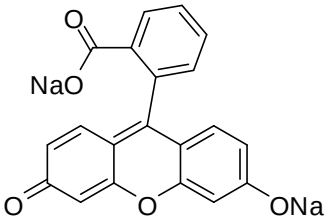

Fluorescite
9

$\lambda_{max\ abs}$ 465 - 490 nm

$\lambda_{max\ emiss}$ 520 - 530 nm

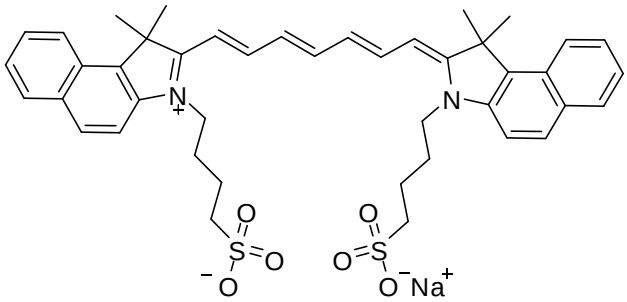

ICG
10

$\lambda_{max\ abs}$ 800 nm

$\lambda_{max\ emiss}$ 820 nm

Figure 2. FDA approved fluorescent contrast agents

1.3. Molecular Electronic Processes

Organic molecules are excited upon light absorption (light: ultraviolet, visible or near infra-red). The excitation involves electron transfer from the highest occupied molecular orbital (HOMO), which is low in energy to the lowest unoccupied molecular orbital (LUMO), which is high in energy. Singlet states and triplet states are the two formal excited electronic states. In the singlet state electron spins are paired even in the presence of a mild magnetic field while in the triplet state the unpaired electron spins interact

with magnetic field to produce three quantized states.[36] In a simplified model (Fig. 3), the absorption of organic molecules causes excitation to singlet states of varying vibrational energy levels. The electron may fall to lower vibrational energy levels in internal conversion (10^{-12} s) or fall to the ground state, emitting fluorescence.[37] Spin conversion to the triplet state may also occur from molecules in the singlet state, the conversion is known as intersystem crossing with a general emission as phosphorescence. It is important to mention that intersystem crossing efficiency is greatly facilitated by heavy atoms such as I, and Br. The heavy atom effect induces spin orbit coupling enhancing phosphorescence quantum yields.

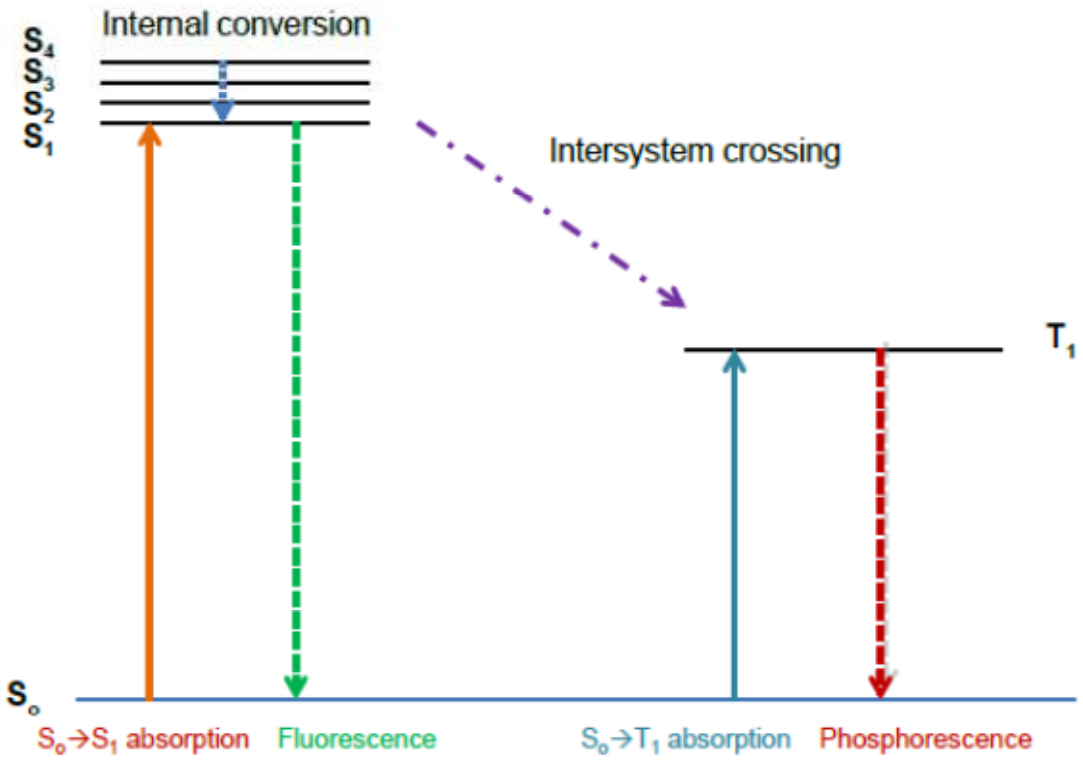

Figure 3. Simplified energy state diagram

1.4. NIR organic PSs and fluorophores

NIR materials are categorized as inorganic and organic, based on their composition. Organic NIR materials include extended π-conjugated chromophores, donor-acceptor type chromophores, some metal complexes as well as ionic dyes. NIR organic based matter has wide applications from its use as heat absorbers or optical filters in electronics, laser printers and charge generation materials[38], information storage materials in optical

disks[39], dye sensitized solar cells and medical applications such as PDT.[40] PSs or fluorochromes absorbing in the NIR region reaches deeper tissues (>500 µm to cm)[41] for therapy and diagnosis respectively. Water, hemoglobin and deoxyhemoglobin have low extinction coefficients in the "so called" therapeutic window (650 – 900 nm), thus absorption by these tissue components is minimum. In addition, in this therapeutic window autofluorescence is reduced and thus background signal is weak.

In general, the molecular design of NIR organic materials is based on tuning the band gap (HOMO – LUMO gap) to low levels.[40] In achieving this, strategies such as extending conjugation, incorporating donor-acceptor charge transfer elements, alternating bond length and at times the use of heavy atoms may be considered. Typical examples can be seen in chromophores like the polyenes with extended conjugation and polymethine units with terminal carbons which bear an electron donating group and the other end bears an acceptor group like the merocyanines, cyanines and hemicyanines. Other polymethines like the highly photostable BODIPY possess a rigidified core with excellent optical properties. Rhodamines with extended conjugation or replacement of O with Si atoms have been developed with fair photostability for bio-imaging. The naturally occurring bacteriochlorophyl-a with NIR absorption between700 – 800 nm has been useful in PDT and tumor imaging.[42] The use of synthetic methods to make stable derivatives has attracted a lot of research interest.

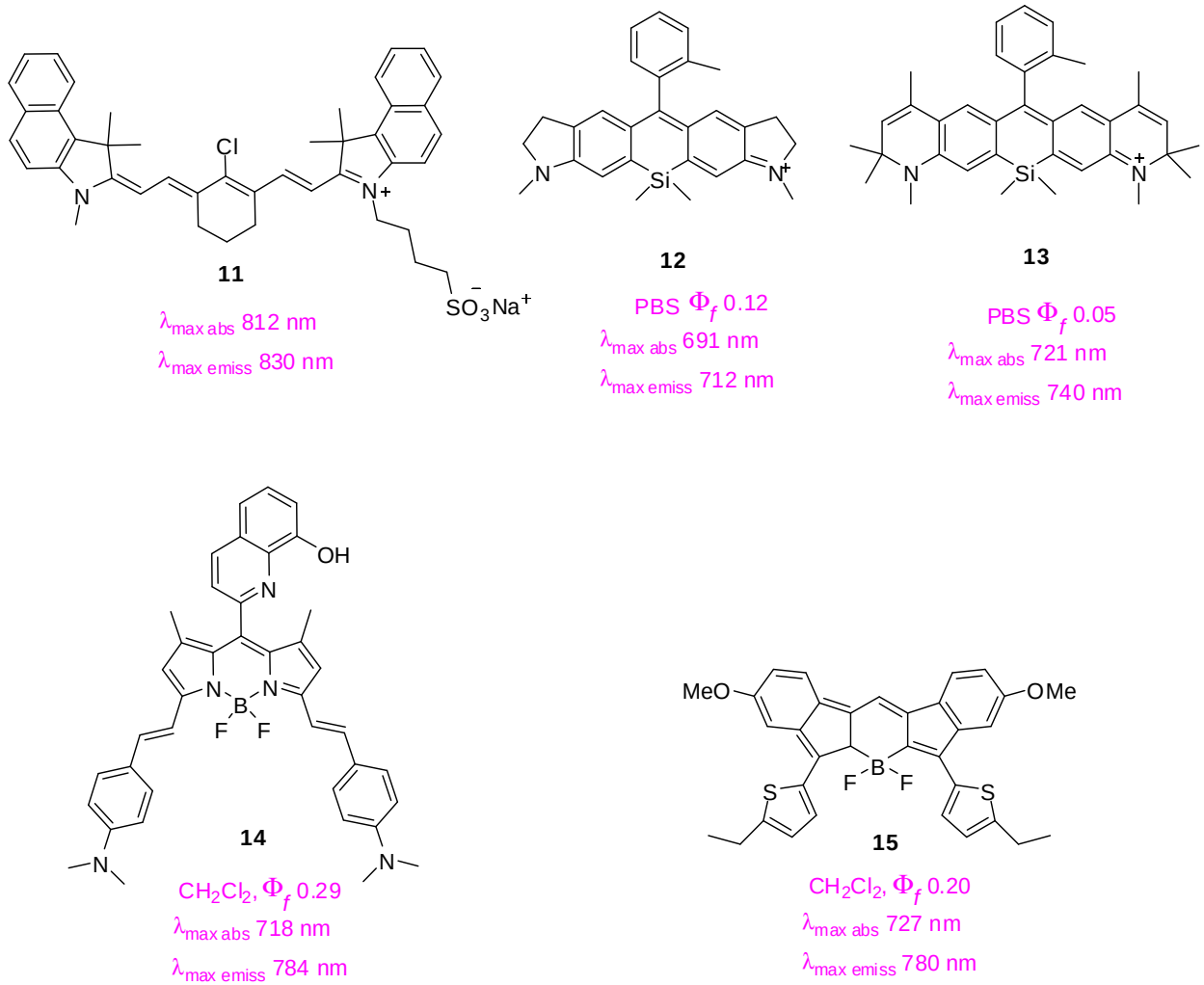

Figure 4. Structures of NIR dyes

The use of donor - acceptor systems in an effort to tune the energy gap of organic substances were remarkable to obtain NIR absorption and emission. Organic materials were designed with electron donor and acceptor moieties linked with either a conjugated (π) or non-conjugated (σ) spacer referred to as D-π-A and D-σ-A respectively. Classic examples were the covalently linked tetrathiafulvalene (TTF) with tetracyano-p-

quinodimethane (TCNQ) and the π-conjugation of TTF with dipyrido [3,2-a:2,3-c]phenazine (Fig. 5).[43, 44]

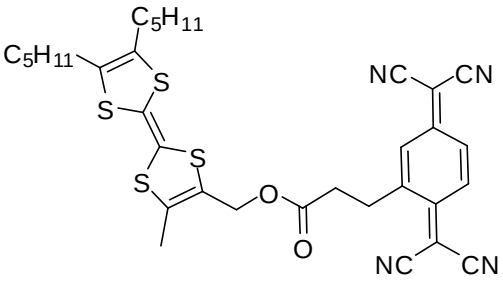

16

$\lambda_{max\ abs}$ 1630 nm

$\lambda_{max\ emiss}$ 2700 nm

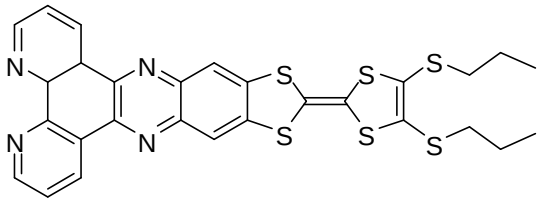

17

CH_2Cl_2, Φ_f 0.01

$\lambda_{max\ abs}$ 535 nm

$\lambda_{max\ emiss}$ 820 nm

Figure 5. Donor-acceptor system based on TTF with an acceptor

1.5. Chemical Strategies for NIR BODIPY Dyes

The quest for NIR BODIPY dyes has attracted great research interest over the years. The progress in building BODIPY dyes with excitability >700 nm is still nascent. The high photostability of the BODIPY chromophore is worthwhile to invest in it for NIR property returns. Currently, among the BODIPY dyes used for PDT and in vivo imaging, none absorbs beyond 700 nm. In an attempt to overcome this hurdle several approaches were be used to attain bathochromic shifts (Fig. 6). 1) Aryl substitution at the 1, 3, 5 and 7-positions of the BODIPY framework impart red-shift.[45, 46] 2) Using Heck-type **(21)** reactions, vinylation at the 2,6-positions with

respective acrylate moieties induced red shifts by about 20–30 nm with monosubstitution and 50–60 nm with di-substitution.[47] Ethynylaryl substitution at the 3,5-positions of the BODIPY framework offers an appealing approach for red shifting. Using arylacetylene via the Sonogashira reaction **(24)** with its halogen-substituted BODIPY coupling partner made it possible to achieving longer wavelengths.[48, 49] 3) The Liebeskind–Srogl coupling with boronic acids or tin-based compounds[50] as well as nucleophilic substitution of halogen-substituted BODIPY at the 3,5-positions with conjugated groups did also induce a red shift.[51, 52] 4) A common route used to obtain long-wavelength BODIPY PSs is styryl substitution via Knoevanegel condensation **(22)**. The versatile nature of styryl substitution produced moderate yields and was achieved in a stepwise fashion from monosubstitution to tetrasubstitution with an appropriate red-shift.[53] Akkaya et. al. offered a sterling observation with insight of the acidity of methyl protons in a tetramethyl-BODIPY, indicating electron densities in the order 2,6 & 1,7 ~ 3,5 (**18**, Fig. 6).[53] The methyl groups in positions 1 and 7 may be similar in acidity to those of 3, 5 methyl groups. 5) The strategy imploring extended conjugation by ring fusion is a smart approach for long wavelength BODIPY dyes. An example is the benzo-fusion following the retro-Diels– Alder reaction of norbornane-derived pyrroles executed by Ono and co workers.[54-57] A method by Hao et al.[58] was developed for functionalized asymmetric benzo-fused BODIPY 6)

Heteroaryl ring fusion **(23)** to the BODIPY core in addition to extending conjugation imparted rigidity and planarity to the chromophore. Our research group including this dissertation and Suzuki et. al. demonstrated the use of the heteroaryl ring fusion approach to obtain NIR absorbing and emitting dyes with excellent optical properties.[59, 60] 7) The aza-BODIPY **(20)** is a unique class that benefits from the replacement of the meso-carbon with a N atom of the BODIPY core. The lone pair electrons on the nitrogen atom engineer a narrow HOMO–LUMO gap by interfering with orbital framework of the pyrroles, hence, the bathochromic shift.[40] The aza-BODIPY analogues, ADPM06, in PDT have shown great promise with their far-red absorption being a strong selling point. Even though significant improvement was made, it did not address the problems of functionalization, water-solubility, NIR BODIPY PS or diagnostic agents. Those are indeed challenges that need to be surmounted.

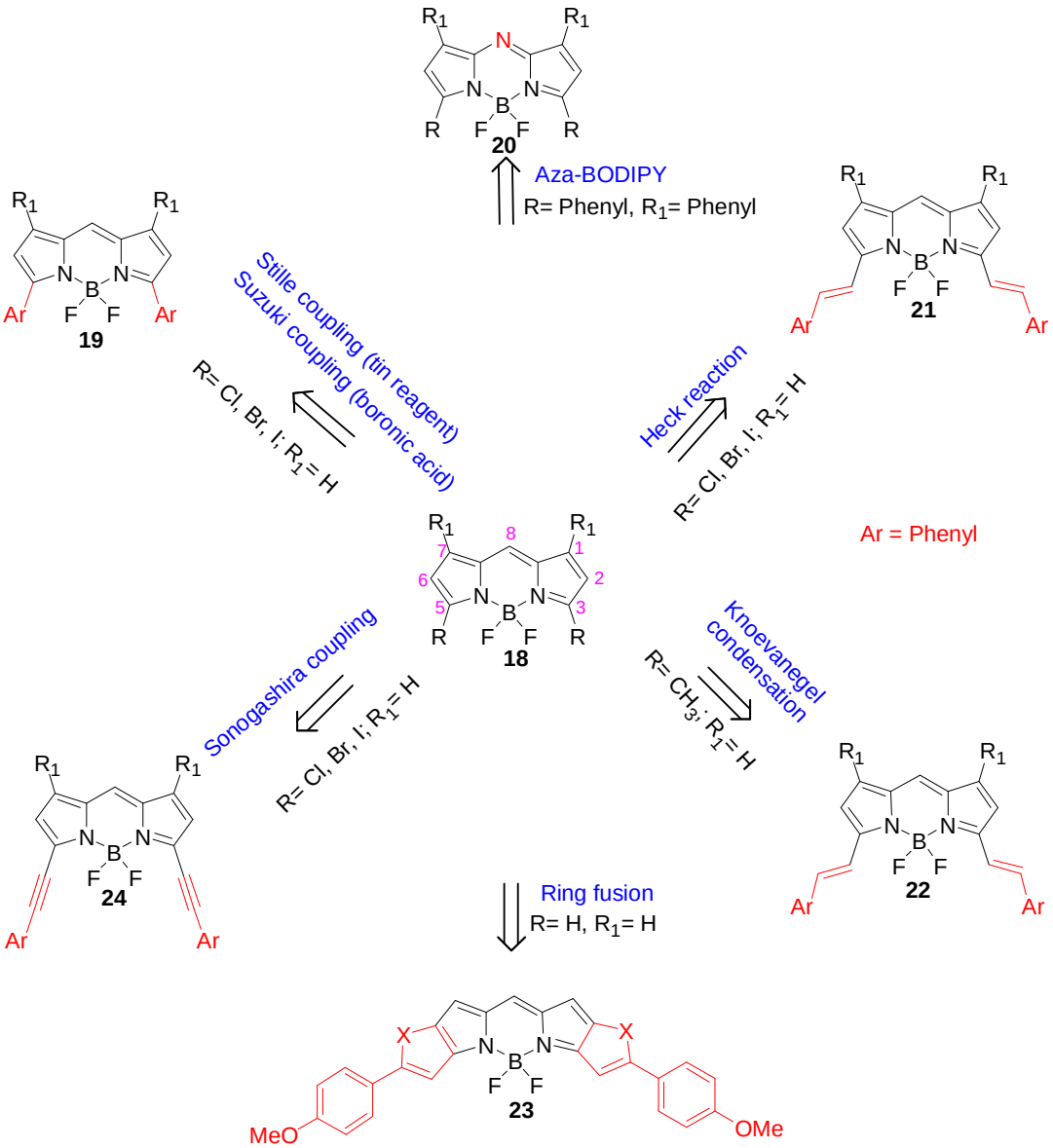

Figure 6. Chemical modification strategies for long-wavelength BODIPY dyes

1.6. Thesis Objective and Outline

Although significant works have been done to develop NIR BODIPY dyes, few have been successful for bio-imaging and PDT applications with excitability > 700 nm. A difficulty in functionalizing NIR organic dyes poses a challenge for biological applications. In this work I developed NIR BODIPY dyes absorbing >700 nm for potential use as PDT agents and in vivo fluorescence imaging probes.

In Chapter 2, since the BODIPY chromophore is noted for low triplet states, fused BODIPY chromophores with extended conjugation were developed and the incorporation of heavy atoms produced NIR singlet oxygen generating BODIPY dyes. Photophysical characterization was carried out accordingly to assess the potential of these new dyes as PSs.

Chapter 3, focused on the development of a robust synthetic strategy to generate NIR BODIPY fluorophores. Taking into account functionalization, incorporating functional groups at the meso position was explored. The challenges faced necessitated the building of a scaffold which is referred to as ‘versatile BODIPY intermediate’. The intermediate which is technically an alkyl halide serves as a unique coupling partner for palladium catalyzed reactions as well as nucleophilic substitution reactions.

In Chapter 4, an *in vivo* efficacy study of my lead BODIPY PS was evaluated. In addition, the design and synthesis of a functionalized dye was performed to improve water solubility. The NIR BODIPY dye had two

carboxylic acid units that altered the pharmacokinetics and offered a platform for conjugation with biomolecules.

Chapter 2

Singlet Oxygen Generation by Novel NIR BODIPY Dyes

2.0. Introduction

In this chapter, my aim was to rationally design highly photostable NIR BODIPY dyes with excitability > 700 nm and large extinction coefficient > 50,000 $M^{-1}cm^{-1}$ which appreciably generates singlet oxygen – the key cytotoxic agent in PDT. The motivation was to further advance the search for more effective second generation PSs for the treatment of tumors by PDT. I hypothesized that fusing thiophene moieties to the BODIPY core and subsequent substitution of other heavy atoms such as bromine would provide a $^1O_2$ generator without compromising the excellent optical properties of BODIPY.

2.1. Singlet Oxygen Applications

2.1.1. Organic Synthesis

The importance of $^1O_2$ in organic synthesis cannot be overemphasized. In solution it is generated using an appropriate PS that absorbs light and converted to the excited triplet state (intersystem crossing). In a type I process, the triplet state PS (94.3 kJ/mol) transfers an electron to biomolecules to form radicals which may interact with molecular

oxygen to yield reactive oxygen species such as hydroxyl ions, superoxides and hydrogen peroxides.[61, 62] In a type II process there is a direct energy transfer to molecular oxygen to form singlet oxygen. $^1O_2$ has a lifetime of 74 minutes in gas phase and solvent dependent solution lifetime (CCl_4: 59 ms, Benzene: 30 µs, H_2O: 3.5 µs).[63] The ene, hetero Diels Alder, [2+2] and [4+2] cycloaddition reactions have successfully made use of $^1O_2$ in chemical transformations (Fig. 7).

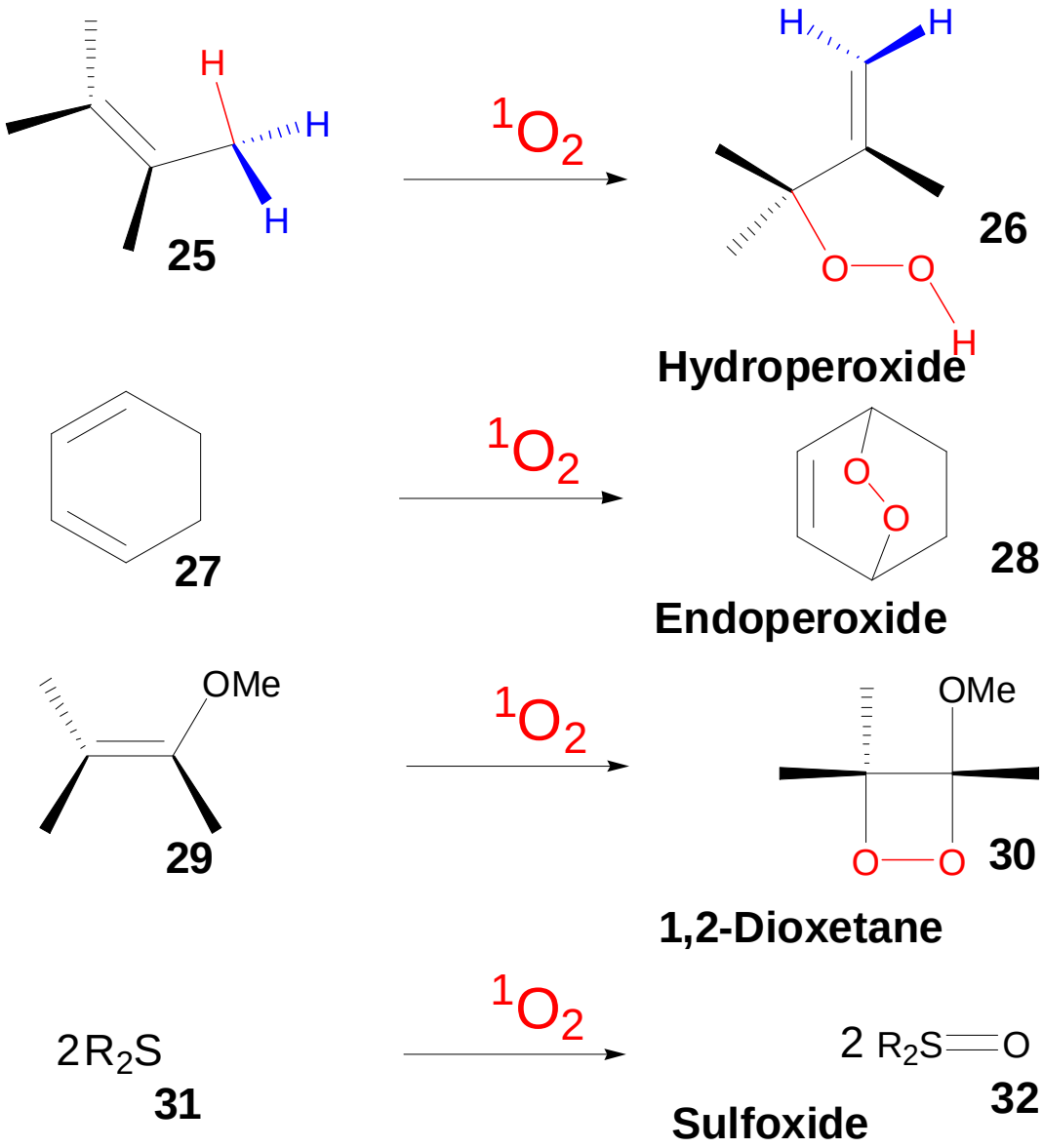

Figure 7. Prototypical reactions of singlet oxygen

2.1.2. PDT

The reactivity of $^1O_2$ makes it a useful cytotoxic agent, hence, its use in the non-invasive treatment of malignancies in PDT. Generators of $^1O_2$ used biologically and in particular in vivo must possess unique optical characteristics towards ideality. The ideal PS must possess the following

characteristics: 1) single pure compound with a chemically defined structure 2) high $^1O_2$ quantum yield Φ_Δ 3) excitability in the NIR region >700 nm with a high molar extinction coefficient 4) moderate fluorescence capacity 5) high photostability, and 6) high phototoxicity with minimal dark toxicity as well as low skin photosensitization in vivo.

2.2. BODIPY PSs

4,4-difluoro-4-bora-3a,4a-diaza-s-indacene (BODIPY), since its first discovery in 1968,[64] has attracted attention for various applications[65] such as biological imaging and labeling,[66] sensors,[67] dye-sensitized solar cells (DSSC),[68] light-emitting materials for electroluminescent devices, and PDT.[69, 70] The photophysical properties of BODIPY dyes display excellent characteristics in relation to other dyes such as intense absorption and emission bands, high photostability, high fluorescence quantum yield, high extinction coefficient, and flexible modification for tuning absorption range and HOMO-LUMO gap.[71] Recently, versatile synthetic approaches made the modifications of BODIPY feasible for achieving variable excited state properties including $^1O_2$ generation by increasing intersystem crossing ($S_1 \rightarrow T_1$ transition) by substituting heavy atoms to the BODIPY core to enhance spin orbit coupling.[72] In current research practice, majority of BODIPY-based PSs used in PDT are developed by the incorporation of heavy atoms, Br and I. Moreover the emergence of heavy-atom free BODIPY PSs is on the rise.[73, 74] The development of BODIPY-based PSs thus far has a

limitation of reaching deeper tissues due to their relatively low absorption wavelength (<700 nm). Only the aza-BODIPY class has advanced in preclinical research. The need to take advantage of the excellent optical and photophysical properties of BODIPY to obtain NIR sensitizers is imperative. A summary of BODIPY PSs in current preclinical use shows the optical properties (fluorescence quantum yield, singlet oxygen quantum yield maximum absorption and emission in various solvents) and their photocytotoxicity values expressed as IC_{50} (or EC_{50}) units (half maximal inhibitory concentration) in respective cell lines (Fig. 8). The summary gives an unambiguous basis to compare the current development to the new singlet oxygen generating NIR BODIPY dyes in this dissertation. Among the BDP PSs in Fig. 8, none has absorption > 700 which is in sharp contrast to our developed sensitizers with remarkable absorption in the NIR range of 720 – 766 nm allowing for deeper tissue penetration for improved treatment. In addition, these dyes show enhanced fluorescence ability especially for **41**, making it useful for multimodal application of diagnosis and therapy.

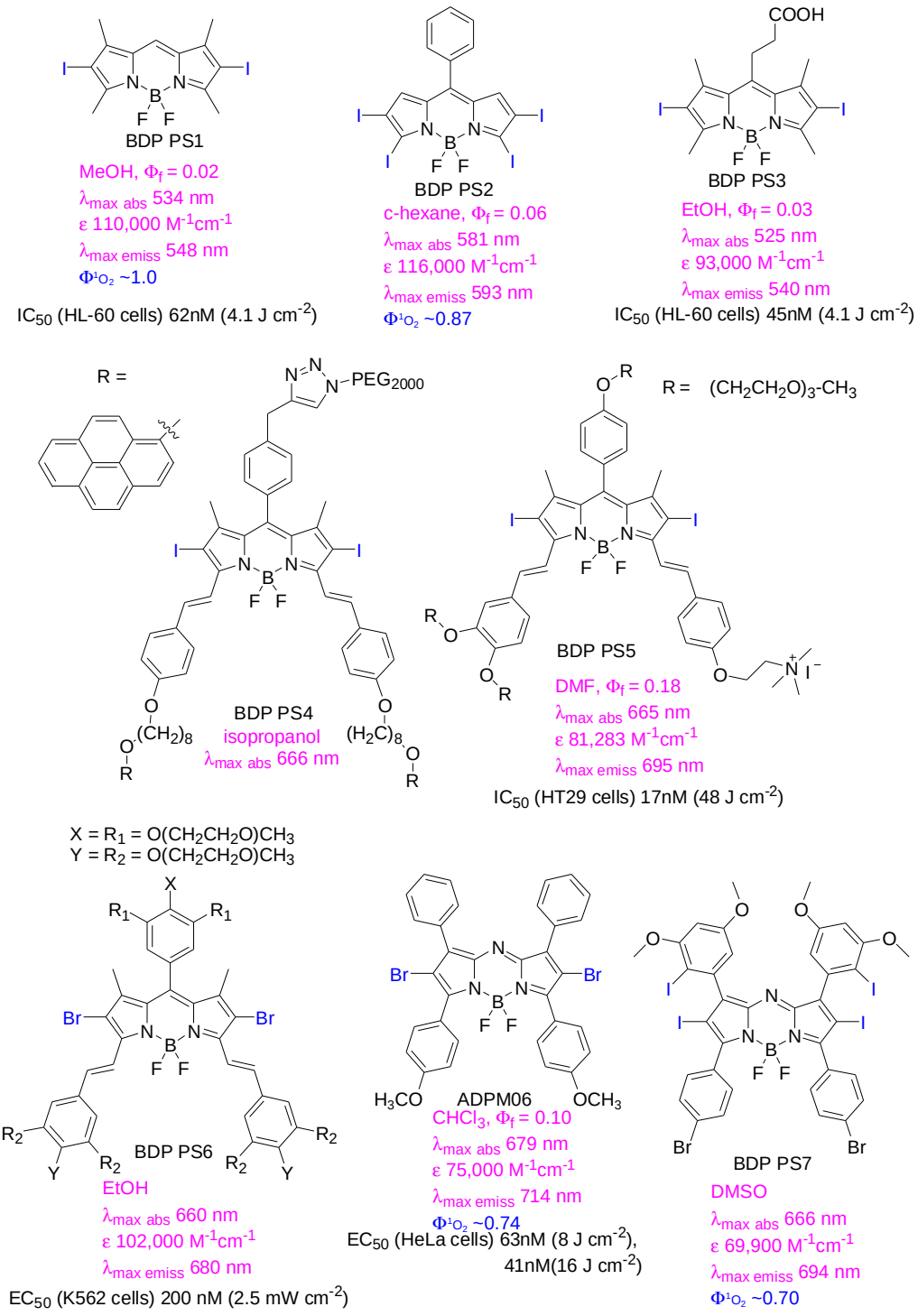

Figure 8. General singlet oxygen generating BODIPY dyes in development[75]

2.3. Synthesis of Novel NIR Dyes

Drawing inspiration from work by Umezawa et al. I approached the synthesis of the BODIPY analogues with a rational incorporation of heavy atoms. Taking the BODIPY core, conjugated chalcogens such as furan and thiophene were fused to pyrrole units via a multi-step pyrrole cyclization. To induce a bathochromic shift to the NIR region I took advantage of the push-pull effect in using the D-π-A strategy where methoxyphenyl units (D) and CF_3 (A) were conjugated through fused BODIPYchromophore.

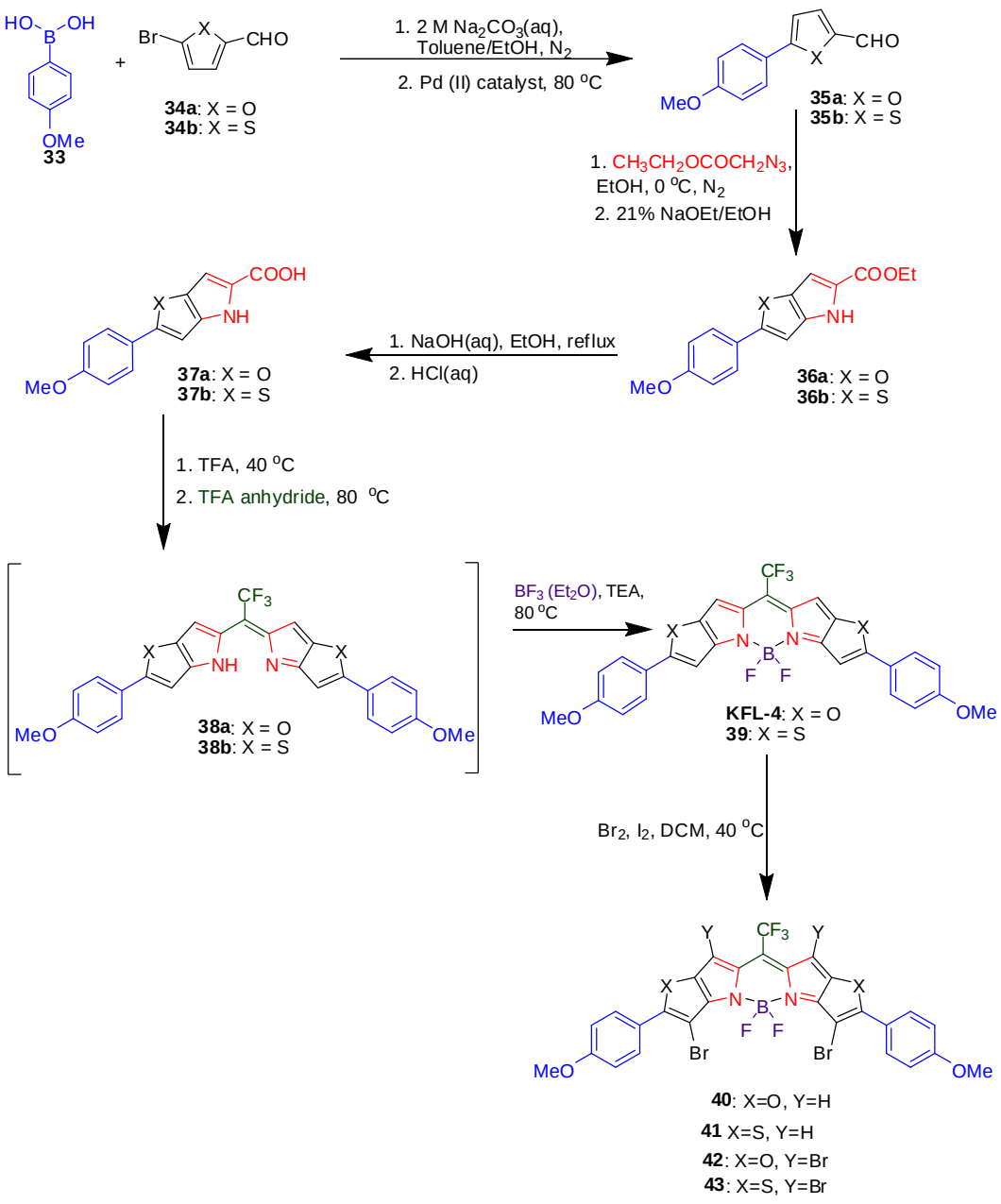

Scheme 1. Synthetic strategy of SO generating NIR BODIPY dyes

2.4. Results and Discussion

2.4.1. Synthesis of BODIPY Derivatives

The first step necessary for the synthesis of compounds **KFL4**, **39 – 43** was the preparation of appropriate modified pyrrole derivatives. The syntheses were summarized in Scheme 1. 2-(4-methoxyphenyl)-4*H*-fura [3, 2-b] pyrrole-5-carboxylic acid, **37a**, a known compound and its thieno analogue, 2-(4-methoxyphenyl)-4*H*-thieno [3, 2-b] pyrrole-5-carboxylic acid **37b**, a new compound; were prepared according to literature procedure.[60] The respective aryl substitution in the first step was carried out following a Suzuki-Miyaura cross coupling in high yields (70 – 80%) employing [1, 1'-bis (diphenylphosphino)-ferrocene] palladium (II) dichloride dichloromethane complex (1:1) as a catalyst. The known furopyrrole (**36a**), and the new thienopyrrole (**36b**), building blocks were synthesized by Hemetsberg-Knittel synthesis in high yields (72-75%) and were characterized by ^{1}H-NMR and ESI - HRMS. The isolable dipyrromethene intermediates (**38a** and **38b**) were formed as a result of a proposed acid mediated decarboxylation and subsequent condensation involving trifluoroacetic anhydride to install a CF_3 group at the meso-position. The isolated intermediates were not characterized but dissolved in toluene with the addition of boron trifluoride etherate and triethylamine under reflux to give the desired BODIPY products **KFL-4** which is a known compound and the new compound **39**. Overall yields were satisfactory. Bromination of

KFL-4 and **39** as well as the degree of bromination exemplified in di (**40**, **41**) and tetra (**42**, **43**) substituted new BODIPY analogues followed an abandoned bromine electrophilic aromatic substitution of pyrroles in the literature.[76] The modified procedure utilizes bromine and trace iodine with varying equivalence in methylene chloride under reflux conditions. The brominated furo-based BODIPY analogues (**40** & **42**) were in slightly higher yields of ~50 % than the thieno-based BODIPY analogues (**41** & **43**) in ~30 %. A direct explanation for the yield variance is not known. Di-brominated BODIPY analogues were obtained using 3 eq. of bromine and 1 mg iodine; while the tetra brominated BODIPY analogues were prepared using 6 eq. bromine and 2 mg iodine. A highly non-polar product was purified by column chromatography and characterized by ^{1}H-NMR and EI-HRMS. The site of bromination of compounds **40** and **41** was confirmed using 1-D NOESY and ROESY respectively. The selective bromination on the furo/thieno rings might be due to the high electron density contributed by the proximal methoxyphenyl donor groups.

2.4.2. Bromination Sites of 40 and 41 by NOESY and ROESY Analysis

Using one dimensional ^{1}H-NMR techniques the sites of bromination for the di-brominated compounds **40** and **41** were determined with helpful insights from Dr. Susan Nimmo of the University of Oklahama NMR facility. Specifically, 1D-selective NOESY and ROESY experiment were employed for **40** and **41** respectively. The interest was in locating ^{1}H – ^{1}H correlation

to affirm the bromination on the furan/thiophene or the pyrrole rings. The principle of these experiments determines ^{1}H – ^{1}H proximity in a molecule by through-space Nuclear Overhauser Effect (NOE). A weak irradiation of the phenyl protons (A) in **KFL-4**/**39**, the precursor of **40/41** resulted in an increase in the population of the higher energy level in nearby non-irradiated protons (B) and (C) through space (Fig. 9). The excess population after undergoing a T1 relaxation to a lower energy level gave signal intensities of the nearby protons (B) and (C). The irradiation of (B) gave signal intensities (A) and (D) suggesting a close proximity between the phenyl protons and the furan/thiophene proton (D). In the NOESY/ROESY of **KFL-4** and **39**, the interaction of D with B was observed. On the other hand, it was not detected in the NOESY/ROESY of **40** and **41**, which is the indicative of bromine substitution on the furan or thiophene instead of the pyrrole ring.

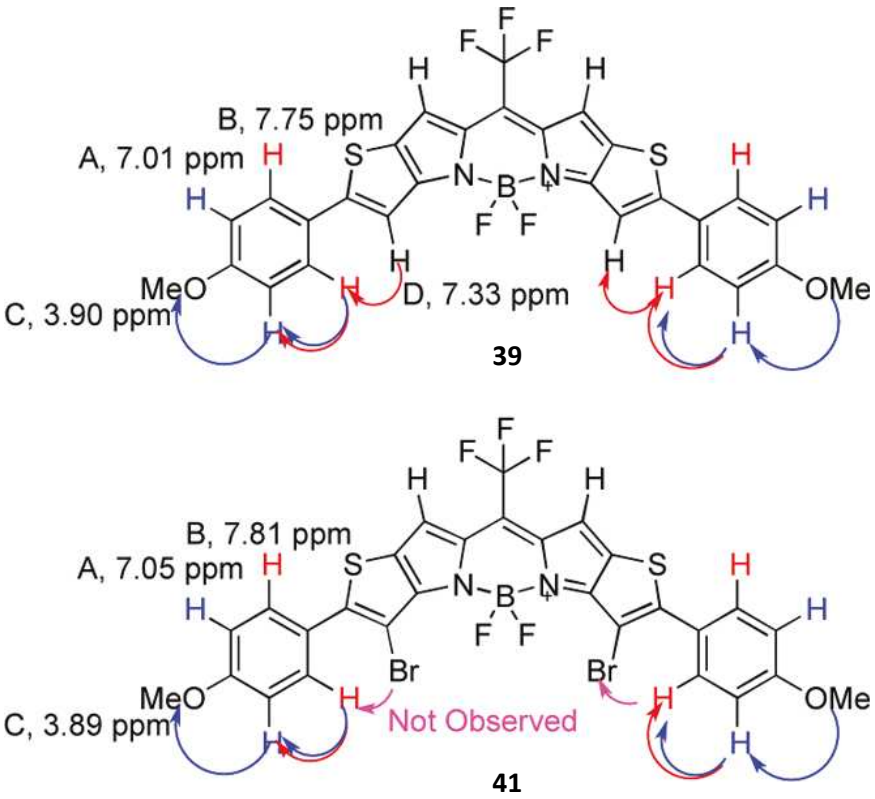

Figure 9. Key NOEs showing sites of bromination in **39** and **41**

2.4.3. Optical Properties of BODIPY Dyes

In solutions of different polarities using $CHCl_3$ and THF, the BODIPY analogues displayed excellent optical properties and sharp bands (Fig. 10). The synthesized dyes in solution showed a vivid green absorption color. The incorporation of the thiophene, **39**, induced red-shifts of 8 nm relative to **KFL4** while maintaining a high molar extinction coefficient of 201 000M^{-1} cm^{-1}. A larger bathochromic shifts of ~20 nm (**KFL4→42**) and ~30 nm (**39 →43**) was observed when four bromine atoms were substituted to the modified core containing furan and thiophene moieties respectively (Table

1). The absorption maximum of **41** was inconsistent with the observed trends as it displayed a blue shift of 11 nm from its parent **39**. The variation was well captured by the TDDFT calculations (Fig. 14) although a cause of this variation is not clear; I could speculate an alteration in geometry by the bromine attachment. All the BODIPY analogues displayed sharp emission bands in the NIR region ranging from 738 – 820 nm, with moderate quantum yields of fluorescence. The effective triplet population of the dyes could have caused the low fluorescence quantum yields of the tetrabrominated analogues.

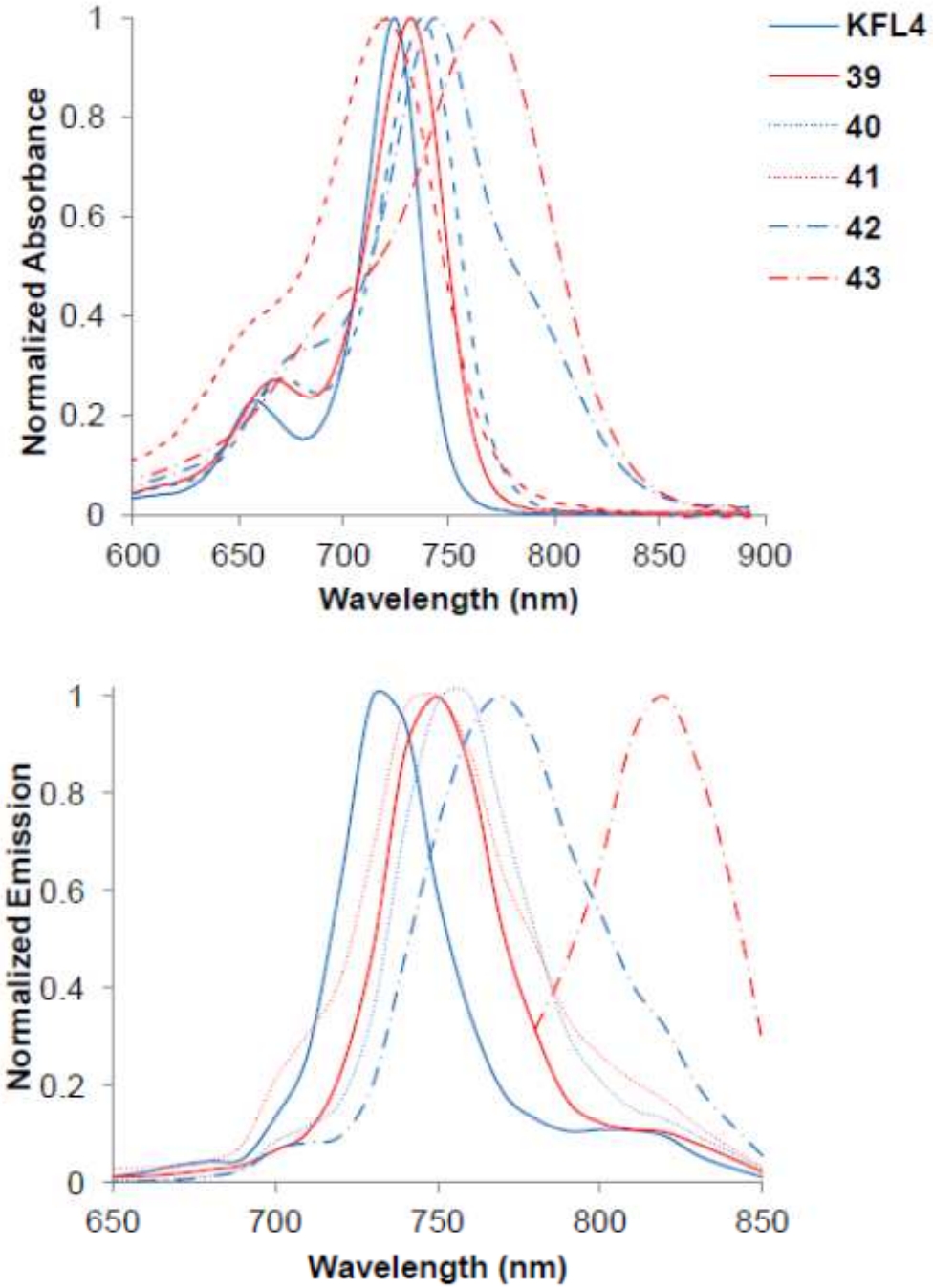

Figure 10. Absorption and emission spectra of NIR BODIPY **KFL4-43** in $CHCl_3$

Table 1. Optical properties of Novel NIR BODIPY analogues

Compound	Solvent	λ_{ab}, nm	λ_{em}, nm	ε, $M^{-1}cm^{-1}$	Φ_f[a]
KFL4	$CHCl_3$	723	738	253 000	0.56
	THF	722	738	229 000	0.56
39	$CHCl_3$	731	754	201 000	0.37
	THF	730	754	179 000	0.39
40	$CHCl_3$	738	756	242 000	0.37
	THF	732	756	203 000	0.28
41	$CHCl_3$	720	754	89 000	0.45
	THF	717	754	64 000	0.17
42	$CHCl_3$	744	765	94 000	0.28
	THF	741	765	139 500	0.11
43	$CHCl_3$	766	820	75 000	0.11
	THF	764	770	51 000	0.04

[a]Reference: **KFL4**

2.4.4. Singlet Oxygen Generation

Employing the indirect method for the determination of singlet oxygen, a comparative study on all analogues in THF solutions was performed. The solutions were irradiated with broadband light, 400 nm - 850 nm, at 0.5 mW/cm^2. Singlet oxygen generation was analyzed experimentally by 1,3-diphenylisobenzofuran (DPBF), a well known singlet

oxygen scavenger. The photooxidation of DPBF was monitored by the decrease of the absorbance band at 410 nm upon irradiation. The experiments were performed at initial concentrations of 5×10^{-6} M of PS and 90×10^{-6} M of DPBF over a period of 18 min. 5-(4-Methoxyphenyl)-10,15,20-triphenyl-21,23 dithiaporphyrin (CMP) was used as a reference PS. Previous experiments established that CMP has a high singlet oxygen quantum yield, $\Phi(^1O_2) = 0.7\text{-}0.8$.[77] Although compounds **39**, **40**, **42** did not show significant photooxidation of DPBF, compounds **41** and **43** showed fast oxidation of DPBF (Fig. 10). A 1.2 fold relative rate of photooxygenation of DPBF by **41** was recorded and a 0.5-fold relative rate for **43** (Table 2). The slower rate of **43** might be attributed to its low molar extinction coefficient at the irradiation wavelength of 764 nm and potential aggregation due to its extreme hydrophobicity.

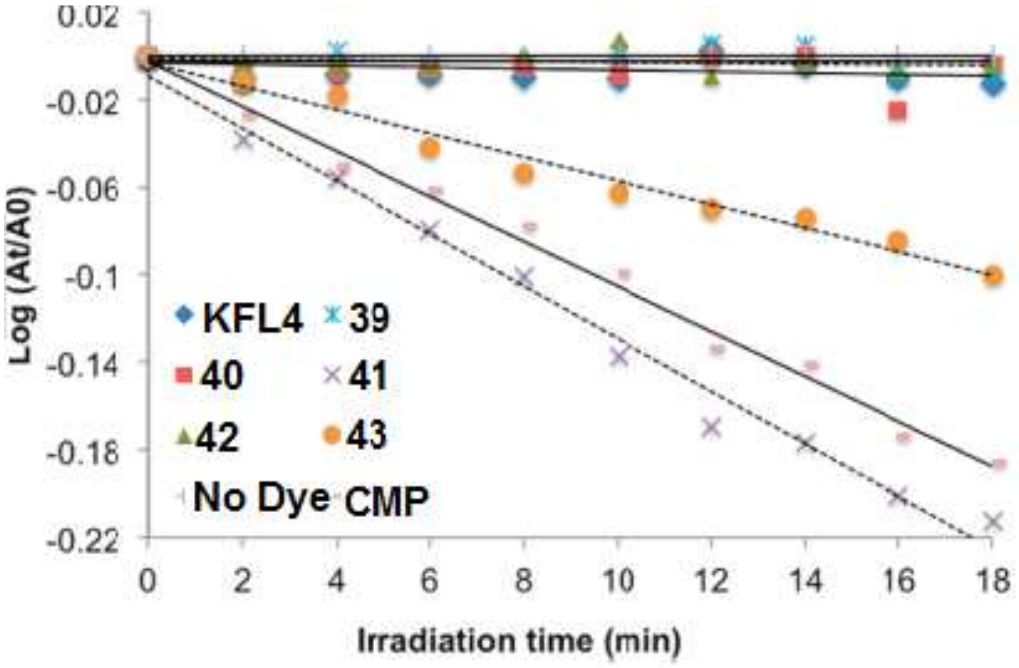

Figure 11. Comparative singlet oxygen generation study of NIR BODIPY analogues

Table 2. Relative rate of DPBF oxidation by **41**, **43** and reference standard

Compound	**CMP**	**41**	**43**
Relative rate	1.0	1.2	0.5

2.4.5. Photostability of BODIPY Analogues

Photostability is one of the required characteristics for fluorescent probes as well as PSs. In particular, NIR dyes that are often photo-unstable require a thorough examination. It is also important to note that a number of second generation PDT agents, for example, bacteriochlorins suffer from photobleaching. Subjecting **39 – 43** to photobleaching kinetic studies in comparison to the clinically approved PDT agent, meta-

tetrahydroxyphenylchlorin (m-THPC) and its NIR absorbing analogue, meta-tetrahydroxyphenylbacteriochlorin (m-THPBC); I observed high resistance to photobleaching. The first order plots revealed that photobleaching of all the NIR BODIPY dyes were slower than that of m-THPBC. In addition, dye **41** had a rate constant of -0.001 min^{-1} and that of **43** was comparable with that of mTHPC at -0.0033 min^{-1}. Photobleaching was observed for dye **40**, with a k value of -0.0055 min^{-1}. Under the irradiation conditions, m-THPC photobleached rapidly at the initial 30 mins over the other BODIPY analogues including **40**.

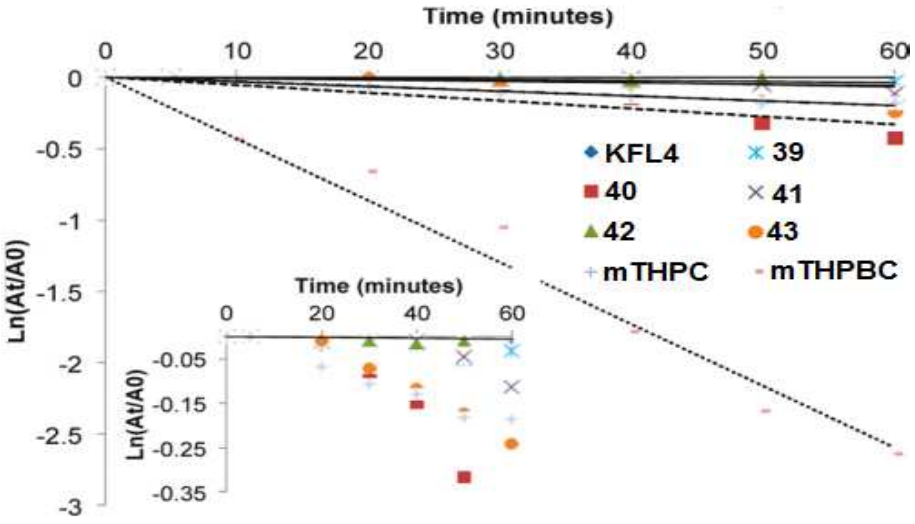

Figure 12. Photobleaching kinetics of BODIPY analogues, m-THPC, and m-THPBC.

Photostability results were obtained by comparing **39 - 43** to m-THPBC. m-THPBC was dissolved in methanol and **39 - 43** were dissolved in THF and the solutions were matched to the same absorbance at T = 0 (m-THPBC = 0.036 mM). These solutions were irradiated with a xenon arc lamp source at an intensity of 100 mW/cm^2 using a water filter and two glass filters (>400 nm and <800 nm). The stability was monitored by UV spectrophotometer over a period of 1 h at 10 min interval following the diminution of band I (m-THPBC = 735 nm) and the bands of **39 - 43** at the respective absorption maxima.

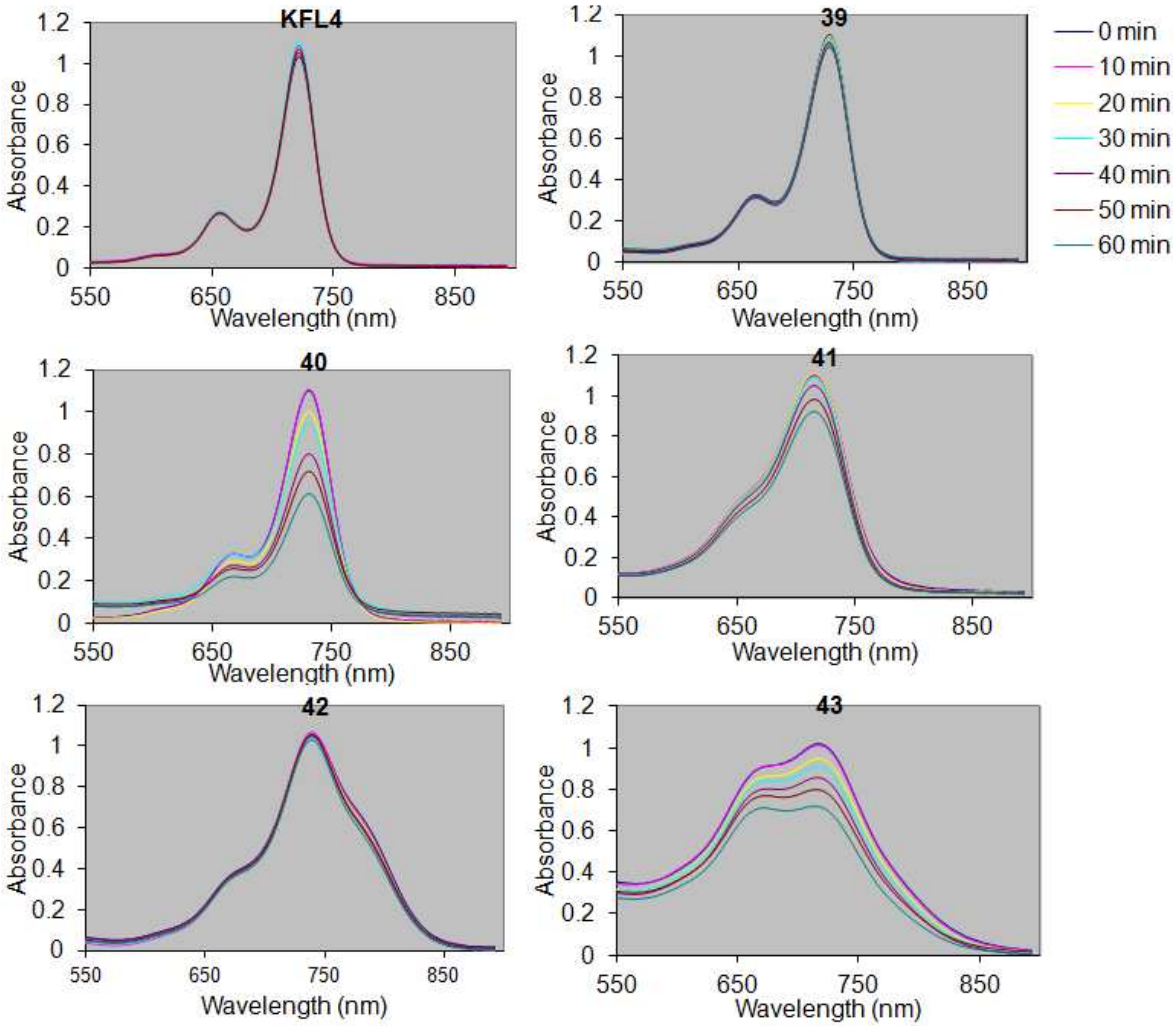

Figure 13. UV spectra obtained during a photobleaching experiment

2.4.6. Computational and Theoretical Insight

To enlighten our understanding of the excited state in predicting the absorption behavior of these BODIPY analogues, theoretical and computational characterization using density functional theory (DFT) was performed.[78] Geometry optimization of these compounds was carried out using the 6-311 G* basis set while the electronic excitations corresponding

to the absorption spectra were calculated with time-dependent-DFT (TDDFT) and the PBEPBE correlation functional in vacuo (gas phase) as expressed by Gaussian 09.[79] The frontier molecular orbital showed electron distribution moving from the HOMO where electrons are spread throughout the molecule and in the LUMO, where the acceptor CF_3 moiety pulls electrons (Fig. 14). The observation affirms the D-π-A strategy. The computationally generated TDDFT calculations predicted strong 0-0 absorption maxima (π – π*) of compounds **39 - 43** in the NIR region with relatively small deviations from the experimental data (ΔE = 0.03 - 0.15 eV) as observed in Table 3. The experimental data obtained from absorption spectra correlated well with calculated excitation energies in vacuo of the analogues as seen in the observed trend (Fig. 15). The differences in spectral shift could be attributed to mainly solvent effects.

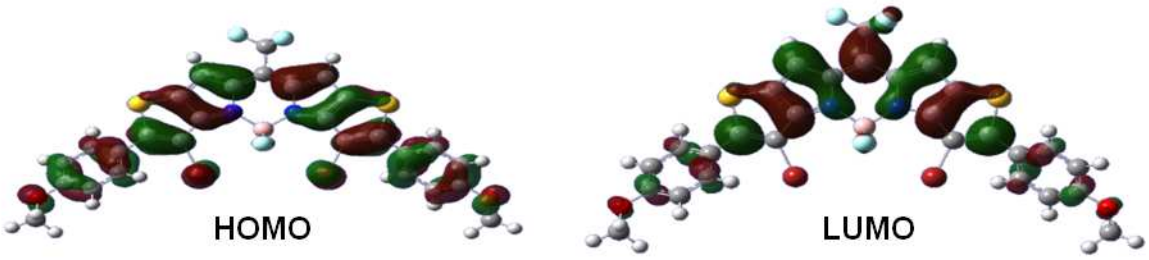

Figure 14. Frontier molecular orbital of BODIPY **41**

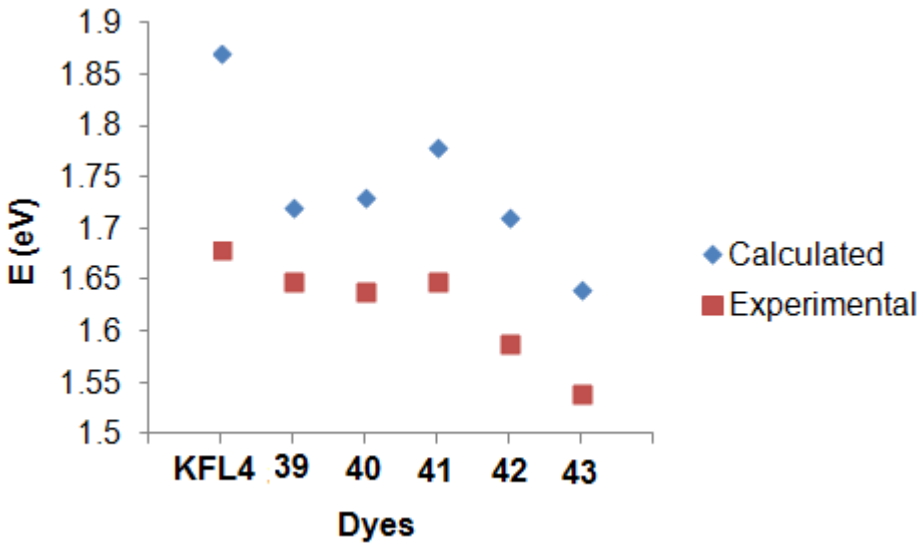

Figure 15. Observed trend for calculated excitation energies and experimental absorption maxima in eV

Table 3. TDDFT-Calculated Excitation Energies for the Lowest Transition (eV, nm), Oscillator Strengths (f), and Experimental Absorption Maxima (exp)

Dye	State	Excitation	E (eV, nm)	f	Exp (eV, nm)
KFL4	S1	H→L (103%)	1.87 (662)	1.66	1.72 (723)
39	S1	H→L (81%)	1.72 (718)	0.47	1.69 (731)
40	S1	H→L (96%)	1.73 (717)	1.28	1.68 (738)
41	S1	H→L (22%)	1.78 (697)	0.54	1.72 (720)
42	S1	H→L (97%)	1.71 (723)	1.23	1.66 (746)
43	S3	H2→L (79%)	1.64 (757)	0.40	1.61 (766)

2.5. Conclusion

In this chapter, I focused on developing novel NIR BODIPY dyes with propensity to generate singlet oxygen, a key cytotoxic agent in PDT. I used the synthetic strategy of ring fusion of furan and thiophene moieties to the BODIPY core for extended π-conjugation in inducing bathochromic shift into the NIR region. Furthermore, in addition to the thiophene moieties, I carried out an aromatic electrophilic substitution with bromine to impart a heavy

atom effect for enhanced ISC in generating $^1O_2$. The chemical strategies employed led to the development of BODIPY dyes with absorption in the NIR from 720 nm – 766 nm and emission of 738 – 820 nm. The brominated sulfur analogues displayed a good generation of $^1O_2$ with high resistance to photobleaching relative to clinically approved Foscan and its NIR absorbing analogue, m-THPBC. The BODIPY dye, **41**, in addition to high $^1O_2$ generation displayed a brightness (BT=ε x Φ_f), 40, 050 and 10, 880 M^{-1} cm^{-1} in $CHCl_3$ and THF, respectively, making it a promising theranostic candidate for PDT and in vivo diagnostics. Moreover, this work confirms the use of computational DFT methods as a useful tool in the design of efficient BODIPY candidates based on the close correlation of experimental to calculated data.

These new sensitizers displayed a great potential for NIR dual-functioning PSs with absorption at long wavelengths and effective generation of both fluorescence and singlet oxygen.

2.6. Experimental Section

2.6.1. General Experimental Procedure

Chemical reagents and solvents of analytical grade were purchased from commercial suppliers (Sigma-Aldrich Co. or Acros Organics) and were used without purification. THF was distilled from Na and benzophenone prior to use. Dichloromethane used was distilled from CaH_2. Air sensitive

reactions were performed under an atmosphere of nitrogen. Nuclear magnetic resonance spectra were recorded in $CDCl_3$, CD_2Cl_2, Acetone-d_6 or DMSO-d_6 on Bruker AM-400 or Varian 300 MHz spectrometers. Chemical shifts are given in parts per million relative to TMS or 7.23 ppm for residual $CHCl_3$ for ^{1}H-NMR and coupling constants were measured in Hz. Electron Impact (EI) using a ThermoFinnigan MAT 95 XL spectrometer and determined at an ionized voltage of 70 eV and Electrospray Ionization (ESI) Mass Spectrometer measurements were recorded on Bruker Mass Spectrometer from SUNY Buffalo and South Dakota State University Mass Spectrometry Facilities respectively. The compounds from furan were synthesized based on the reference.[60]

Geometry optimization was carried out using Gaussian 09 and Spartan 08 modules.

2.6.2. 4-methoxyphenylboronic acid (33)*.[80] Magnesium (4.20 g, 174 mmol) was placed in a dry 2-neck round bottom flask and dry THF (50 ml) was added and refluxed for 2 h. 4-bromoanisole (27.20 g, 145 mmol) in dry THF (100 ml) was added slowly and after 5 h the reflux was stopped and the solution was cooled to room temperature. The cooled solution (4-methoxypheny magnesium bromide) was slowly added to trimethylborate (19.60 g, 188 mmol) in dry THF (100 ml) at 0 ℃ via a cannula. After stirring the reaction mixture overnight at room temperature, the reaction was

filtered and the solid obtained immersed in water. The aqueous solution was acidified with 1 N HCl (aq.) and extracted with ethyl acetate (3 times). The organic layer was washed with water and dried over anhydrous Na_2SO_4 and the solvent removed under vacuum. The solid residue was purified by recrystallization from toluene to obtain a pure white solid, **33** (19.60 g, 89 % [based on ^{1}H-NMR]). ^{1}H-NMR ($CDCl_3$) δ: 8.17 (d, J = 8.6 Hz, 2H), 7.02 (d, J = 8.6 Hz, 2H), 3.89 (s, 3H), B-OH (not observed).*Known

2.6.3. 5-(4-methoxyphenyl)-furan-2-carbaldehyde (35a)*.[60] 33 (4.85 g, 31.9 mmol) and 5-bromo-2-furaldehyde (5.59 g, 31.9 mmol) were dissolved in toluene (200 ml). Ethanol (50 ml) and 2 M aqueous Na_2CO_3 (30 ml) was added and nitrogen was bubbled through the reaction mixture for 30 min. [1,1-bis(diphenylphosphino)-ferrocene] palladium (II)dichloride dichloromethane complex (1:1) (167 mg, 0.20 mmol) was added and heated to 80 ℃ for 14 h. The reaction mixture was coo led and the ethanol evaporated under vacuum. The resulting solution was washed with water and brine and dried over anhydrous Na_2SO_4 and concentrated to obtain a brown liquid. Column chromatography (silica gel) was used to purify the compound by gradient elution with ethyl acetate: hexane (5:95 – 25:75) as mobile phase with the target compound eluting at 20:80 ethyl acetate: hexane (monitored by TLC) as a yellow liquid (4.10 g, 85% [based on ^{1}H-NMR]). ^{1}H-NMR ($CDCl_3$) δ: 9.53 (s, 1H), 7.66 (d, J = 8.8 Hz, 2H), 7.25 (d, J

= 8.8 Hz, 1H) 6.87 (d, *J* = 8.8 Hz, 2H), 6.65 (d, *J* = 8.8 Hz, 1H), 3.76 (s, 3H). *Known

2.6.4. Ethylazidoacetate*.[81] Ethylbromoacetate (6.40 g, 38.5 mmol) was dissolved in acetone and transferred into a round bottom flask. While stirring at room temperature (25 ℃) dissolved sodium azide (5.0 g, 77 mmol) in water was added slowly. Stirring was continued for 1.5 h and the reaction was stopped. The acetone was evaporated and dichloromethane was used to extract the compound. The extract was washed with water and dried over anhydrous $MgSO_4$ and concentrated to obtain a pale yellow liquid (4.35 g, 87 % [based on ^{1}H-NMR]). ^{1}H-NMR ($CDCl_3$, 400 MHz): δ 4.20 (q, *J* = 7.1 Hz, 2H), 3.82 (s, 2H), 1.25 (t, *J* = 7.1 Hz, 3H). IR: (KBr, cm^{-1}): 2110 ($\nu_{N\equiv N}$).*Known

2.6.5. 2-(4-Methoxyphenyl)-4H-furo[3,2-b]pyrrole-5-carboxylic acid ethyl ester (36a)*.[60] Ethylazidoacetate (13.0 g, 100 mmol) and 5-(4-methoxyphenyl)-furan-2-carbaldehyde (**35a**) (5.8 g, 29 mmol) were dissolved in anhydrous ethanol (250 ml) and stirred at 0 ℃ under a nitrogen atmosphere. 21 % NaOEt in EtOH solution (42.9 ml, 100 mmol) was added dropwise to the mixture and stirring continued for 2 h. A saturated solution of ammonium chloride was added to form a yellow precipitate which was collected by filtration and vacuum dried. The resulting brown residue was dissolved in toluene and refluxed for 1.5 h to complete the cyclization of the derived pyrrole. The solvent was evaporated and purified by column

chromatography (silica gel) using gradient elution of ethyl acetate – hexane (5 – 30 → 95 – 70) to obtain a brown solid (3.00 g, 48 % [based on ^{1}H-NMR]). ^{1}H-NMR ($CDCl_3$, 400 MHz) δ: 8.67 (s, 1H), 7.59 (d, *J* = 8.8 Hz, 2H), 6.87 (d, *J* = 8.8 Hz, 2H), 6.72 (s, 1H), 6.50 (s, 1H), 4.27 (q, *J* = 7.1 Hz, 2H), 3.78 (s, 3H), 1.31 (t, *J* = 7.1 Hz, 3H).*Known

2.6.6. Ethyl 2-(4-methoxyphenyl)-4H-thieno[3,2-b]pyrrole-5-carboxylate (36b): Ethylazidoacetate (5.01 g, 38.8 mmol) and 5-(4-methoxyphenyl)thiophene-2-carbaldehyde (**35b)** (2.12 g, 9.7 mmol) was dissolved in anhydrous EtOH (250 ml) under a nitrogen atmosphere at 0 ℃ and stirred for 20 min. 21% NaOEt in EtOH solution (2.64 g, 38.8 mmol) was added dropwise at 0 ℃ over 20 min. The reaction t urned dull orange in color. After 30 min, the reaction solution was taken out of the ice bath and stirred for an additional 1.5 h. A saturated aqueous solution of NH_4Cl (10 ml) was added dropwise to facilitate precipitation. The yellow precipitate was collected by vacuum filtration and washed with water. The washed solid was collected and allowed to dry. The dried solid was dissolved in 30 ml of toluene and refluxed for 1.5 h to complete the cyclization of the derived pyrrole. Toluene was removed and the residue purified by column chromatography (silica gel) using gradient elution with ethyl acetate – hexane (5 – 30 → 95 – 70) to give a yellow amorphous solid (1.00 g, 47 %, [based on ^{1}H-NMR]). ^{1}H-NMR ($CDCl_3$, 400 MHz): δ 8.95 (s, 1H), 7.55 (d, *J* = 8.0 Hz, 2H), 7.11 (s, 1H), 7.07 (s, 1H), 6.93 (d, *J* = 8.0 Hz, 2H), 4.34 (q, *J*

= 7.1 Hz, 2H), 3.84 (s, 3H), 1.39 (t, *J* = 7.1 Hz, 3H). HRMS (EI) (m/z): Calculated for $C_{16}H_{15}NO_3S$: 301.0773; Found: 301.0826 $[M]^+$.

2.6.7. 2-(4-Methoxyphenyl)-4H-thieno[3,2-b]pyrrole-5-carboxylic acid (37b): 36b (0.30 g, 1.1 mmol) was dissolved in EtOH (~10 ml). NaOH (0.62 g, 15.5 mmol) in water (5 ml) was added to the solution and refluxed for 1 h. The reaction was cooled to room temperature and further cooled in an ice bath. The reaction mixture was then acidified with concentrated HCl. The precipitate was filtered, washed with water and dried under vacuum. A dark green solid was obtained (0.22 mg, 70 % [based on ^{1}H-NMR]). ^{1}H-NMR (DMSO-d_6, 400 MHz): δ 12.36 (s, 1H), 11.93 (s, 1H), 7.60 (d, *J* = 8.0 Hz, 2H), 7.22 (s, 1H), 7.01 (s, 1H), 6.99 (d, *J* = 8.0 Hz, 2H), 3.79 (s, 3H). HRMS ESI (m/z): Calculated for $C_{14}H_{11}NO_3S$: 273.0460; found: 273.0459 $[M+H]^+$.

2.6.8. 2,8-Di(4-methoxyphenyl)-11-trifluoromethyl-dithieno[2,3-b]-[3,2-g]-5,5-difluoro-5-bora-3a,4a-dithio-s-indacene (39). 37b (0.20 g, 0.7 mmol) was dissolved in TFA (10 ml) at 40 ℃, an intense green color appeared. Trifluoroacetic anhydride (2 ml) was added at 40 ℃ and the temperature was then raised to 80 ℃ and stirring was continued for 30 min, all under a nitrogen atmosphere. The reaction was quenched as it was poured into aqueous $NaHCO_3$ solution containing crushed ice. The dark green precipitate was filtered, washed with water and dried in vacuo. The solid was dissolved in dry toluene (47 ml) and stirred for 5 min at room temperature under a nitrogen atmosphere for complete dissolution. Boron

trifluoride diethetate (1 ml) and triethylamine (0.5 ml) were added and the temperature was raised to 80 ℃ and stirring continued for 30 min. After cooling, the reaction solution was diluted with toluene and washed with aqueous $NaHCO_3$, water and brine. The solvent was evaporated to obtain a crude mixture, which was purified by column chromatography (silica gel) using chloroform/hexane (80:20) as the mobile phase. A green metallic solid was obtained (73 mg, 33 % [based on ^{1}H-NMR]). ^{1}H-NMR (CD_2Cl_2, 400 MHz): δ 7.76 (d, *J* = 8.0 Hz, 4H), 7.34 (s, 2H), 7.32 (s, 2H), 7.03 (d, *J* = 8.0 Hz, 4H), 3.91 (s, 6H). HRMS EI (m/z): Calculated for $C_{28}H_{18}BF_5N_2O_2S_2$: 584.0823; Found: 584.0825 $[M]^+$.

2.6.9. 3,7-Dibromo-2,8-di(4-methoxyphenyl)-11-trifluoromethyl-difuro[2,3-b]-[3,2-g]-5,5-difluoro-5-bora-3a,4a-diaza-s-indacene (40). **KFL-4** (0.06 g, 0.1 mmol) along with I_2 (0.001 g) were dissolved in CH_2Cl_2 (15 ml). A solution of Br_2 (0.10 g, 0.7 mmol) in CH_2Cl_2 (5 ml) was added dropwise and stirred at 40 ℃ for 12 h. The reaction mixture was neutralized with aqueous Na_2CO_3 solution and the aqueous layer was separated from the organic layer. The aqueous layer was further extracted with diethyl ether and the combined organic layers were dried over anhydrous Na_2SO_4 and the solvents removed by evaporation under vacuum to obtain a brown solid (40 mg, 52 % [based on ^{1}H-NMR]). ^{1}H-NMR ($CDCl_3$, 400 MHz) *δ*: 8.21 (d, *J* = 9.0 Hz, 4H), 7.03 (d, *J* = 9.0 Hz, 4H), 6.80 (s, 2H), 3.84 (s, 6H).

HRMS EI (*m/z*): Calculated for $C_{28}H_{16}BBr_2F_5N_2O_4$: 709.9470; found: 709.9519 $[M]^+$.

2.6.10. 3,7-Dibromo-2,8-di(4-methoxyphenyl)-11-trifluoromethyl-dithieno[2,3-b]-[3,2-g]-5,5-difluoro-5-bora-3a,4a-diaza-s-indacene (41). Following the method used to prepare compound **40**, the starting material **39** (0.05 g, 0.1 mmol), was used with I_2 (0.001 g) and Br_2 (0.04 g, 0.3 mmol) to obtain compound **41** (25 mg, 37 % [based on ^{1}H-NMR]). Interestingly, while one doublet peak for four protons at 2-position of 4-methoxyphenyl groups was observed from the other BODIPY derivatives, compound **41** showed two doublet peaks for the corresponding four protons. It might be due to hindered rotation of methoxyphenyl group by the substituted bromines in **41**. ^{1}H-NMR (CD_2Cl_2, 300 MHz) δ: 7.84 (d, J = 9.0 Hz, 2H), 7.76 (d, J = 9.0 Hz, 2H), 7.64 (s, 1H), 7.05 (dd, J = 9.0 Hz, 4H), 3.89 (s, 6H). HRMS EI (*m/z*): Calculated for $C_{28}H_{16}BBr_2F_5N_2O_2S_2$: 741.9013; found: 741.8978 $[M]^+$.

2.6.11. 3,7,9,12-Tetrabromo-2,8-di(4-methoxyphenyl)-11-trifluoromethyl-difuro[2,3-b]-[3,2-g]-5,5-difluoro-5-bora-3a,4a-diaza-s-indacene (42). KFL-4 (0.13 g, 0.2 mmol) along with I_2 (0.002 g) were dissolved in CH_2Cl_2 (15 ml). A solution of Br_2 (0.33 g, 2.1 mmol) in CH_2Cl_2 (5 ml) was added dropwise and stirred at 40 ℃ for 12 h. The reaction mixture was neutralized with aqueous Na_2CO_3 solution (20 %) and the aqueous layer was separated from the organic layer. The aqueous layer

was further extracted with diethyl ether and the combined organic layers were dried over anhydrous Na_2SO_4 and the solvents removed by evaporation to obtain a brown solid (61 mg, 30 % [based on ^{1}H-NMR]). ^{1}H-NMR ($CDCl_3$, 300 MHz) δ: 8.20 (d, J = 8.9 Hz, 4H), 6.97 (d, J = 8.9 Hz, 4H), 3.84 (s, 6H). HRMS EI (*m/z*): Calculated for $C_{28}H_{14}BBr_4F_5N_2O_4$: 867.7659; found: 867.7673 $[M]^+$.

2.6.12. 3,7,9,12-Tetrabromo-2,8-di(4-methoxyphenyl)-11-trifluoromethyl-dithieno[2,3-b]-[3,2-g]-5,5-difluoro-5-bora-3a,4a-diaza-s-indacene (43). Following the method used to prepare compound **42**, the starting material **39** (0.09 g, 0.2 mmol), was used with I_2 (0.002 g) and Br_2 (0.29 g, 2.0 mmol) to obtain compound **43** (27 mg, 20 % [based on ^{1}H-NMR]). ^{1}H-NMR ($CDCl_3$, 300 MHz) δ: 7.71 (d, J = 9.2 Hz, 4H), 6.96 (d, J = 9.2 Hz, 4H), 3.81 (s, 6H). HRMS EI (*m/z*): Calculated for $C_{28}H_{14}BBr_4F_5N_2O_2S_2$: 899.7202; found: 899.7197 $[M]^+$.

Chapter 3

Versatile Synthesis of NIR BODIPY Dyes via Palladium Catalyzed Cross-coupling

3.0. Introduction

The development of NIR organic probes for non-invasive optical imaging and photo-induced light therapy is an attractive enterprise for medical applications. Difficult synthesis, lack of photostability, limited opportunities for functionalization, and poor solubility for use biologically are a number of challenges in the development of NIR organic probes. The photostability, high molar extinction coefficient, sharp absorption and emission bands of BODIPY are well known and so make it a reliable chromophore for use in diagnosis and therapy. However, synthesis for NIR BODPY analogs still remains a major challenge. To address this problem, a versatile but robust strategy is needed, which involves a flexible and facile synthesis to obtain customizable target analogues and intelligent incorporation of functional moieties to maintain their excellent photophysical properties.

In this chapter, I created a reactive fused BODIPY aryl halide intermediate (**BDP635**, Scheme 2) displaying versatility with multiple Pd-catalyzed cross coupling reactions as well as nucleophilic substitution reactions (Fig. 16). A stepwise consideration of the strategy for NIR BODIPY involved 1) preparation of versatile BODIPY aryl halide coupling

partner absorbing in the visible region, 2A) Pd- catalyzed cross coupling reactions of the BODIPY aryl halide such as Suzuki, Stille, Heck for extended conjugation, or 2B) nucleophilic substitution reactions of the BODIPY aryl halide for modest red-shifting. 3) Once NIR BODIPY cores were obtained, these could be further modified with various functional groups to modulate their physicochemical properties such as water solubility and tendency of aggregation (Chapter 4).

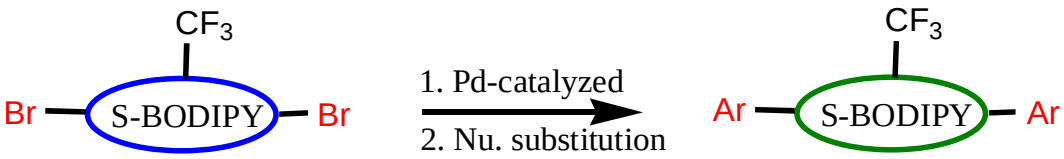

Figure 16. Schematic diagram of versatile synthetic strategy

3.1. Synthesis of Versatile BODIPY Aryl Halide

The BODIPY core is known for its high electron density and therefore, susceptible to electrophilic substitution reaction. Selective halogenation of the BODIPY exposes it to a plethora of reactions from nucleophilic to transition metal catalyzed cross coupling. Simple BODIPY units have been used in this regard with their 3, 5 and 2, 6 positions halogenated for coupling or substitution to aryl moieties. Motivated by the prototypes of short-wavelength absorbing dyes, I rationally designed the scaffold which benefits from ring fusion of aromatic heterocycles to the BODIPY core but maintains the electronic properties of the BODIPY core.

To achieve the versatile BODIPY aryl halide (**BDP635**), I synthesized the pyrrole building block (**46**) from bromo-thiophene carbaldehyde (**44**) by first reacting it with ethylazido acetate (**45**) and then heating at high temperatures (Scheme 2). The ester was subjected to basic hydrolysis. The carboxylic version of the modified pyrrole (**47**) was formed after acidification. The bromo-substituted modified pyrrole (**47**) underwent a condensation via an acid catalyzed decarboxylation of the pyrrole and with a subsequent reaction with TFA anhydride installed a CF_3 at the meso-position of the formed dipyrromethene unit. The di-bromo BODIPY alkyl halide is prepared by the reaction of the dipyrromethene unit with boron trifluoride and triethylamine.

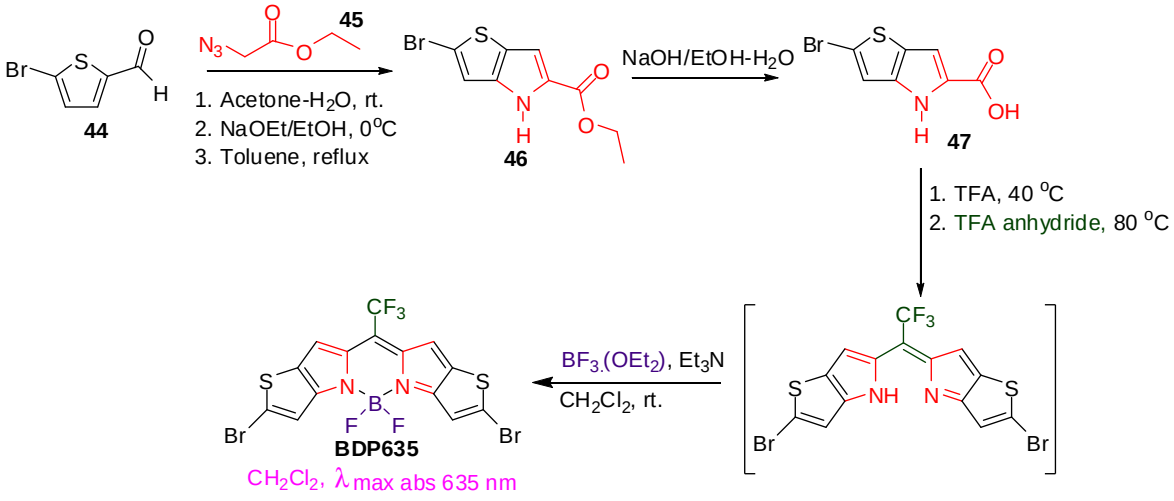

Scheme 2. Synthetic approach for **BDP635**

3.2. Results and Discussion

3.2.1. Synthesis of BDP635

The preparation of starting material, 2-bromo-4*H*-thieno[3, 2-b]pyrrole-5-carboxylic acid, **47,** a known compound, followed the Hemetsberg-Knittel synthesis of ethylazidoacetate (**45**) and 5-bromo-2-carbaldehyde (**44**) with subsequent hydrolysis led to **47** in high yields (75%) isolated by precipitation and filtration. Compound **47** was subjected to the established condensation with TFA and trifluoroacetic anhydride. The isolable dipyrromethene solid was not characterized but used in the next step involving a reaction with boron electrophile, BF_3 etherate in the presence of triethylamine to obtain the new BODIPY halide, **BDP635**. The desired BODIPY was isolated by silica-gel column chromatography by pouring the solution through the column to obtain the pure blue solution. A standard work-up was not used due to the decomposition of the target compound upon rotary evaporation that might be a result of a reaction of residual TEA with the highly electrophilic BODIPY product. The purified **BDP635** was characterized by ^{1}H-NMR and EI-HRMS.

3.2.2. X- Ray Structure of BDP635

The **BDP635** single crystal of a monoclinic system was obtained by slow evaporation from a clear blue, concentrated solution of **BDP635** in CH_2Cl_2 at room temperature in a round bottom flask. The black plate-like crystal of dimensions 0.44 x 0.41 x 0.08 mm was used for the structural analysis. Measurements were performed using a diffractometer with a Bruker APEX CCD area detector and graphite-monochromated Mo Kα radiation (λ = 0.71073 Å). The sterically crowded boron center maintained a geometry almost tetrahedral with an N-B-N angle of 105.1 (2) ^{o}, while the C-F-C and remained close to tetrahedral geometry at 106.7 (2) ^{o} and 106.3 (2) ^{o}. The Br-C bond lengths were identical at 1.861 (3) Å. The BODIPY core remained planar in fusion with the thiophene aromatic.

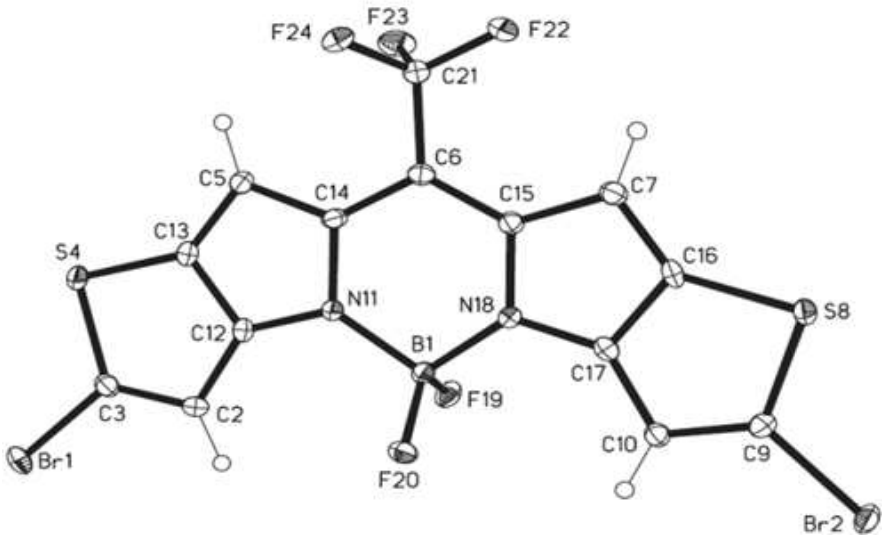

Figure 17. ORTEP view of the X-ray crystal structure of **BDP635**. The displacement ellipsoids were drawn at the 50 % probability level.

3.2.3. Quantum chemistry and theoretical approach

To gain insight into the electronic properties of the so called versatile BODIPY alkyl halide, **BDP635**, electron density maps of the frontier molecular orbitals (HOMO and LUMO) were calculated using density functional theory (DFT) calculations in tandem with the Becke's three-parameter hybrid functional[82] and the Lee–Yang–Parr correlation (B3LYP). [83] Gaussian 09 with an appropriate basis set of 6-311G* was used for the calculations. **BDP635** showed similar electron density maps to the previously synthesized NIR BODIPY dyes with the exception of donor fragments. In the ground state, the electrons at HOMO are held in the fused BODIPY chromophore and once excited (LUMO), the electrons move to the trifluoromethyl electron withdrawing unit at the meso position (Fig. 18). The observed electron flow is expected in the design strategy for the donor-acceptor system. To gain insight into the excited states as a result of the strong absorption band in the visible region, a TDDFT excited state calculation at the B3LYP/6-311G* level in vacuo and the C-PCM model was performed, giving rise to a variation of ~135 nm between calculated vs. experimental (Fig. 18). Considering the strong $S_o \rightarrow S_1$ transitions with oscillator strength ~0.12, the variation could be attributed to solvent effects. On the whole, the insight offered confidence as it supported the rational of

building NIR absorbing BODIPY with a building block strongly absorbing in the visible range.

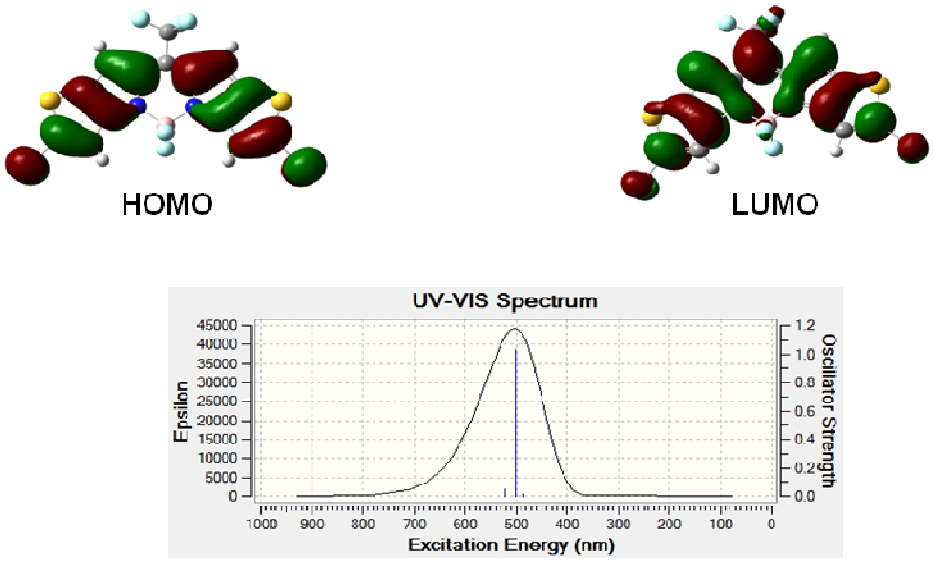

Figure 18. FMO of **BDP635** and excited state UV prediction

3.3. Palladium-catalyzed Cross Coupling

Carbon-carbon bond formation reactions are essential in chemical synthesis for a wide spectrum of uses mainly via cross coupling reactions. Transition metals have played an active role in promoting several cross-coupling reactions.[84] Copper, palladium, nickel and recently Iron have been employed largely. Palladium is arguably the most used and thoroughly investigated.[85] To a large extent palladium uses iodides and bromides as its

organic acceptors but recently alkyl phosphines, N-heterocyclic carbenes and aryl chlorides have become applicable.[86]

3.3.1. Suzuki cross coupling

With the establishment of organoborons and alkylhalides, phosphines or triflates as useful reagents for carbon-carbon bond formation I capitalized on the benefits of Suzuki cross coupling to extend the BODIPY and consequently push its absorption towards NIR (Fig. 19). Among the benefits considered were the 1) mild conditions, 2) commercial availability or established methodology for boronic acids, 3) functional group tolerance and less toxic by-products generated.

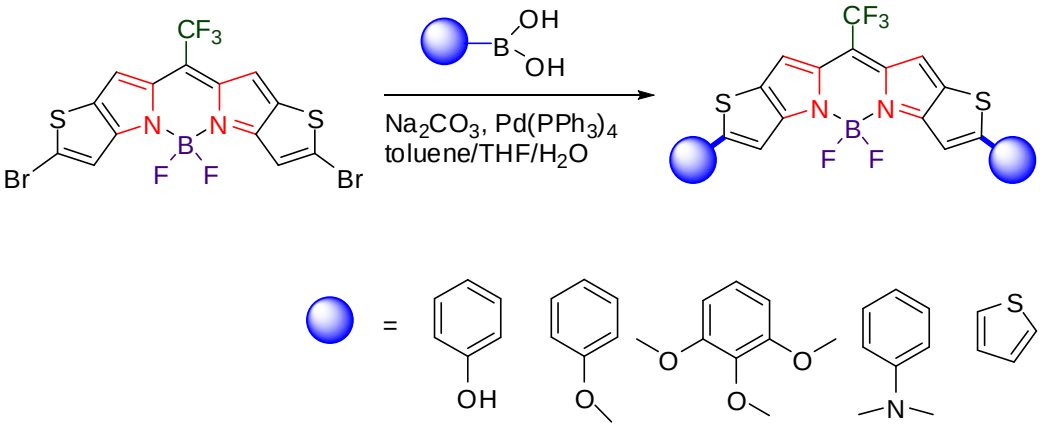

Scheme 3. Suzuki reaction coupling

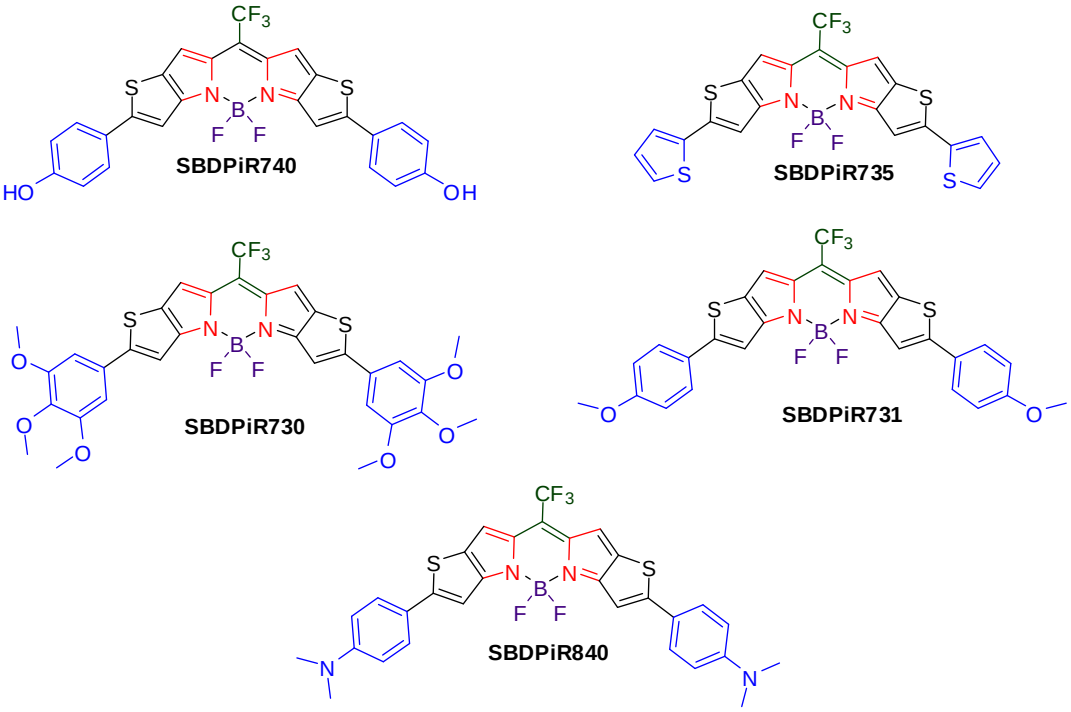

Figure 19. Structures of **SBDPiRs** via Suzuki coupling

3.3.2. Heck reaction

In the D-π-A system an approach to extend the π-conjugated system sandwiched by the donor and acceptor systems was performed. Hence the Heck reaction offered us a useful tool for building substituted olefins.

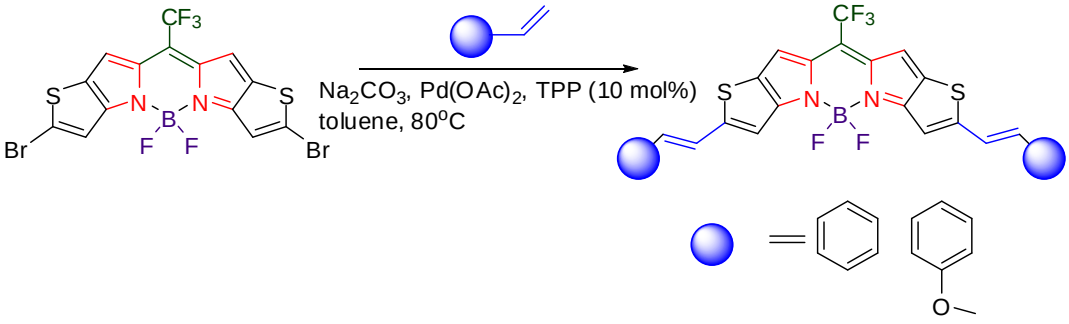

Scheme 4. Heck reaction coupling

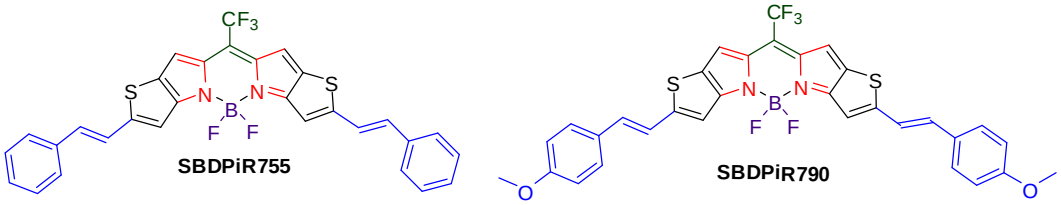

Figure 20. Structures of SBDPiR via Heck reaction

3.3.3. Stille coupling

A great alternative to the organoborane reagent are the organostannanes (organotin) as typified in the Stille cross coupling. It was rationed that building an organic electrophile would be an excellent coupling partner for organostannanes. In addition, the wide functional group

tolerance, less sensitivity to moisture and relatively easier preparation of organotins made it a worthwhile venture to pursue.

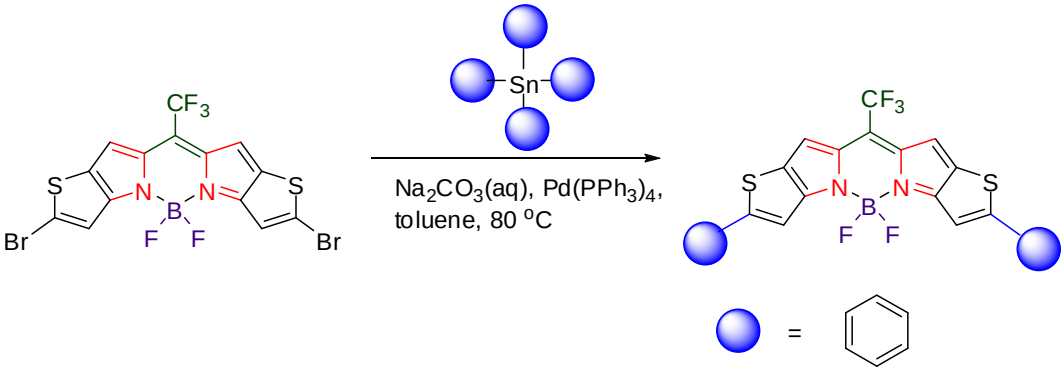

Scheme 5. Stille cross-coupling reaction

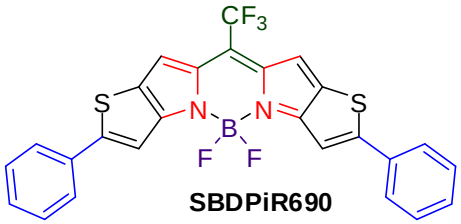

Figure 21. Structure of **SBDPiR** via Stille coupling

3.3.4. Nucleophilic substitution

In order to explore the reactivity of the key intermediate as a BODIPY electrophile, substitution reactions with nucleophiles from the chalcogen group; O and S was performed (Fig. 22). Relatively fast

reactions were observed with appreciably moderate to high yields, confirming the versatility of **BDP635**.

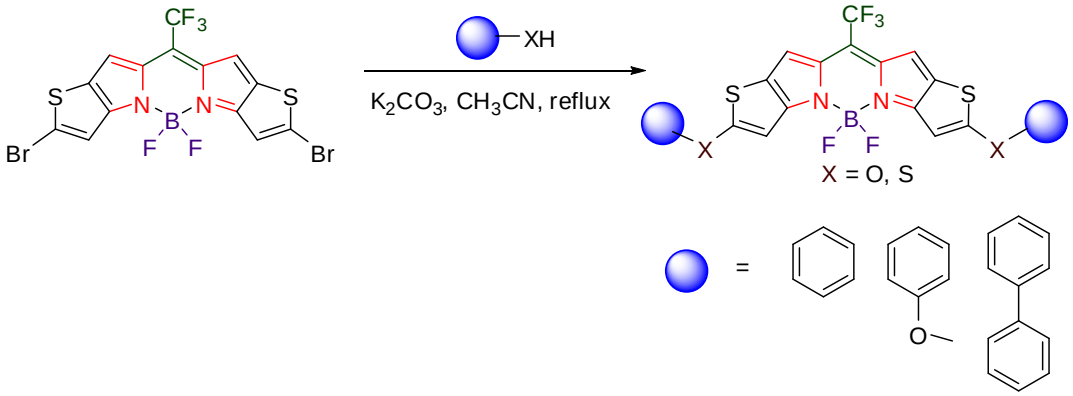

Scheme 6. Nucleophilic substitution reaction

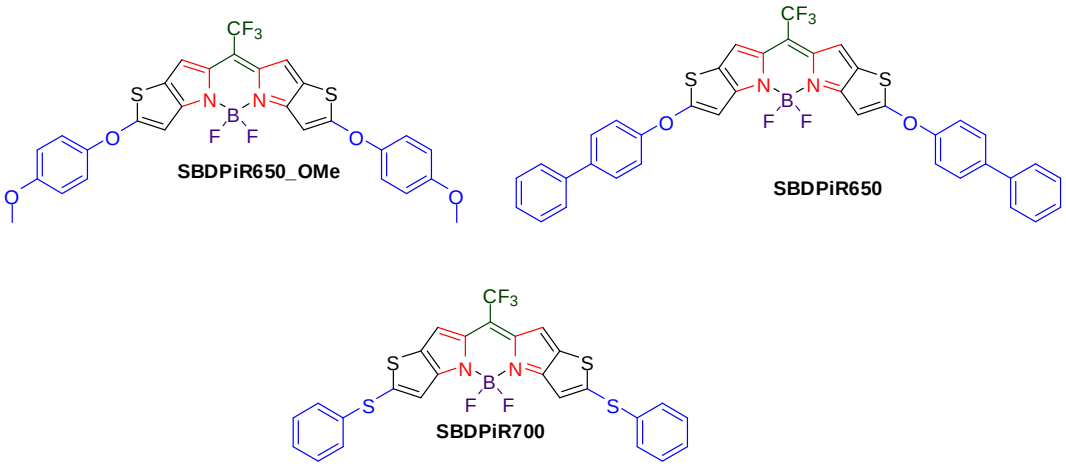

Figure 22. Structures of SBDPiR via nucleophilic substitution reaction

3.4. Results and Discussion

3.4.1. Synthesis

According to mesomeric structures of the indigenous BODIPY core, the 2, 6 (β) positions bear the least positive charge; making it susceptible to electrophilic attack. Using the indigenous core as a prototype an estimate that the 2, 8 positions of the modified thieno-pyrrole BODIPY (**BDP635**) bears similar electronic properties was made. In addition, the CF_3 group at the meso position renders the BODIPY as a more electrophilic organic moiety for various reactions. **BDP635** was used in several palladium catalyzed cross coupling reactions, displaying similar reactivity as an organic electrophile in comparison to various halogenated BODIPY reported in literature.

First, in the Suzuki cross coupling **BDP635** showed excellent reactivity in comparison to that of the hexabromo-BODIPY reported in the literature.[87] In this Pd-catalyzed cross coupling reaction, our dibromo-modified BODIPY (**BDP635**) reacted with different aryl boronic acids in a three component solvent system of water, THF and toluene, using $Pd(PPh_3)_4$ as catalyst with Na_2CO_3 as a base. The reaction was heated at 80 ℃ for 2-3 h depending on arylboronic acid (Scheme 3). All compounds except **SBDPiR731** were new compounds obtained in satisfactory yields. Compounds **SBDPiR740**, **SBDPiR735**, **SBDPiR731**, **SBDP730** (Fig. 19)

were obtained using 4-hydroxyphenylboronic acid, thiopheneboronic acid, methoxyphenylboronic acid and 3, 4, 5-trimethoxyphenyl boronic acid respectively in moderate yields of ~50 %. **SBDPiR730** was synthesized to demonstrate the relatively facile and cost effective approach in making the known (made by our research group) **SBDPiR730** in scheme 1 as compound **39**. The use of N,N-dimethylaminophenylboronic acid resulted in **SBDPiR840**, most red-shifted in the synthesized dye series. The enhanced resonance effect in the N, N-dimethylaminophenylboronic acid might have contributed to the relatively faster reaction in relation to the other substrates in the series.

Second, the reactivity of **BDP635** was further validated in the Heck coupling reaction as relatively milder conditions were applied to obtain desired NIR BODIPY in relation to the 3,5 halogenated BODIPY in literature.[48] In an anhydrous toluene solution of, **BDP635** with respective styrene and 4-methoxystyrene substrates were heated to 80 ℃ for 6 h. Palladium (II) acetate was used as catalyst and triphenylphosphine as ligand. It is interesting to point out that shorter reaction times yielded the monosubstituted analogues as observed on TLC and UV-vis spectroscopy but were not isolated and characterized. The commonly used base for Heck coupling, triethylamine, was not employed for these substrates as I suspect a possible nucleophilic attack of the base with **BDP635**, instead, Na_2CO_3 was used. **SBDPiR755** and **SBDPiR790** (Fig. 20) were obtained in decent

yields of 25 – 30 %. A remarkable bathochromic shift was observed due to the external olefin added to the existing BODIPY π-system to afford a D-π-π-A system.

Third, **BDP635** was allowed to react under the Stille coupling reaction conditions for 1 h with equimolar portions of tetraphenyltin reagent. $Pd(PPh_3)_4$ was used as catalyst with an aqueous solution of Na_2CO_3 (1M) to afford the **SBDPiR690** (Fig. 21) in a di-substituted fashion.

Finally, I demonstrated S_NAr reactions on **BDP635** with varied nucleophiles such as thiophenol, 4-methoxyphenol and biphenylphenol to afford **SBDPiR700**, **SBDPiR650_OMe** and **SBDPiR650** (Fig. 22) respectively. **BDP635** showed similar reactivity to that of 3,5-dihalogenated BODIPY[52] and bromoBODIPYs developed by Jiao et al.[51] The reaction conditions for the substrates utilized minimal amount of acetonitrile and K_2CO_3 as base to establish the S_NAr. The reaction yields were good in the order of 70 %.

All substrates were purified by silica gel column chromatography and characterized by ^{1}H-NMR and EI-HRMS. All synthesized analogs were new compounds except **SBDPiR731** (**39**) which was synthesized first by our earlier study.[59]

The reaction conditions and yields of the palladium-catalyzed coupling reactions as well as S_NAr reactions of **BDP635** are summarized in Table 4.

Table 4: Summary of reaction conditions of palladium catalyzed and nucleophilic substitution of **SBDPiRs**

Reagent	Solvent	Temp/ºC	Reaction time/h	Product	Yield/ %
4-Methoxyphenol	CH_3CN	reflux	1	**SBDPiR650_OMe**	25
4-Phenylphenol	CH_3CN	reflux	1	**SBDPiR650**	70
Thiophenol	CH_3CN	reflux	0.5	**SBDPiR700**	30
Tetraphenyltin	Toluene	80	1	**SBDPiR690**	30
Styrene	Toluene	80	6	**SBDPiR755**	20
4-Methoxystyrene	Toluene	80	6	**SBDPiR790**	25
4-Hydroxyboronic acid	Tol/THF/H_2O[a]	80	3	**SBDPiR740**	54
4-methoxyphenylboronic acid	Tol/THF/H_2O[a]	80	3	**SBDPiR731**	50
3,4,5-trimethoxyphenyl boronic acid	Tol/THF/H_2O[a]	80	2	**SBDPiR730**	45
N,N-dimethylphenyl boronic acid	Tol/THF/H_2O[a]	80	2	**SBDPiR840**	20
2-thiopheneboronic acid	Tol/THF/H_2O[a]	80	1	**SBDPiR735**	50

Tol – toluene; [a] 1:1:1(v/v)

3.4.2. Optical Properties of SBDPiRs

The **SBDPiRs** showed excellent photophysical with high extinction coefficients sharp absorption and emission bands similar to the cyanines and phthalocyanines. The high extinction coefficient could be attributed to

the planarity of these **SBDPiRs** as shown by the X-ray single crystal analysis of the precursor **BDP635**. The optical characteristics validated the rational approach used in the design. The previous D-π-A strategy was adopted displaying absorption spectra with lowest energy absorbing maximally 650 – 840 nm which corresponds to the 0-0 band of $S_o \rightarrow S_1$ (π-π*) transition of the BODIPY framework. The nucleophilic substituted **SBDPiRs** exhibited lowest absorption maxima among the series due to the break in conjugation as a result of the heteroatom (O, S) insertion. The impact of the sulfur heavy atom in **SBDPiR700** gave a pronounced bathochromic shift relative its oxygen analogues. In contrast, the Suzuki and Stille made **SBDPiRs** as a result of uninterrupted conjugation to aromatics (**SBDPiR690**), heteroaromatics (**SBDPiR735**) and aromatics bearing donor moieties such as the 4-methoxyphenyl, 4-hydroxyphenyl and 3,4,5-trimethoxyphenyl (**SBDPiR730**, **SBDPiR731, SBDPiR740**) displayed enhanced red-shift towards NIR absorption. Interestingly, **SBDPiR840** having 4-*N*,*N*-dimethylaminophenyl group as a donor moiety showed a large $S_o \rightarrow S_1$ transition with the lowest energy, presumably, as a result of the intramolecular charge transfer (ICT) imposed by the dimethylaminophenyl substituent, which significantly reduced the HOMO-LUMO gap.

The fluorescence spectra of these **SBDPiRs** showed emission in the NIR from 660 nm to >800 nm making them similar or better than cyanine

dye series which are widely used. The sharp emission bands and almost no spectral overlap with its absorption band as observed (Fig. 23) render these **SBDPiRs** akin to available quantum dots.[88] In addition, possibility of spectral separation puts the **SBDPiRs** in a potential position for use in cellular and in vivo imaging as well as multicolor assays.

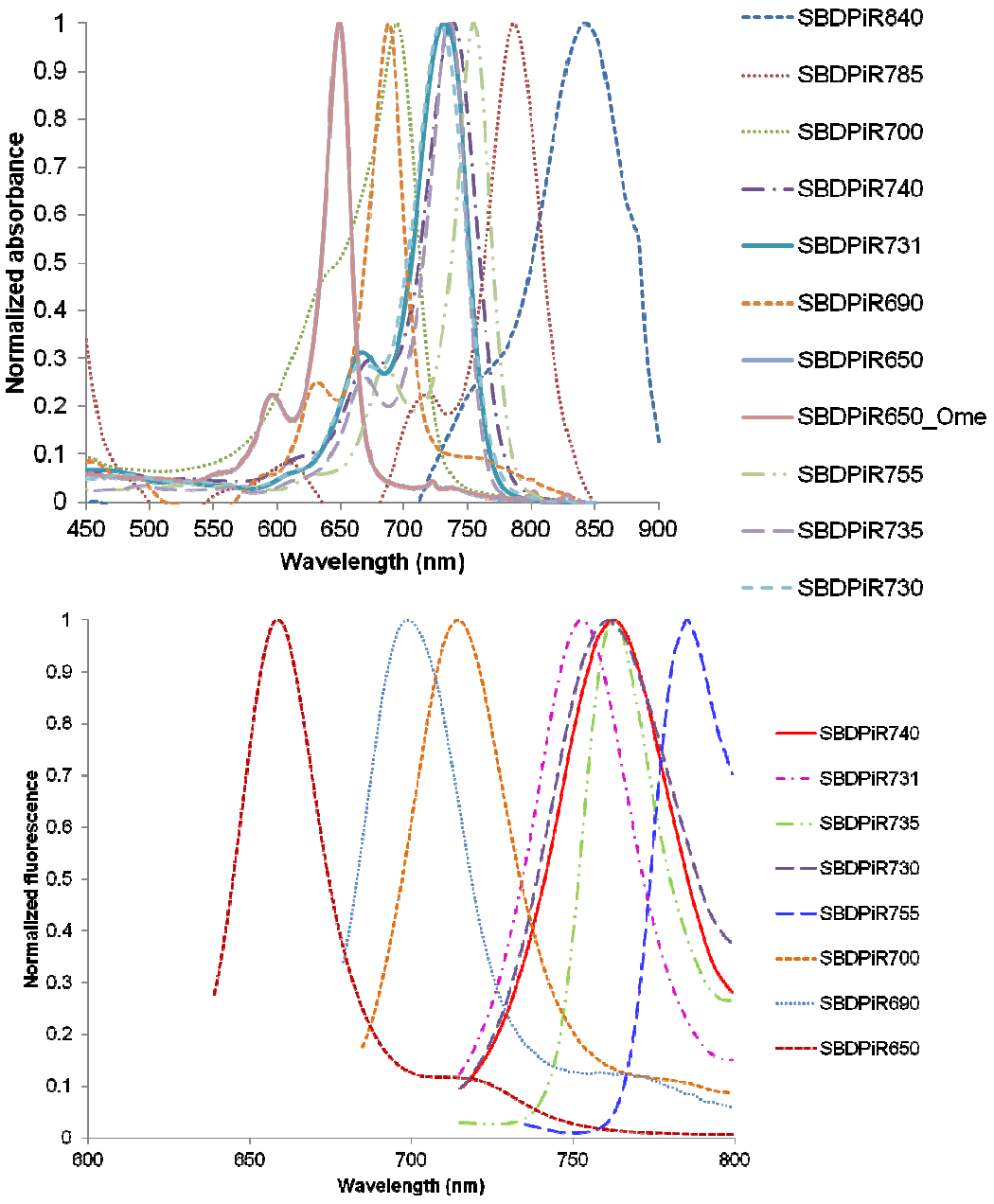

Figure 23. Absorption and emission spectra of **SBDPiRs**

Table 5. Optical properties of **BDP635** and **SBDPiRs**

Dye	λ_{abs}, nm	λ_{flu}, nm	ε, M^{-1} cm^{-1}
BDP	635	650	-
SBDPiR650_OMe	649	660	118 000
SBDPiR650	649	660	83 000
SBDPiR690	688	700	120 000
SBDPiR700	694	715	105 000
SBDPiR730	728	761	140 000
SBDPiR731	731	755	185 000
SBDPiR735	733	763	125 000
SBDPiR740	738	763	101 000
SBDPiR755	753	785	110 000
SBDPiR790	786	-	85 000
SBDPiR840	841	-	-

3.5. *In vivo* imaging with SBDPiR790

3.5.1. Materials and Methods

Female Balb/c mice were purchased from NCI (Federick, MD). Mice were housed and handled in the College of Pharmacy animal facility, University of Oklahoma Health Sciences Center, Oklahoma City, OK. All animal experiments were approved by IACUC, University of Oklahoma

Health Science Center (personal approval was offered). Injection solution of **SBDPiR790** was prepared by solubilizing it in DMSO (4 mM) and then it was diluted with 1 % Tween 80 - 5 % dextrose solution (PBS). The solution was filtered through a 0.2 µm sterile syringe filter before i.p. injection.

BALB/c mice bearing colon-26 cells (mouse colon carcinoma cells) were used for this study. 6-8 week old Balb/c mice were shaved and depilated with hair removal cream (Nair) at the upper back. The mice were subcutaneously inoculated with colon 26 cells at the neck region with 1 x 10^{-6} cells in 0.1 ml PBS solution. Tumors with 4-6 mm diameter size were made in a week. The *in vivo* Xtreme imaging system (Carestream Health, Inc.) was used in acquiring images as mice were kept under safe anaesthesia using Isoflurane. The instrumental conditions for the imaging were as follows: fluorescence mode with excitation 760 nm and emission 830 nm; exposure time 5 sec; F/stop: 2 and pixel 2 x 2. Images collected were then processed using the Carestream MI imaging software to equally adjusted minima and maxima scale.

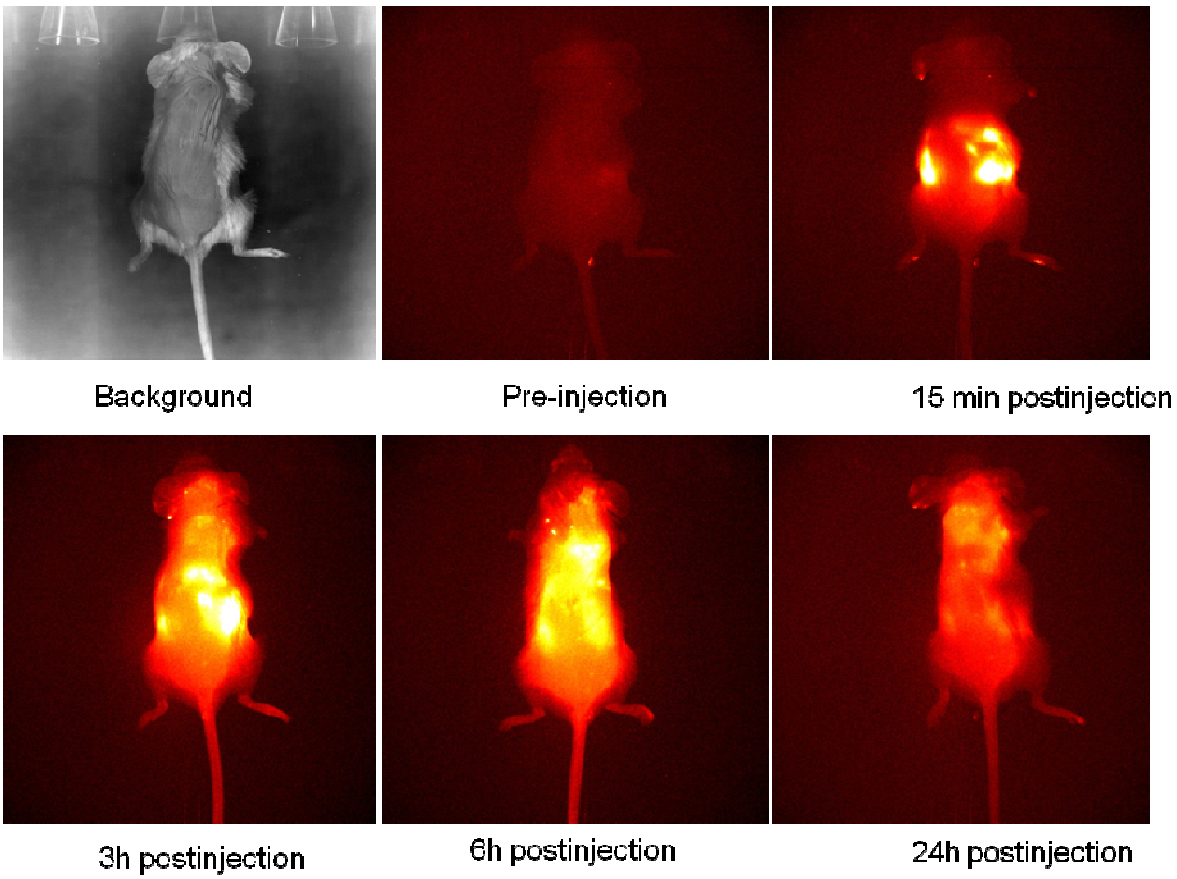

Figure 24. Time dependent *in vivo* images with **SBDPiR790** in BALB/c mice bearing colon-26 tumor

3.5.2. Result and Discussion

All mice received 2.5 μmol/kg of **SBDPiR790** (MW=636.11 g/mol) solution in PBS (0.2 ml) via i.p. injection. Images were taken at 0 (before), 15 min, 3, 6, 24 h post-injection. **SBDPiR790** showed relatively clear images with time-dependent manner (Fig. 24). At 15 min, it seemed the most of the dye still remained in the peritoneal cavity. At 3 h, all skin area showed relatively bright emission with intense bright spots in mid-body (presumably kidney or peritoneal cavity). At 6 h, most of skin area showed

some emission but an intense emission was observed in the tumor area. At 24 h, skin showed lower emission intensity than at 3 and 6 h time points but brighter emission was observed at the tumor site than other body. Even though more thorough examination is needed, these results clearly demonstrated the potential of **SBDPiR790** for NIR in vivo optical imaging. Particularly **SBDPiR790** can be a practical alternative to the sole clinically approved NIR probe, ICG. The stability, and excellent photophysical properties of **SBDPiR790** and its lipophilic character make it useful for varied applications including cancer diagnosis and neurological imaging taking advantage of its ability to cross the blood-brain barrier.

3.6. Conclusion

The synthesis of novel NIR BODIPYs, the **SBDPiRs**, followed a rational approach in their design that was carefully executed. In this strategy, I designed a building block to be used as an intelligent scaffold of which several NIR BODIPY dyes were developed. The building block **BDP635** was designed and synthesized as a reactive brominated fused BODIPY chromophore with absorption in the visible region, λ_{max} = ~635 nm. The BODIPY aryl halide was referred to as ‘versatile’ due to its reactivity towards various palladium catalyzed coupling partners as well as nucleophilic reagents. Using varying coupling partners such as boronic acids, organo tin compounds, and arylvinyl molecules, Suzuki, Stille and

Heck reactions were successfully performed. Moreover, nucleophiles such as substituted phenols and thiophenol worked remarkably well for the nucleophilic substitution reactions. Interestingly, the range of NIR dyes generated possessed characteristics (sharp absorption and emission and high molar extinction coefficient) similar to approved fluorescence dyes with an added advantage of flexible tuning to achieve dyes with absorptivity > 800 nm. In addition, I demonstrated the potential of one of the dyes for *in vivo* optical imaging. I propose this strategy and this class of **SBDPiRs** for use as *in vivo* imaging probes. These could also be further developed as PSs with slight modifications to enhance the intersystem crossing such as bromination and iodination.

3.7. Experimental Section

3.7.1. 2-Bromo-4H-thieno [3, 2-b] pyrrole-5-carboxylic acid (47)*: 46 (0.30 g, 1.1 mmol) was dissolved in EtOH (10 ml). NaOH (0.62 g, 15.5 mmol) in water (4.9 ml) was added and refluxed for 1 h. The reaction was cooled to room temperature and then chilled in an ice bath to acidify the mixture with concentrated HCl. The precipitate was filtered, washed with water and dried under vacuum. A grey solid was obtained (0.22 mg, 70 % [based on ^{1}H-NMR]). ^{1}H-NMR (DMSO-d_6, 300 MHz): δ 12.76 (s, 1H), 12.15 (s, 1H), 7.21 (s, 1H), 6.99 (s, 1H). HRMS ESI (m/z): Calculated for

$C_7H_4BrNO_2S$: 246.0812; found: 246.0833 $[M+H]^+$. *Known with slight modification.

3.7.2. 2,8-Di(bromo)-11-trifluoromethyl-dithieno[2,3-b]-[3,2-g]-5,5-difluoro-5-bora-3a,4a-dithio-s-indacene (BDP635): 47 (1.0 g, 1.8 mmol) was dissolved in TFA (25 ml) and heated to 40 ℃ for 15 min. An intense red color appeared. Trifluoroacetic anhydride (9 ml) was added and the temperature was then raised to 80 ℃ with continued stirring for 4 h. A deep blue color was observed. The reaction solution was allowed to cool and poured into an aqueous $NaHCO_3$ solution with crushed ice. The solution containing precipitates was then filtered and the solid was dried in vacuo. The dry solid was dissolved in CH_2Cl_2 (250 ml) and stirred for 5 min at room temperature under a nitrogen atmosphere. Boron trifluoride dietherate (4 ml) and triethylamine (3 ml) were added and the reaction was stirred at room temperature for 1 h. The reaction solution was passed through a silica gel column using CH_2Cl_2 as eluent. An intense blue solution was obtained as pure compound which appeared as a bluish-green metallic solid (160 mg, 16 % [based on ^{1}H-NMR]). ^{1}H-NMR ($CDCl_3$, 300 MHz): δ 7.31 (s, 2H), 7.24 (s, 2H). HRMS EI (m/z): Calculated for $C_{14}H_4BBr_2F_5N_2S_2$: 529.8200; Found: 529.8170$[M]^+$.

3.7.3. 2,8-Di(4-hydroxyphenyl)-11-trifluoromethyl-dithieno[2,3-b]-[3,2-g]-5,5-difluoro-5-bora-3a,4a-diaza-s-indacene (SBDPiR740): To a 1:1:1 toluene/THF/H_2O solution of **BDP635** (0.19 g, 0.36 mmol) was added 4-

hydroxyboronic acid (0.20 g, 1.43 mmol) and Na_2CO_3 (0.11 g 1.05 mmol). The reaction solution was purged by bubbling nitrogen gas through for 10 min. A catalytic amount of $Pd(PPh_3)_4$ (~5 mol %) was added and the reaction heated to 80 ℃ for 2 h. After completion of the reaction as judged by TLC, the reaction was diluted with 5 ml water and extracted with diethyl ether. The combined organic layer was washed with water and brine and dried over anhydrous Na_2SO_4. The dried mixture was purified by silica-gel column chromatography using ethyl acetate – hexane (50:50) as eluent. A dark green solid was obtained (102 mg, 54 %, [based on ^{1}H-NMR]). ^{1}H-NMR (acetone-d_6, 300 MHz): δ 7.84 (d, J = 9.0 Hz, 4H), 7.52 (s, 2H), 7.37 (s, 2H) 7.03 (d, J = 9.0 Hz, 4H). HRMS EI (m/z): Calculated for $C_{26}H_{14}BF_5N_2O_2S_2$: 556.0510; Found: 556.0520 $[M]^+$.

3.7.4. 2,8-Di(4-methoxyphenyl)-11-trifluoromethyl-dithieno[2,3-b]-[3,2-g]-5,5-difluoro-5-bora-3a,4a-diaza-s-indacene (SBDPiR731): To a 1:1:1 toluene/THF/H_2O solution of **BDP635** (0.10 g, 0.2 mmol) was added 4-methoxyphenylboronic acid (0.12 g, 0.8 mmol) and Na_2CO_3 (0.06 g 0.6 mmol). The reaction solution was purged by bubbling nitrogen gas through for 10 min. A catalytic amount of $Pd(PPh_3)_4$ (~5 mol %) was added and the reaction heated to 80 ℃ for 2 h. After completion of the reaction as judged by TLC, the reaction was diluted with 5 ml water and extracted with diethyl ether. The combined organic layer was washed with water and brine and dried over anhydrous Na_2SO_4. The dried mixture was purified by silica-gel

column chromatography using ethyl acetate – toluene (5:95) as eluent. A dark green solid was obtained (53 mg, 50 % [based on ^{1}H-NMR]). ^{1}H-NMR (CD_2Cl_2, 400 MHz): δ 7.76 (d, *J* = 8.0 Hz, 4H), 7.34 (s, 2H), 7.32 (s, 2H), 7.03 (d, *J* = 8.0 Hz, 4H), 3.91 (s, 6H). HRMS EI (m/z): Calculated for $C_{28}H_{18}BF_5N_2O_2S_2$: 584.0823; Found: 584.0825 $[M]^+$.

3.7.5. 2,8-Di(thiophenyl)-11-trifluoromethyl-dithieno[2,3-b]-[3,2-g]-5,5-difluoro-5-bora-3a,4a-diaza-s-indacene (SBDPiR735): To a 1:1:1 toluene/THF/H_2O solution of **BDP635** (0.10 g, 0.2 mmol) was added 2-thiopheneboronic acid (0.10 g, 0.8 mmol) and Na_2CO_3 (0.06 g 0.6 mmol). The reaction solution was purged by bubbling nitrogen gas through for 10 min. A catalytic amount of $Pd(PPh_3)_4$ (~5 mol %) was added and the reaction heated to 80 ℃ for 30 min. After completion of the reaction as judged by TLC, the reaction was diluted with 5 ml water and extracted with diethyl ether. The combined organic layer was washed with water and brine and dried over anhydrous Na_2SO_4. The dried mixture was purified by silica-gel column chromatography using ethyl acetate – toluene (5:95) as eluent. A dark green solid was obtained (51 mg, 50 % [based on ^{1}H-NMR]). ^{1}H-NMR (CD_2Cl_2, 300 MHz): δ 7.24 (m, 2H), 7.53 (s, 2H), 7.54 (s, 2H), 7.34 (s, 2H), 7.57 (m, 4H). HRMS EI (m/z): Calculated for $C_{22}H_{10}BF_5N_2S_4$: 535.9740; Found: 535.9725 $[M]^+$.

3.7.6. 2,8-Di(3,4,5-trimethoxyphenyl)-11-trifluoromethyl-dithieno[2,3-b]-[3,2-g]-5,5-difluoro-5-bora-3a,4a-diaza-s-indacene (SBDPiR730): To a

1:1:1 toluene/THF/H_2O solution of **BDP635** (0.12 g, 0.2 mmol) was added 3,4,5-trimethoxyphenylboronic acid (0.19 g, 0.9 mmol) and Na_2CO_3 (0.07 g 0.7 mmol). The reaction solution was purged by bubbling nitrogen gas through for 10 min. A catalytic amount of $Pd(PPh_3)_4$ (~10 mol %) was added and the reaction heated to 80 ℃ for 1 h. After completion of the reaction as judged by TLC, the reaction solution was diluted with 10 ml toluene and the water layer separated. The organic layer was washed with water and brine and dried over anhydrous Na_2SO_4. The dried mixture was purified by silica-gel column chromatography using ethyl acetate – toluene (5:95) as eluent. A dark green solid was obtained (54 mg, 45 % [based on ^{1}H-NMR]). ^{1}H-NMR (CD_2Cl_2, 300 MHz): δ 7.36 (s, 2H), 7.32 (s, 2H), 6.98 (s, 4H), 3.93 (s, 12H), 3.87 (s, 6H). HRMS EI (m/z): Calculated for $C_{32}H_{26}BF_5N_2O_6S_2$: 704.1245, Found: 704.1226 $[M]^+$.

3.7.7. 2,8-Di(4-N,N,dimethylaminophenyl)-11-trifluoromethyl-dithieno[2,3-b]-[3,2-g]-5,5-difluoro-5-bora-3a,4a-diaza-s-indacene (SBDPiR840):

To a 1:1:1 toluene/THF/H_2O solution of **BDP635** (0.12 g, 0.2 mmol) was added 4-N,N,dimethylaminophenylboronic acid (0.11 g, 0.7 mmol) and Na_2CO_3 (0.07 g 0.7 mmol). The reaction solution was purged by bubbling nitrogen gas through for 10 min. A catalytic amount of $Pd(PPh_3)_4$ (~10 mol %) was added and the reaction heated to 80 °C for 2 h. After completion of the reaction as judged by TLC, the reaction was diluted with 10 ml toluene and the water layer separated. The organic layer was washed

with water and brine and dried over anhydrous Na_2SO_4. The dried mixture was purified by silica-gel column chromatography using toluene as eluent. A dark green solid was obtained (24 mg, 20 % [based on ^{1}H-NMR]). ^{1}H-NMR (CD_2Cl_2, 300 MHz): δ 7.68 (d, *J* = 6.0 Hz, 4H), 7.37 (s, 2H), 7.34 (s, 2H), 7.40 (d, *J* = 6.0 Hz, 4H), 3.07 (s, 9H), HRMS EI (m/z): Calculated for $C_{30}H_{24}BF_5N_4S_2$: 610.1456, Found: 610.1470 $[M]^+$.

3.7.8. 2,8-Di(styryl)-11-trifluoromethyl-dithieno[2,3-b]-[3,2-g]-5,5-difluoro-5-bora-3a,4a-diaza-s-indacene (SBDPiR755): In a one-neck flask **BDP635** (0.08 g, 0.2 mmol), styrene (0.04 g, 0.4 mmol), $Pd(OAc)_2$ (20 mol %), triphenylphosphine (20 mol %), Na_2CO_3 (0.06 g 0.6 mmol) were dissolved in anhydrous toluene (3 ml). The reaction solution was heated to 80 ℃ with stirring under N_2 (g) for 6 h. After completion (monitored by TLC) the reaction was diluted with 10 ml toluene and washed with water and brine and dried over anhydrous Na_2SO_4. The dried mixture was purified by silica-gel column chromatography using toluene as eluent. A black solid was obtained (17 mg, 22 % [based on ^{1}H-NMR]). ^{1}H-NMR (CD_2Cl_2, 300 MHz): δ 7.59 (d, *J* = 8.0 Hz, 4H), 7.39 (d, *J* = 8.0 Hz, 4H), 7.26 (s, 3H), 7.20 (s, 1H), 7.12 (s, 2H). HRMS EI (m/z): Calculated for $C_{30}H_{18}BF_5N_2S_2$: 576.0925; Found: 576.0906 $[M]^+$.

3.7.9. 2,8-Di(4-(methoxy-phenyl)vinyl)-11-trifluoromethyl-dithieno[2,3-b]-[3,2-g]-5,5-difluoro-5-bora-3a,4a-diaza-s-indacene (SBDPiR790): In a one-neck flask **BDP635** (0.08 g, 0.2 mmol), 4-methoxystyrene (0.04 g, 0.4

mmol), $Pd(OAc)_2$ (20 mol %), triphenylphosphine (20 mol %), Na_2CO_3 (0.06 g 0.6mmol) were dissolved in anhydrous toluene (3 ml). The reaction solution was heated to 80 ℃ with stirring under N_2 (g) for 6 h. After completion (monitored by TLC) the reaction was diluted with 10 ml toluene and washed with water and brine and dried over anhydrous Na_2SO_4. The dried mixture was purified by silica-gel column chromatography using toluene as eluent. A dark brown solid was obtained (20 mg, 25 % [based on ^{1}H-NMR]). ^{1}H-NMR (CD_2Cl_2, 300 MHz): δ 7.44 (d, *J* = 9.0 Hz, 4H), 7.17 (s, 2H), 7.16 (s, 2H), 7.15 (s, 2H), 6.99 (s, 2H), 6.88 (d, *J* = 9.0 Hz, 4H). HRMS EI (m/z): Calculated for $C_{32}H_{22}BF_5N_2O_2S_2$: 636.1136; Found: 636.1120 $[M]^+$.

3.7.10. 2,8-Di(phenyl)-11-trifluoromethyl-dithieno[2,3-b]-[3,2-g]-5,5-difluoro-5-bora-3a,4a-diaza-s-indacene (SBDPiR690): In a one-neck flask **BDP635** (0.03 g, 0.1 mmol), tetraphenyltin (0.03 g, 0.1 mmol), $Pd(OAc)_2$ (20 mol %), triphenylphosphine (20 mol %), Na_2CO_3 (2 ml, 1 M aq.) were dissolved in toluene (3 ml). The reaction solution was heated to 80 ℃ with stirring under N_2 (g) for 1 h. After completion (monitored by TLC) the reaction was diluted with 10 ml toluene and washed with water and brine and dried over anhydrous Na_2SO_4. The dried mixture was purified by silica-gel column chromatography using toluene as eluent. A green solid was obtained (10 mg, 30 % [based on ^{1}H-NMR]). ^{1}H-NMR (CD_2Cl_2, 300 MHz): δ 7.52 (d, *J* = 8.0 Hz, 4H), 7.40 (s, 2H), 7.31 (peaks overlap, 6H),

7.24 (s, 2H). HRMS EI (m/z): Calculated for $C_{26}H_{14}BF_5N_2S_2$: 524.0612; Found: 524.0599 $[M]^+$.

3.7.11. 2,8-Di(thiophenoxy)-11-trifluoromethyl-dithieno[2,3-b]-[3,2-g]-5,5-difluoro-5-bora-3a,4a-diaza-s-indacene (SBDPiR700): BDP635 (0.03 g, 0.06 mmol), thiophenol (0.02 g, 0.14 mmol), and K_2CO_3 (0.02 g, 0.14 mmol) were dissolved in anhydrous CH_3CN (3 ml). The reaction solution was heated to 80 ℃ with stirring under N_2 (g) for 30 min, the reaction turns brick red. After completion (monitored by TLC) the reaction was diluted with 10 ml ether and washed with 1 M Na_2CO_3 (aq.) and dried over anhydrous Na_2SO_4. The dried mixture was purified by silica-gel column chromatography using toluene as eluent. A green solid was obtained (10 mg, 30 % [based on ^{1}H-NMR]). ^{1}H-NMR (CD_2Cl_2, 300 MHz): δ 7.62 (d, J = 6.0 Hz, 4H), 7.47 (d, J = 6.0 Hz, 4H), 7.24 (s, 2H), 7.15 (s, 2H), 6.91 (s, 2H). HRMS EI (m/z): Calculated for $C_{26}H_{14}BF_5N_2S_4$: 588.0053; Found: 588.0037 $[M]^+$.

3.7.12. 2,8-Di(4-methoxyphenoxy)-11-trifluoromethyl-dithieno[2,3-b]-[3,2-g]-5,5-difluoro-5-bora-3a,4a-diaza-s-indacene (SBDPiR650_OMe): BDP635 (0.06 g, 0.1 mmol), 4-methoxyphenol (0.06 g, 0.3 mmol), and K_2CO_3 (0.05 g, 0.4 mmol) were dissolved in anhydrous CH_3CN (3 ml). The reaction solution was heated to 80 ℃ with stirring under N_2 (g) for 30 min. After completion (monitored by TLC) the reaction was dried, dissolved in CH_2Cl_2 and washed with water and brine and dried over anhydrous

Na_2SO_4. The dried mixture was purified by silica-gel column chromatography using hexane as eluent. A blue solid was obtained (15 mg, 25 %, [based on ^{1}H-NMR]). ^{1}H-NMR (CD_2Cl_2, 300 MHz): δ 7.09 (d, *J* = 8.0 Hz, 4H) 7.00 (s, 2H), 6.85 (d, *J* = 8.0 Hz, 4H), 6.21 (s, 2H), 3.77 (s, 6H). HRMS EI (m/z): Calculated for $C_{28}H_{18}BF_5N_2O_4S_2$: 616.0721; Found: 616.0724 $[M]^+$.

3.7.13. 2,8-Di(biphenyl-4-yloxy)-11-trifluoromethyl-dithieno[2,3-b]-[3,2-g]-5,5-difluoro-5-bora-3a,4a-diaza-s-indacene (SBDPiR650): BDP635 (0.06 g, 0.1 mmol), 4-phenylphenol (0.06 g, 0.3 mmol), and K_2CO_3 (0.05 g, 0.4 mmol) were dissolved in anhydrous CH_3CN (3 ml). The reaction solution was heated to 80 ℃ with stirring under N_2 (g) for 30 min. After completion (monitored by TLC) the reaction was diluted with 10 ml toluene and washed with water and brine and dried over anhydrous Na_2SO_4. The dried mixture was purified by silica-gel column chromatography using ethyl acetate – hexane (50:50) as eluent. A reddish-brown solid was obtained (42 mg, 70 % [based on ^{1}H-NMR]). ^{1}H-NMR ($CDCl_3$, 300 MHz): δ 7.52 (m, 3H), 7.49 (m, 5H) 7.43 (m, 5H), 7.30 (d, *J* = 9.0 Hz, 3H), 7.20 (s, 1H), 6.80 (d, *J* = 9.0 Hz, 2H), 6.39 (s, 1H). HRMS EI (m/z): Calculated for $C_{38}H_{22}BF_5N_2O_2S_2$: 708.1136; Found: 708.1121 $[M]^+$.

Chapter 4

Functionalization of NIR BODIPY and Biological Evaluation

4.0. Introduction

Generally, targeted therapies are developed to reduce side effects. For example, the side effects associated with conventional cancer chemotherapy can be reduced by molecular-targeted cancer therapy.[89] The use of molecular probes and photonic agents for in vivo therapy requires high selectivity or specificity to the diseased site. Although second generation fluorescent probes and PDT agents relied on passive targeting of tumor vasculature, not all diseased locations can take advantage of this targeting approach. Moreover, destruction of central tumor vasculature by some second generation PS though effective cannot be used for peripheral vasculature. Active targeting became a useful tool to enhance target specificity. Active targeting involves the covalent conjugation of probes to targeting vectors such as ligands, peptides and antibodies to improve the affinity of these probes to target sites based on corresponding receptors or antigens. Among the several targeted therapies the use of monoclonal antibodies (mAb) has received greatest attention with the FDA approval of ~25 mAb therapeutics.[90, 91]

The conjugation of these targeting biomolecules to PSs or fluorescent probes requires appropriate functional groups on the PS/probes. The

challenges with most NIR absorbing chromophores are high hydrophobicity and limited potential for functionalization. In this chapter, I attempted the functionalization of NIR BODIPYs by 1) meso-functionalized approach and 2) extended functionalization from a modified BODIPY core.

Among the BODIPY analogs, **SBDPiR715** showed excellent photophysical properties, balanced fluorescence emission and effective singlet oxygen generation, as a dual functioning PS for theranostic application (PDD guided PDT). Thus, I performed pilot in vivo studies with **SBDPiR715** to gauge its potential for dual-functioning PS. Indeed, SBDPiR715 showed bright in vivo images and ablation of large tumors. However, since it is highly lipophilic and planar to readily form aggregates, I functionalized **SBDPiR715** with carboxylic acid moieties to increase water solubility and reduce the aggregation tendency. The di-carboxyl group functionalized **SBDPiR715** can also be used for further modifications such as conjugation to delivery vectors via an ester bond.

4.1. Synthesis of Meso-Functionalized NIR BODIPY, 50

The meso-functionalized NIR BODIPY was designed by adding a carboxy phenyl group at the meso position of the thiophene-fused BODIPY core (**50**, Scheme 7). I hypothesized that it would form D-π-A system where 4-methoxyphenyl fragments act as donor moieties to push electrons through the highly conjugated fused BODIPY framework to the carboxy

phenyl group (an acceptor). The synthesis utilized previous approach to build a modified fused pyrrole substrate (Scheme 1). The pyrrole substrate **47** was decarboxylated under thermal, copper catalyzed conditions to obtain free pyrrole at the 2-position. Mono methyl-terephthalate **49** was activated using thionyl chloride to generate a reactive electrophile for condensation with the modified free pyrrole. A subsequent boron chelation step was performed which afforded the target compound **50**.

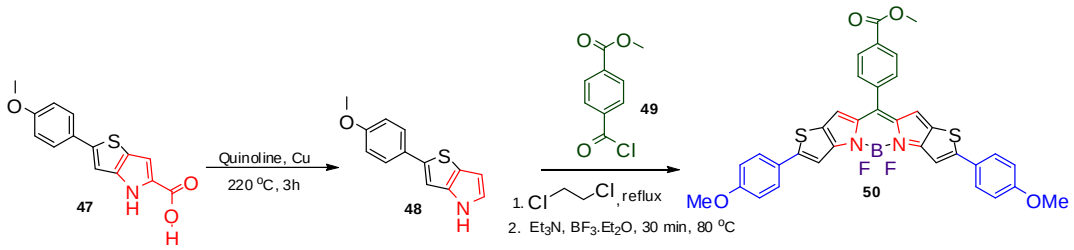

Scheme 7. Synthetic approach for meso-functionalized NIR BODIPY

4.2. Results and Discussion

4.2.1. Synthesis

The synthesis of compound **50** required the preparation of the pyrrole intermediate **48** (scheme 7). The methoxyphenylthienopyrrole, **48** is a new compound and quite challenging to make it in respectable yields. A basic decarboxylation approach using NaOH in ethylene glycol as well as acid promoted decarboxylation with TFA generated very low yields (<10 %). Other decarboxylation methods such as transition-metal catalyzed decarboxylation often used for phenyl-substituted carboxylic acids proved

unsuccessful. However, the use of doubly distilled quinoline and copper (I) oxide at high temperatures of 220 ℃ as reported in literature[92] obtained an improved yield of 40 %. The compound was carefully handled as it was exposed to minimal amount of light. The purification was done using a modified (1 % TEA) silica-gel column chromatography. The final functionalized BODIPY bearing a phenyl carboxylate at the meso-position was achieved by using the reactive 4-chlorocarbonyl-benzoic acid methyl ester (**49**) and the heterocycle (**48**). The reaction followed a synthetic protocol used by Burgess et al. giving similar reaction yields (3 %).[46]

4.2.2. Optical properties

The solution of **50** in $CHCl_3$ gave a vivid bluish-green color. The observation was an account of a strong 0-0 absorption at 685 nm. The molar extinction coefficient was remarkably lower (85 000 $M^{-1}cm^{-1}$) than the CF_3 meso substituted analogues (~200 000 $M^{-1}cm^{-1}$). That could be attributed to the free rotation of the phenyl carboxylate ring at the meso-position to the fluorophore that broke the planarity of the structure. In addition, the free rotation accounts for the relatively low fluorescence.

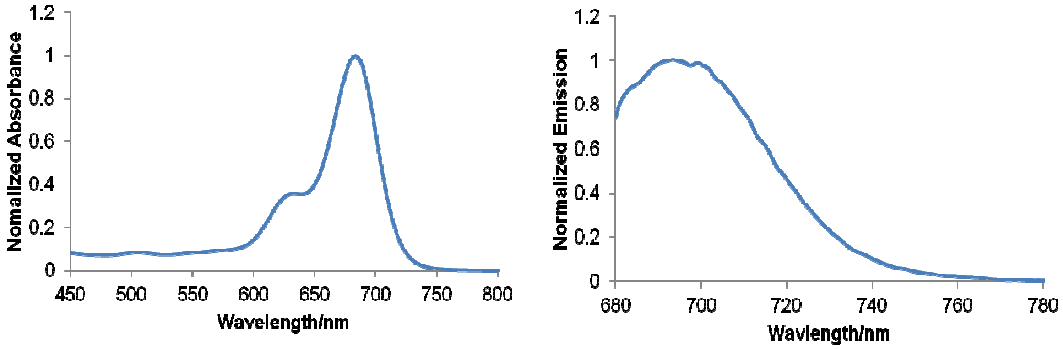

Figure 25. Optical spectra of Meso-functionalized NIR BODIPY, **50**

4.2.3. Theoretical insight

Geometry optimization was performed using the Spartan08 computational suite. The single point energy optimization with a PM3 semi-empirical model in vacuo was utilized. I observed the electron density as reasoned, localized at the donor region, methoxyphenyl group in the HOMO. The effect of the acceptor, phenylcarboxylate, though showed electron pull may be relatively weak. That may account for the shorter absorption wavelength at 685 nm in solution as a result of relatively lower HOMO – LUMO band gap.

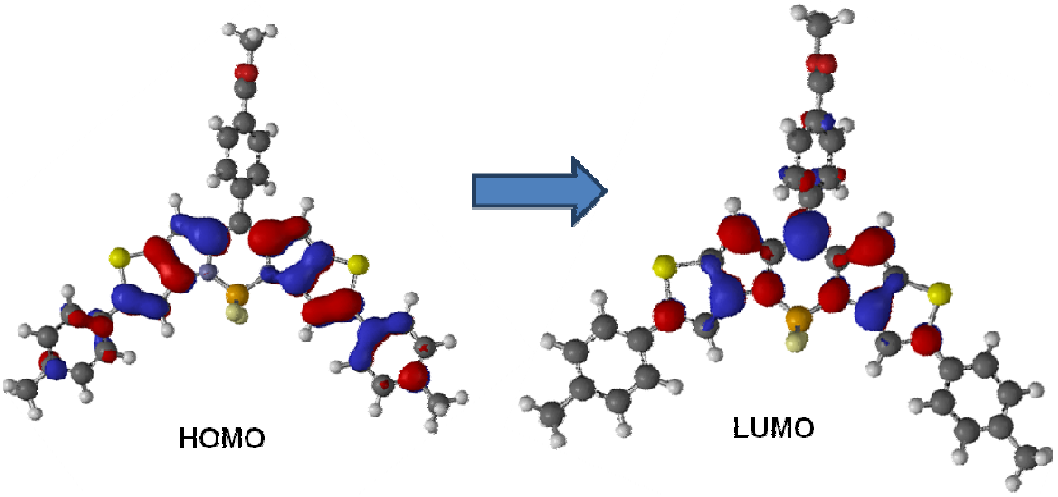

Figure 26. Geometry optimization of meso-functionalized NIR BODIPY, **50**

4.3. Di-carboxylic acid Functionalized SBDPiR

The di-carboxylic acid analog **53** was designed to improve water solubility and to reduce aggregation tendency of highly planar compound. In addition, the carboxylic acid groups could be used for the conjugation to delivery vectors or delivery vehicles. I took advantage of the functional group tolerance of the Suzuki coupling to attach hydroxyl groups as evidenced in **SBDPiR740** (Scheme 8). I furthermore performed a substitution reaction with ethylbromoacetate. To transform the fluorescence dye **51** to dual functioning PS **52**, the BODIPY core was brominated. The synthesis was completed by basic hydrolysis of the ester groups of **52** to obtain free carboxylic acids of **53**.

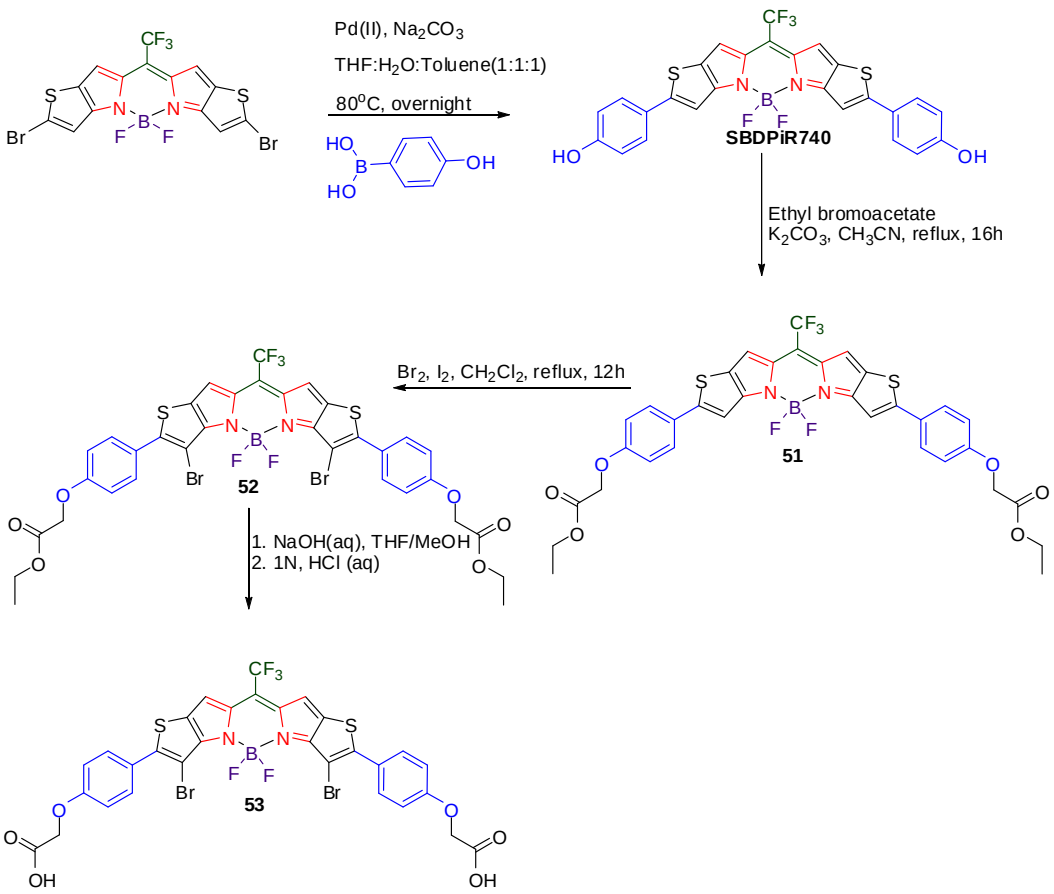

Scheme 8. Synthesis of functionalized NIR BODIPY, **53**

4.4. Results and Discussion

4.4.1. Synthesis

Generating di-carboxylic acid functionalized NIR BODIPY needed a starting material with a functional group. From the earlier synthesis of the SBDPiRs, I used **SBDPiR740** as the starting point, taking advantage of its hydroxyl groups (Scheme 3). I performed O-alkylation via a nucleophilic substitution reaction with ethylbromoacetate in acetonitrile under reflux conditions for 16 h. Surprisingly, acetone did not work as a solvent for the

BODIPY substrate in the current work. I strategically carried out an electrophilic bromination via the established methodology (Scheme 1 in Chapter 2) using bromine and trace iodine in DCM under reflux. The bromination was done before the final step to avoid any interfering reactions with the carboxylic acids of **53**. Basic hydrolysis with 0.2 N NaOH (aq.) in a mixture of THF/MeOH with subsequent reflux afforded the final compound **53** in good yield (60 %). The carboxylic acids at the periphery are platforms for conjugation to targeting vectors. All compounds were purified by silica-gel column chromatography with the exception of **53** (precipitated after acidification) and were characterized by ^{1}H-NMR and EI-HRMS.

4.4.2. Singlet oxygen generation and Photostability.

A singlet oxygen generation experiment on **53** using the indirect method of DPBF photooxidation was performed. There were strong similarities of the behavior of **53** towards DPBF with **41**. In addition, the photostability of **53** showed relatively better than the clinically approved m-THPC (Foscan). It was established that the functionalization of these novel PSs do not affect their excellent photophysical behavior (Fig. 26). The photooxidation of DPBF was monitored by UV-vis spectrophotometer at 410 nm. Within 20 min the oxidation rate compared to that of **41**, indicating that compound **53** is also a potent singlet oxygen generator despite the functionalization. Additionally, less than 30 % of **53** photobleached under

the harsh light illumination condition over a period of an hour, which is a strong evidence for photostability.

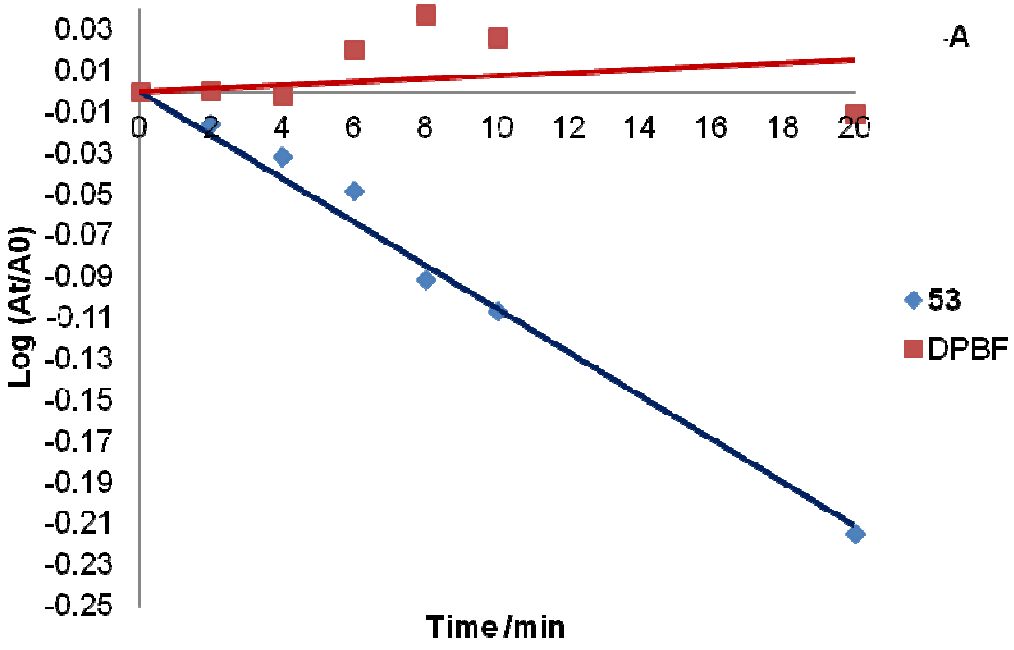

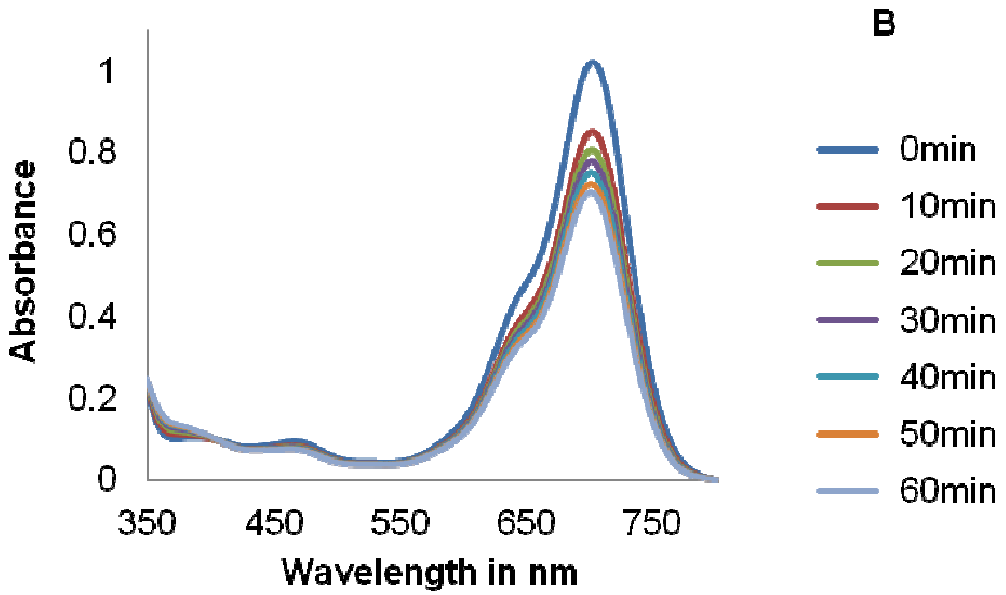

Figure 27. Comparative SO generation by DPBF (**A**) and Photostability (**B**)

4.5. *In Vivo* Optical imaging with 53

Optical imaging was performed with an IVIS Spectrum small-animal *in vivo* imaging system (Caliper LS). The Living Image Software v3.0 (Caliper LS) was used to analyze images and measurements of fluorescent signals. Excitation and emission wavelengths of 720 nm and 760 nm, respectively were used to acquire in vivo fluorescent images of **53** (M.W=830.20 g/mol). All images were attained using a 1-s exposure time and an f/stop of 1, with a sampling of multiple angles with animal under Isoflurane anaesthesia. Animals were injected with 2.5 µmol/kg (2 mg/kg) of **53** via i.p. administration.

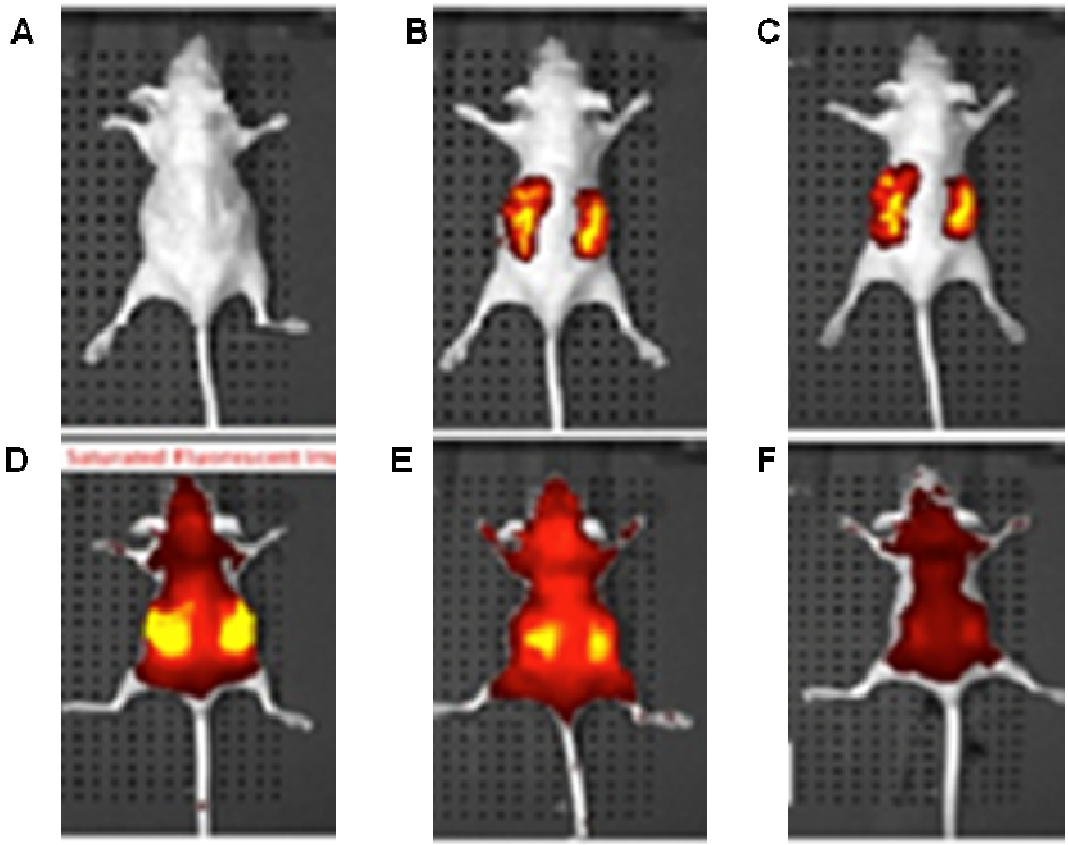

Figure 28. Time-dependant fluorescent images of 53 in nude mouse (from top left: (**A**) 0, (**B**) 5, (**C**) 10 min, (**D**) 3, (**E**) 6, (**F**)12 h after i.p. injection)

The *in vivo* imaging study of **53** proved its potential as an *in vivo* optical imaging probe. Bright fluorescence signal was detected from mouse (Fig. 27). At 5 and 10 min, two bright areas were observed in the mid-body, presumably, due to the PS in peritoneal cavity before absorption to the system (blood). At 3 and 6 h, most skin showed bright emission and two clear bright spots also observed, probably kidneys. At 12 hr, the intensity of

skin was lower than 3 and 6 h images. Most of 53 might be cleared out from the system.

4.6. *In Vivo* Drug Biodistribution and PDT of 41

4.6.1. Materials and Methods

4.6.1.1. PS

To obtain an injection solution of **41**, the emulsifier Tween 80 was used. Tween 80 is a nonionic surfactant, frequently used in vivo as solubilizing agent for highly lipophilic therapeutics. The formulation procedure required dissolving the PS in a minimal amount of Tween 80 (100 µl). The paste was allowed to stand overnight. 5% Dextrose in phosphate-buffered saline (PBS) solution was added and the solution was sonicated for 1 h. The resulting green solution was filtered through a 0.2 µm membrane filter. To ensure the accuracy of the concentration, which might vary due to partial solubility of the PS, the exact concentration was confirmed by UV-visible spectral analysis of the solutions prior to dosing.

4.6.1.2. Cells

Colon-26 mouse carcinoma cells were obtained from the American Type Culture Collection (ATCC) and cultured in minimum essential medium supplemented with 10% (v/v) fetal calf serum (FCS), 50 U ml^{-1} penicillin, 50

µg ml^{-1} streptomycin and 1% (v/v) L-glutamine. The cells were maintained in 5% CO_2 (v/v) and 21% O_2 (v/v) at 37^oC.

4.6.1.3. Animal Models

All animal experiments were approved by IACUC of the University of Oklahoma Health Science Center. Female BALB/c mice were received purchased from Charles River at 6–8 week old. Balb/c mice were shaved on the upper back and depilated with Nair (Carter-Wallace Inc., New York, NY, USA). Mice were anesthetized with an i.p. injection of ketamine/xylazine cocktail (90 mg kg^{-1} ketamine and 10 mg kg^{-1} xylazine). One million colon-26 cells were injected subcutaneously in one dorsal neck area suspended in 100 ml PBS. Tumors grew predictably in all the mice and reached a size of 4- to 6-mm diameter in 5–7 days or 8 – 11 mm in 14 – 16 days after injection, at which time they were used for PDT.

4.6.1.4. Drug efficacy studies: PDT Protocol

Compound **41** in 1% Tween 80 - 5% Dextrose solvent was injected i.p. at a dose of 3 µmol/kg (2.2 mg/kg) and 5 µmol/kg (3.7 mg/kg) in 0.2 ml solution. Tumors were irradiated 6 h, 24 h or 32 h after the injection using a Lumacare LC-122M with a fiber-optic light delivery system (Lumacare, Newport Beach, CA, USA) emitting light at 700 nm (±40 nm). The

illuminating spot had a diameter of 1.2 cm and was positioned so that the entire tumor and a surrounding 2–3 mm area of normal tissue were exposed to light. No evident temperature increase was detected at the site of irradiation. Mice were anesthetized as described above and the tumor-bearing limb positioned under the spot. Total dose of 200 – 300 mW/cm^2 was delivered for 30 min (360 – 540 J cm^{-2}). Mice bearing colon-26 tumors were also irradiated without having received injection of **41**. Another group of animals was treated with **41** i.p. without irradiation. After irradiation, mice were allowed to recover in an animal cotton blanket until they resumed normal activity. A positive tumor response was ascribed to tumors that appeared flat blackened or reddened scarp and necrotic tissue within a few days after PDT. Animals were considered cured after complete tumor regression and the absence of a palpable tumor.

A mass tumor necrosis was observable after a few hours – a day following PDT treatment with the development of necrosis and eschar. Tumor healing however took ~30 days with remodeling of the damaged or scarred tissue. The protocol treated larger tumors (8 - 11 mm diameter) that are rarely used pre-clinically. No weight loss or other visual signs of toxicity was observed at the treatment dose of 5 µmol/kg (3.7 mg/kg). There was no effect on the group treated with light alone.

4.6.1.5. Drug biodistribution

Mice were injected via i.p. with **41** (5 µmol/kg/3.7 mg/kg). After 24 h postinjection, the mice (n=3) were euthanized by CO_2 inhalation. Tissues were excised from major organs and tumor. Collected tissues were rinsed with PBS and blotted dry. One hundred milligram of excised tissue was homogenized with $CHCl_3$ (1 ml). The homogenates were centrifuged at 5160 *g* for 20 min and the supernatant used for fluorescence measurement (excitation at 710 nm and emission at 754 nm). The amount of compound in each sample was evaluated relative to the standard curve and expressed in ‘‘mg/g of tissue’’ unit.

4.7. Results and Discussion

Compound **41**-mediated PDT studies demonstrated under varying drug-light interval of 6 h (n = 3), 24 h (n = 4) and 32 h (n = 3) respectively (Fig. 28) has shown to be an exciting new class of phototherapeutic agent, possessing significant potential for preclinical development. The *in vivo* response to **41** PDT used the colon 26 tumor bearing mice to determine drug-light combination tolerance. I employed two approaches in the treatment; 1) traditional PDT protocol frequently used in our lab with a 24 h drug-light interval with a starting tumor size of ~85 mm^3. 2) Treatment of larger tumor sizes (~650 mm^3) with 6 h and 32 h drug-light interval for preferential drug accumulation at the tumor site.

Within 3 weeks control groups of tumor alone (control, n = 4) and tumor with 24 h drug-light interval (light only, n = 3) reached high tumor volumes at consistent rates. In the same period the treatment groups experienced mass necrosis and eschar within a day. For the 6 and 24 h drug-light interval treatment groups, the observed necrosis spread to neighboring skin regions probably due to **41** in the skin causing skin photosensitization (Fig. 29 and Fig. 30). In the 32 h treatment group there seemed to be a preferential accumulation of the drug in the tumor region leading to a confinement of necrosis to the tumor region (Fig. 31). All the treatment groups showed complete tumor ablation as monitored for 90 days.

In this study I showed compound **41** was well tolerated with high efficacy in vivo employing short to long drug-light intervals. The observed cure in the colon 26 bearing tumor model and in two treatment groups larger than clinical tumor sizes is encouraging. In addition, the in vivo response compares to the well established aza-BODIPY, **ADPM06**,[93] for preclinical indication as well as the vascular targeting TOOKAD developed in 2002 and in current clinical trials for prostate cancer.[94] Compound **41**-mediated PDT showed promise as a useful lead candidate with properties as an ideal second generation PS such as high extinction coefficient (89,000 $M^{-1}cm^{-1}$), good fluorescence property (BT = 40,050 $M^{-1}cm^{-1}$) valuable for imaging. The dual functioning ability of compound **41** as a diagnostic and therapeutic agent and its high photostability places it ahead

of almost all the clinically approved agents such as Photofrin (630 nm, ε 1,170 $M^{-1}cm^{-1}$), a non-single compound and Foscan (650 nm, ε 39,000 $M^{-1}cm^{-1}$) in current clinical use for superficial malignancies. I also demonstrated the use of compound **41**-mediated PDT for treatment of larger tumors of volume ~650 mm^3, taking advantage of its NIR excitability. The hydrophobic nature of **41** poses a disadvantage as its clearance from biological systems may be delayed. Approaches to functionalize compound **41** with water solubilizing groups such as carboxylic acids, sulfonate groups may be a useful venture.

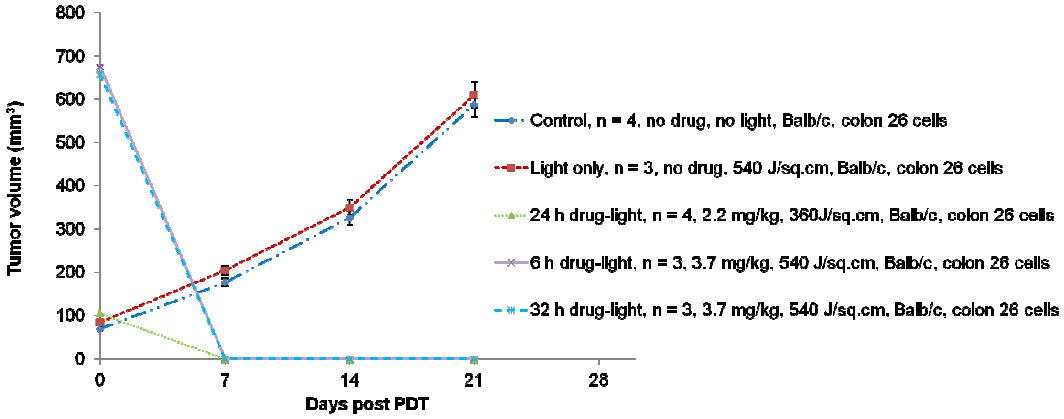

Figure 29. *In vivo* response to Compound **41**-mediated PDT (*standard error of mean used*)

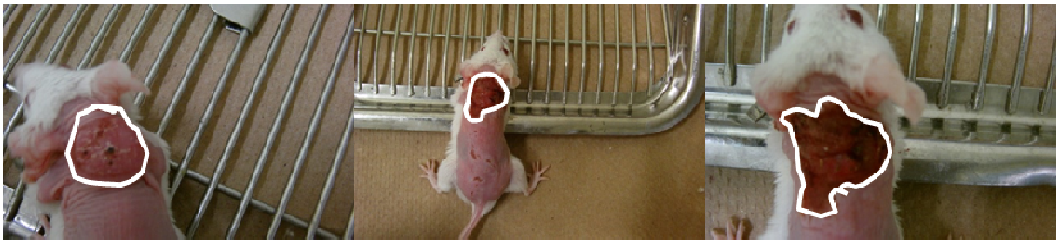

Figure 30. *In vivo* response to **41**-mediated PDT at 6 h drug-light interval *(white line → tumor [untreated] and necrotic [treated] boundary)*

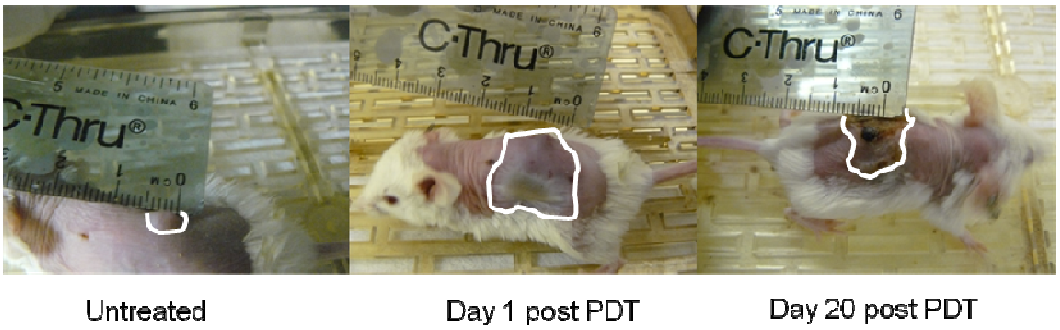

Figure 31. *In vivo* response to **41**-mediated PDT at 24 h drug-light interval *(white line → tumor [untreated] and necrotic [treated] boundary)*

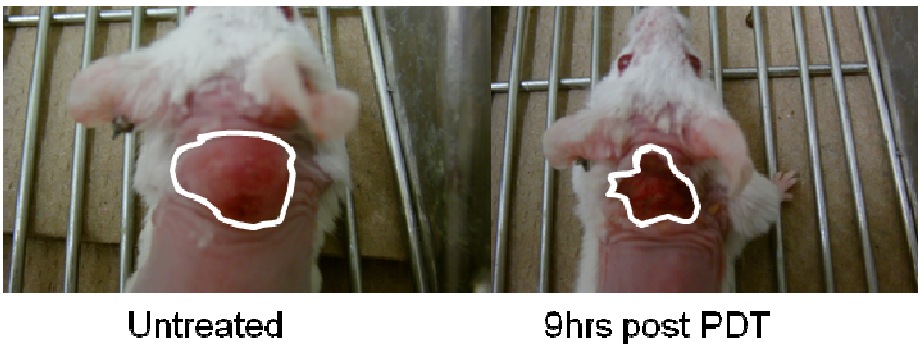

Figure 32. *In vivo* response to **41**-mediated PDT at 32 h drug-light interval *(white line → tumor [untreated] and necrotic [treated] boundary)*

I also showed that **41** has an organ biodistribution pattern (Fig. 32) consistent with a wide range of PSs.[95] The innate fluorescence property of **41** enabled its biodistribution in various organs after systemic delivery intraperitoneally. In the biodistribution study, I observed a higher accumulation of **41** in the liver and spleen. The observation might be as a result of the general knowledge of hydrophobic agent's elimination from an organism through the bile-gut pathway. I also speculated that the high content of LDL receptors in the liver, spleen and kidney might influence the result as **41** is hydrophobic. Contrary to my expectation, I observed slightly higher PS localization in the skin over tumor.

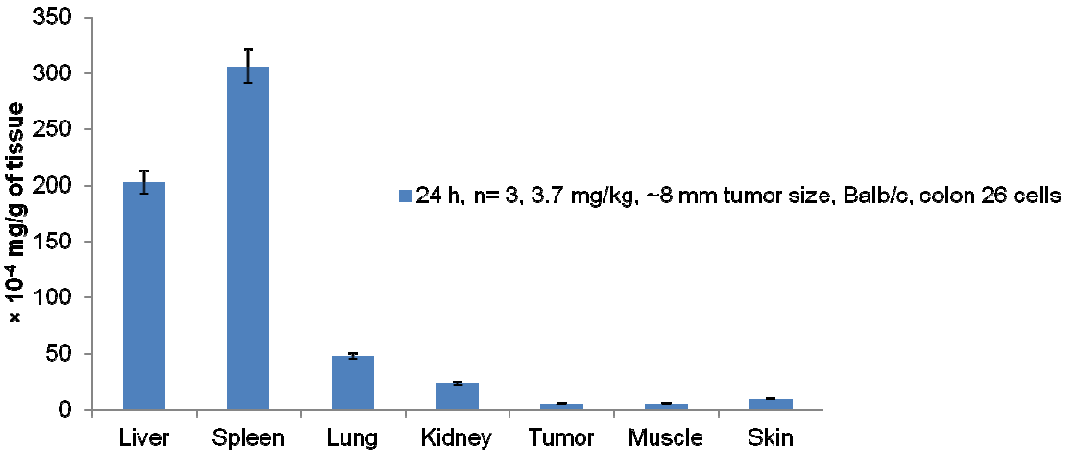

Figure 33. Time-dependant biodistribution of **41** in organs (*Standard deviation used*).

4.8. Conclusion

In this chapter, I demonstrated the ability to functionalize the NIR BODIPY by facile synthetic methods without compromising the excellent photophysical properties they possess. I performed meso-functionalization on the thieno fused BODIPY core to obtain compound **50**. Its optical properties after characterization looked great but suffered from a low yield from the condensation step. Furthermore, I show the biological applicability of these NIR dyes in vivo; both as an imaging agent and as therapeutic agent. Compound **41** showed severe necrosis and extreme tumor ablation with high cure rates monitored over a 90 day period. Compound **41** and its functionalized form, **53** possess an inherent fluorescent ability useful for dual application of diagnosis and therapy. Based on the study I propose **41** as a viable theranostic candidate for tumor visualization (diagnosis) and treatment (therapy).

4.9. Experimental Section

4.9.1. 2-(4-Methoxy-phenyl)-4H-thieno[3,2-b]pyrrole (48): 2-(4-Methoxy-phenyl)-4H-thieno[3,2-b]pyrrole-5-carboxylic acid (0.50 g, 1.8 mmol), Cu powder (0.18 g, 1.3 mmol) was dissolved in doubly distilled quinoline (10 ml) and refluxed at 220 ℃ for 3 h. The reaction mix ture was cooled to room temperature and the copper filtered out. The filtrate was poured into cold water and acidified with 2 N HCl to pH 4. The solution was extracted with

ethyl acetate, washed with 10 % HCl, 10 % $NaHCO_3$, brine and water. The solution was dried over anhydrous Na_2SO_4 and evaporated to dryness. The mixture was purified by silica-gel column modified with 1 % triethylamine using CH_2Cl_2 as eluent to afford a yellowish-grey solid (164 mg, 40 % [based on ^{1}H-NMR]). ^{1}H-NMR (CD_2Cl_2, 300 MHz): δ 8.5 (bs, 1H), 7.57 (d, *J* = 9.0 Hz, 2H), 7.18 (s, 1H), 6.87 (d, *J* = 9.0 Hz, 2H), 3.89 (s, 3H) HRMS EI (*m/z*): Calculated for $C_{13}H_{11}NOS$: 229.0561; found: 229.0532 $[M]^+$

4.9.2. 4-Chlorocarbonyl-benzoic acid methyl ester (49)*:[96] Terephthalic acid monomethyl ester (0.25 g, 1.4 mmol) was dissolved in thionyl chloride (5 ml) and refluxed for 1 h. Excess thionyl chloride was removed in vacuo to give an off-white solid. The solid was dissolved in anhydrous benzene (7 ml) and the solvent evaporated. The procedure was repeated 3 times and the solid dried at high temperatures to remove residual solvent. 273 mg was obtained at 93 % yield. *Known

4.9.3. 2,8-Di(4-Methoxy-phenyl)-11-benzoic acid methyl ester-dithieno[2,3-b]-[3,2-g]-5,5-difluoro-5-bora-3a,4a-diaza-s-indacene (50): **48** (0.16 g, 0.7 mmol) and **49** (0.07 g, 0.4 mmol) were dissolved in 1,2-dichloroethane and the solution was refluxed for 72 h. The solution was cooled to room temperature and TEA and boron trifluoride etherate was added. The mixture was refluxed for 30 min. under He (g) atmosphere. The solution was washed with water and brine and the residue was purified by silica-gel column chromatography using ethyl acetate – toluene (5:95) as

eluent. A green solid was obtained (5 mg, 3%, [based on ^{1}H-NMR]). ^{1}H-NMR ($CDCl_3$, 300 MHz): δ 8.12 (d, *J* = 9.0 Hz, 2H), 7.60 (d, *J* = 9.0 Hz, 4H), 7.44 (d, *J* = 9.0 Hz, 2H), 7.41 (s, 2H), 6.88 (d, *J* = 9.0 Hz, 4H), 6.67 (s, 2H), 3.80 (s, 3H), 3.92 (s, 6H). HRMS EI (*m/z*): Calculated for $C_{35}H_{25}BF_2N_2O_4S_2$: 650.1317; found: 650.1321 $[M]^+$.

4.9.4. 2,8-Di(4-Ethoxycarbonylmethoxy-phenyl)-11-trifluoromethyl-dithieno[2,3-b]-[3,2-g]-5,5-difluoro-5-bora-3a,4a-diaza-s-indacene (51): SBDPiR740 (0.10 g, 0.2 mmol), ethylbromoacetate (0.12 g, 0.7 mmol) and K_2CO_3 (0.05, 0.4 mmol) were dissolved in anhydrous CH_3CN under N_2 atmosphere. The solution was heated at 80 ℃ for 16 h. After the complete consumption of the starting material (monitored by TLC), the reaction was stopped. The solvent was removed and the residue was dissolved in CH_2Cl_2. The resulting solution was washed with water and dried over anhydrous Na_2SO_4. The mixture was purified by recrystallization from ethyl acetate/cyclohexane mixture to afford a green solid (91 mg, 70 % [based on ^{1}H-NMR]). ^{1}H-NMR ($CDCl_3$, 300 MHz) δ: 7.67(d, *J* = 9.0 Hz, 4H), 7.48 (s, 2H), 7.32 (s, 2H), 6.97 (d, *J* = 9.0 Hz, 4H), 4.70 (s, 4H), 4.27 (q, *J* = 7.1 Hz, 4H), 1.30 (t, *J* = 7.1 Hz, 6H) HRMS EI (*m/z*): Calculated for $C_{34}H_{24}BBr_2F_5N_2O_6S_2$: 728.1245; found: 728.1227 $[M]^+$

4.9.5. 3,7-Dibromo-2,8-di(4-Ethoxycarbonylmethoxy-phenyl)-11-trifluoromethyl-dithieno[2,3-b]-[3,2-g]-5,5-difluoro-5-bora-3a,4a-diaza-

s-indacene (52): 51 (0.07 g, 0.1 mmol) along with I_2 (0.001 g) was dissolved in CH_2Cl_2 (15 ml). A solution of Br_2 (0.04 g, 0.3 mmol) in CH_2Cl_2 (5 ml) was added dropwise and stirred at 40 ℃ for 12 h. The reaction mixture was neutralized with aqueous Na_2CO_3 solution and the aqueous layer was separated from the organic layer. The aqueous layer was further extracted with diethyl ether and the combined organic layers were dried over anhydrous Na_2SO_4 and the solvents removed by evaporation to obtain a brown solid (40 mg, 52 % [based on ^{1}H-NMR]). ^{1}H-NMR (CD_2Cl_2, 300 MHz) δ: 7.73 (d, J = 9.0 Hz, 4H), 7.40 (s, 2H), 7.01 (d, J = 9.0 Hz, 4H), 4.70 (s, 4H), 4.25 (q, J = 7.1 Hz, 4H), 1.30 (t, J = 7.1 Hz, 6H) HRMS EI (*m/z*): Calculated for $C_{34}H_{24}BBr_2F_5N_2O_6S_2$: 885.9435; found: 885.9419 $[M]^+$.

4.9.6. 3,7-Dibromo-2,8-di(4-Carboxymethoxy-phenyl)-11-trifluoromethyl-dithieno[2,3-b]-[3,2-g]-5,5-difluoro-5-bora-3a,4a-diaza-s-indacene (53): 52 (0.04 g, 0.04 mmol) was dissolved in a 1:1 mixture of THF/MeOH and 0.4 N NaOH (aq.) was added. The reaction was refluxed for 2 h. The THF/MeOH was removed under vacuum and diluted with water and acidified with 1N HCl. The precipitate was filtered and dried (23 mg, 63 % [based on ^{1}H-NMR]). ^{1}H-NMR (CD_2Cl_2, 300 MHz) δ: 7.73 (d, J = 9.0 Hz, 4H), 7.40 (s, 2H), 7.01 (d, J = 9.0 Hz, 4H), 4.70 (s, 4H) HRMS EI (*m/z*): Calculated for $C_{34}H_{24}BBr_2F_5N_2O_6S_2$: 829.8809; found: 829.8819 $[M]^+$.

Chapter 5

Conclusion and Perspective

The non-invasive diagnosis and therapy of disease indications with light is an emerging modality. In vivo preclinical and clinical applications underscore the usefulness of fluorescence imaging and PDT in establishing reliable prognosis and disease treatment, particularly for cancer and other malignancies. To further the course of these modalities efficient NIR absorbing fluorophores and PSs are needed. More specifically, dyes absorbing >700 nm with inherent excellent photophysical properties is a requisite. These properties should include: 1) high photostability, 2) sharp absorption and emission bands, 3) high molar extinction coefficient, 4) appreciable fluorescence quantum yield/ singlet oxygen quantum yield, and 5) potential for functionalization. Since current clinically approved PSs for PDT lack absorption in the region >700 nm and only one NIR fluorescence dye is FDA approved, it is obvious that the search for efficient, NIR PS and alternative NIR fluorophores is a necessity.

In this dissertation, I focused mainly on the design and synthesis of NIR BODIPY dyes to: 1) provide improved photodynamic response and 2) generate efficient fluorophores for fluorescence imaging. I took advantage of ring fusion to the BODIPY core as a unique synthetic strategy as well as

D-π-A systems and the incorporation of heavy atoms such as, sulfur, and bromine to establish unprecedented longer wavelength dyes in these BODIPY analogues. The established synthetic protocol is robust and versatile, offering a facile and flexible approach to customizable NIR BODIPYs for variegated research. The biological function of these novel classes of NIR BODIPY was explored for in vivo photodynamic response to ablate tumors and in vivo optical imaging for monitoring and diagnosis.

In the first part of this dissertation, I demonstrated that fusing of a thiophene fragment to the BODIPY core as well as electrophilic substitution with bromine would induce intersystem crossing leading to singlet oxygen generation as well as impart red shift towards NIR. I successfully built the thieno-fused BODIPY unit following the D-π-A system along with its furo-fused analogues and additionally incorporated the bromine atoms for singlet oxygen generation. All the analogues showed strong absorption in the NIR from 720 – 766 nm in $CHCl_3$ and strong emission of 738 – 820 nm. The sulfur containing analogues showed appreciable singlet oxygen generation comparable to the core-modified porphyrins, which is a well studied class of chromophores in our research group. Photobleaching kinetics showed the high photostability of these NIR BODIPYs in comparison to m-THPC (clinically approved PDT agent) and its NIR analogue m-THPBC. In this work, a lead candidate was obtained with appreciable fluorescence

quantum yield. I therefore, propose the candidate as a dual-functional agent for PDT and diagnosis or better still for fluorescence-guided PDT.

Secondly, I aimed at developing NIR fluorescent probes and PDT agents with a propensity towards functionalization. The search led to the design of a robust but versatile synthetic procedure relying on the synthesis of a BODIPY alkyl halide absorbing in the visible region and reactive towards nucleophilic substitution and transition-metal catalyzed chemical transformation with aryl moieties. I successfully synthesized the SBDPiRs with sterling optical absorption in the NIR from 650 – 840 nm. I used the nucleophilic substitution of substituted phenols and thiophenols to generate SBDPiRs with excitability 650 – 700 nm. Suzuki and Stille coupling was used to generate SBDPiRs with excitability 688 – 740 nm and the Heck coupling was used to obtain SBDPiRs with 755 – 786 nm excitability. The study indicated a viable alternative to the cynanines and phthalocynines with the NIR absorption and high molar extinction coefficient of the SBDPiRs.

Finally, I demonstrated the functionalization of these NIR BODIPY and their biological application as photodynamic agents and fluorescence imaging probes. I synthesized functional NIR BODIPY fluorophore bearing a carboxylate moiety at the meso-position in mimicking the D-π-A system

(compound **50**). In addition, a PDT agent bearing free-carboxylic acid units was synthesized and its potential for in vivo imaging was explored using Balb/c mice at a therapeutic dose of 2.5 µmol/kg (2 mg/kg). The drug biodistribution of a lead candidate was performed and this established the lipophilic nature of the drug as localization in the skin was higher relative to the tumor after 24 h. I used an established PDT protocol to show complete tumor ablation with varying drug-light interval after intra-peritoneal delivery of drug. A 6 h and 24 h drug-light interval showed skin phototoxicity while a 32 h drug light interval showed no skin photosensitization. This drug displayed intense fluorescent signals in an in vivo imaging setup, confirming our earlier assertion.

Overall, these studies push the boundaries for the search of effective NIR photodynamic agents and fluorescent probes for improved photodynamic response and fluorescence imaging in vivo. Our design and synthesis strategy would be useful to obtain functional NIR BODIPYs for the described applications.

References

1. Awuah, S.G. & You, Y. Boron dipyrromethene (BODIPY)-based photosensitizers for photodynamic therapy. *RSC Adv.* **2**, 11169-11183 (2012).

2. Weissleder, R. A clearer vision for in vivo imaging. *Nat. Biotechnol.* **19**, 316-317 (2001).

3. Plaetzer, K., Krammer, B., Berlanda, J., Berr, F. & Kiesslich, T. Photophysics and photochemistry of photodynamic therapy: fundamental aspects. *Laser Med. Sci.* **24**, 259-268 (2009).

4. Foote, C.S. Definition of type I and type II photosensitized oxidation. *Photochem. Photobiol.* **54**, 659 (1991).

5. Brancaleon, L. & Moseley, H. Laser and non-laser light sources for photodynamic therapy. *Laser Med. Sci.* **17**, 173-186 (2002).

6. Mang, T.S. Lasers and light sources for PDT: past, present and future. *Photodiagn. Photodyn. Ther.* **1**, 43-48 (2004).

7. Juzeniene, A., Peng, Q. & Moan, J. Milestones in the development of photodynamic therapy and fluorescence diagnosis. *Photochem. Photobiol. Sci.* **6**, 1234-1245 (2007).

8. Weishaupt, K.R., Gomer, C.J. & Dougherty, T.J. Identification of singlet oxygen as the cytotoxic agent in photoinactivation of a murine tumor. *Cancer Res.* **36**, 2326-2329 (1976).

9. Moan, J. & Sommer, S. Oxygen dependence of the photosensitizing effect of hematoporphyrin derivative in NHIK 3025 cells. *Cancer Res.* **45**, 1608-1610 (1985).

10. Pass, H.I. Photodynamic therapy in oncology: mechanisms and clinical use. *J. Nat. Cancer Inst.* **85**, 443-456 (1993).

11. Henderson, B.W. & Dougherty, T.J. How does photodynamic therapy work? *Photochem. Photobiol.* **55**, 145-157 (1992).

12. DeRosa, M.C. & Crutchley, R.J. Photosensitized singlet oxygen and its applications. *Coord. Chem. Rev.* **233–234**, 351-371 (2002).

13. Schmidt, R. Photosensitized Generation of Singlet Oxygen. *Photochem. Photobiol.* **82**, 1161-1177 (2006).

14. Montalti, M. & Murov, S.L. Handbook of photochemistry. (CRC/Taylor & Francis, Boca Raton; 2006).

15. Brown, J.M. & Wilson, W.R. Exploiting tumour hypoxia in cancer treatment. *Nat. Rev. Cancer.* **4**, 437-447 (2004).

16. Moan, J. On the diffusion length of singlet oxygen in cells and tissues. *J. Photochem. Photobiol. B: Biology* **6**, 343-344 (1990).

17. Kuimova, M.K., Yahioglu, G. & Ogilby, P.R. Singlet oxygen in a cell: spatially dependent lifetimes and quenching rate constants. *J. Am. Chem. Soc.* **131**, 332-340 (2009).

18. Niedre, M., Patterson, M.S. & Wilson, B.C. Direct Near-infrared Luminescence Detection of Singlet Oxygen Generated by Photodynamic Therapy in Cells In Vitro and Tissues In Vivo. *Photochem. Photobiol.* **75**, 382-391 (2002).

19. Wilkinson, F., Helman, W.P. & Ross, A.B. Rate constants for the decay and reactions of the lowest electronically excited singlet-state of molecular-oxygen in solution - an expanded and revised compilation. *J. Phys. Chem. Ref. Data* **24**, 663-1021 (1995).

20. Wilkinson, F., Helman, W.P. & Ross, A.B. Quantum yields for the photosensitized formation of the lowest electronically excited singlet-state of molecular-oxygen in solution. *J. Phys. Chem. Ref. Data* **22**, 113-262 (1993).

21. von Tappeiner, H. & Jesionek, A. Therapeutische versuche mit fluoreszierenden stoffen. *Muenche Med. Wochenschr.* **47**, 2042-2044 (1903).

22. v. Tappeiner, H. Die photodynamische Erscheinung (Sensibilisierung durch fluoreszierende Stoffe). *Ergebnisse der Physiologie, biologischen Chemie und experimentellen Pharmakologie* **8**, 698-741 (1909).

23. Policard, A. A study on the available aspects of experimental tumours examined by Wood's light. *Cr. Soc. Biol.* **91**, 1423-1424 (1924).

24. Lipson, R.L. & Baldes, E.J. The photodynamic properties of a particular hematoporphyrin derivative. *Arch. Dermatol.* **82**, 508-516 (1960).

25. Lipson, R.L., Baldes, E.J. & Olsen, A.M. The use of a derivative of hematoporhyrin in tumor detection. *J. Natl. Cancer Inst.* **26**, 1-11 (1961).

26. Lipson, R.L., Baldes, E.J. & Olsen, A.M. Hematoporphyrin derivative: a new aid for endoscopic detection of malignant disease. *J. Thorac. Cardiovasc. Surg.* **42**, 623-629 (1961).

27. Lipson, R.L., Baldes, E.J. & Gray, M.J. Hematoporphyrin derivative for detection and management of cancer. *Cancer* **20**, 2255-2257 (1967).

28. Lipson, R.L., Baldes, E.J. & Olsen, A.M. Further Evaluation of the Use of Hematoporphyrin Derivative as a New Aid for the Endoscopic Detection of Malignant Disease. *Dis. Chest.* **46**, 676-679 (1964).

29. Auler, H. & Banzer, G. Untersuchungen uber die Rolle der Porphyrine beigeschwulstkranken Menschen und Tieren. *Z. Krebsforsch.* **53**, 65-68 (1942).

30. Dougherty, T.J., Grindey, G.B., Fiel, R., Weishaupt, K.R. & Boyle, D.G. Photoradiation therapy. II. Cure of animal tumors with hematoporphyrin and light. *J. Natl. Cancer Inst.* **55**, 115-121 (1975).

31. Kelly, J.F. Haematoporphyrins in the diagnosis and treatment of carcinoma of the bladder. *Proc. R. Soc. Med.* **68**, 527-528 (1975).

32. Kelly, J.F., Snell, M.E. & Berenbaum, M.C. Photodynamic destruction of human bladder carcinoma. *Br. J. Cancer* **31**, 237-244 (1975).

33. Agostinis, P. et al. Photodynamic Therapy of Cancer: An Update. *Ca-Cancer J. Clin.* **61**, 250-281 (2011).

34. Kosaka, N., Ogawa, M., Choyke, P.L. & Kobayashi, H. Clinical implications of near-infrared fluorescence imaging in cancer. *Future Oncol.* **5**, 1501-1511 (2009).

35. Kosaka, N., Mitsunaga, M., Longmire, M.R., Choyke, P.L. & Kobayashi, H. Near infrared fluorescence-guided real-time endoscopic detection of peritoneal ovarian cancer nodules using intravenously injected indocyanine green. *Int. J. Cancer* **129**, 1671-1677 (2011).

36. J., T.N. Modern Molecular Photochemistry. (University Science Books, Sausalito; 1991).

37. Lakowicz, J.R. Principles of fluorescence spectroscopy, Edn. 3rd. (Springer, New York; 2006).

38. Law, K.Y. Organic Photoconductive Materials - Recent Trends and Developments. *Chem. Rev.* **93**, 449-486 (1993).

39. Peng, Z.H., Geise, H.J., Zhou, X.F. & Peng, B.X. Near infrared absorbing dyes for optical disks. *B. Soc. Chim. Belg.* **105**, 739-742 (1996).

40. Qian, G. & Wang, Z.Y. Near-Infrared Organic Compounds and Emerging Applications. *Chem-Asian J.* **5**, 1006-1029 (2010).

41. Weissleder, R. A clearer vision for in vivo imaging. *Nat. Biotechnol.* **19**, 316-317 (2001).

42. Pandey, R.K. et al. Nature: A rich source for developing multifunctional agents. Tumor-imaging and photodynamic therapy. *Laser Surg. Med.* **38**, 445-467 (2006).

43. Perepichka, D.F. et al. A covalent tetrathiafulvalene-tetracyanoquinodimethane diad: Extremely low HOMO-LUMO gap, thermoexcited electron transfer, and high-quality Langmuir-Blodgett films. *Angew. Chem Int. Edit.* **42**, 4636-4639 (2003).

44. Jia, C.Y. et al. An experimental and computational study on intramolecular charge transfer: A tetrathiafulvalene-fused dipyridophenazine molecule. *Chem-Eur. J.* **13**, 3804-3812 (2007).

45. Mei, Y.J., Bentley, P.A. & Wang, W. A selective and sensitive chemosensor for Cu^{2+} based on 8-hydroxyquinoline. *Tetrahedron Lett.* **47**, 2447-2449 (2006).

46. Chen, J., Burghart, A., Derecskei-Kovacs, A. & Burgess, K. 4,4-difluoro-4-bora-3a,4a-diaza-s-indacene (BODIPY) dyes modified for

extended conjugation and restricted bond rotations. *J. Org. Chem.* **65**, 2900-2906 (2000).

47. Thivierge, C., Bandichhor, R. & Burgess, K. Spectral dispersion and water solubilization of BODIPY dyes via palladium-catalyzed C-H functionalization. *Org. Lett.* **9**, 2135-2138 (2007).

48. Rohand, T., Qin, W.W., Boens, N. & Dehaen, W. Palladium-catalyzed coupling reactions for the functionalization of BODIPY dyes with fluorescence spanning the visible spectrum. *Eur. J. Org. Chem.*, 4658-4663 (2006).

49. Jiao, L.J. et al. Long wavelength red fluorescent dyes from 3,5-diiodo-BODIPYs. *Org. Biomol. Chem.* **8**, 2517-2519 (2010).

50. Han, J.Y., Gonzalez, O., Aguilar-Aguilar, A., Pena-Cabrera, E. & Burgess, K. 3- and 5-Functionalized BODIPYs via the Liebeskind-Srogl reaction. *Org. Biomol. Chem.* **7**, 34-36 (2009).

51. Jiao, L.J. et al. Regioselective Stepwise Bromination of Boron Dipyrromethene (BODIPY) Dyes. *J. Org. Chem.* **76**, 9988-9996 (2011).

52. Rohand, T., Baruah, M., Qin, W.W., Boens, N. & Dehaen, W. Functionalisation of fluorescent BODIPY dyes by nucleophilic substitution. *Chem. Commun.*, 266-268 (2006).

53. Buyukcakir, O., Bozdemir, O.A., Kolemen, S., Erbas, S. & Akkaya, E.U. Tetrastyryl-Bodipy Dyes: Convenient Synthesis and Characterization of Elusive Near IR Fluorophores. *Org. Lett.* **11**, 4644-4647 (2009).

54. Wada, M. et al. Synthesis and optical properties of a new class of pyrromethene-BF2 complexes fused with rigid bicyclo rings and benzo derivatives. *Tetrahedron Lett*. **42**, 6711-6713 (2001).

55. Shen, Z. et al. Boron-diindomethene (BDI) dyes and their tetrahydrobicyclo precursors - en route to a new class of highly emissive fluorophores for the red spectral range. *Chem-Eur. J.* **10**, 4853-4871 (2004).

56. Goeb, S. & Ziessel, R. Convenient synthesis of green diisoindolodithienylpyrromethene-dialkynyl borane dyes. *Org. Lett.* **9**, 737-740 (2007).

57. Ulrich, G., Goeb, S., De Nicola, A., Retailleau, P. & Ziessel, R. Synthesis of bisisoindolomethene dyes bearing anisole or ethylthiophene residues for red and near-IR fluorescence. *Synlett*, 1517-1520 (2007).

58. Jiao, L.J. et al. Synthesis and Functionalization of Asymmetrical Benzo-Fused BODIPY Dyes. *J. Org. Chem.* **75**, 6035-6038 (2010).

59. Awuah, S.G., Polreis, J., Biradar, V. & You, Y. Singlet Oxygen Generation by Novel NIR BODIPY Dyes. *Org. Lett.* **13**, 3884-3887 (2011).

60. Umezawa, K., Nakamura, Y., Makino, H., Citterio, D. & Suzuki, K. Bright, color-tunable fluorescent dyes in the visible-near-infrared region. *J. Am. Chem. Soc.* **130**, 1550-1554 (2008).

61. Foote, C.S. Definition of Type-I and Type-Ii Photosensitized Oxidation. *Photochem. Photobiol.* **54**, 659-659 (1991).

62. Silverman, S.K. & Foote, C.S. Singlet Oxygen and Electron-Transfer Mechanisms in the Dicyanoanthracene-Sensitized Photooxidation of 2,3-Diphenyl-1,4-Dioxene. *J. Am. Chem. Soc.* **113**, 7672-7675 (1991).

63. Turro, N.J. Modern Molecular Photochemistry. (University Science Books, Sausalito; 1991).

64. Treibs, A. & Kreuzer, F.H. Di- and Tri-Pyrrylmethene Complexes with Di-Fluoro Boron. *Liebigs Ann. Chem.* **718**, 208-& (1968).

65. Wood, T.E. & Thompson, A. Advances in the chemistry of dipyrrins and their complexes. *Chem. Rev.* **107**, 1831-1861 (2007).

66. Zheng, Q.D., Xu, G.X. & Prasad, P.N. Conformationally restricted dipyrromethene boron difluoride (BODIPY) dyes: Highly fluorescent, multicolored probes for cellular imaging. *Chem-Eur. J* .**14**, 5812-5819 (2008).

67. Benniston, A.C. & Copley, G. Lighting the way ahead with boron dipyrromethene (Bodipy) dyes. *Phys. Chem. Phys.* **11**, 4124-4131 (2009).

68. Erten-Ela, S. et al. A panchromatic boradiazaindacene (BODIPY) sensitizer for dye-sensitized solar cells. *Org. Lett.* **10**, 3299-3302 (2008).

69. Ziessel, R., Bonardi, L., Retailleau, P. & Camerel, F. New difluoro-boradiazaindacene shaped with gallate platforms. *Cr. Chim.* **11**, 716-733 (2008).

70. Yogo, T., Urano, Y., Ishitsuka, Y., Maniwa, F. & Nagano, T. Highly efficient and photostable photosensitizer based on BODIPY chromophore. *J. Am. Chem. Soc.* **127**, 12162-12163 (2005).

71. Loudet, A. & Burgess, K. BODIPY dyes and their derivatives: Syntheses and spectroscopic properties. *Chem. Rev.* **107**, 4891-4932 (2007).

72. Adarsh, N., Avirah, R.R. & Ramaiah, D. Tuning Photosensitized Singlet Oxygen Generation Efficiency of Novel Aza-BODIPY Dyes. *Org. Lett.* **12**, 5720-5723 (2010).

73. Huang, L., Yu, X.R., Wu, W.H. & Zhao, J.Z. Styryl Bodipy-C-60 Dyads as Efficient Heavy-Atom-Free Organic Triplet Photosensitizers. *Org. Lett.* **14**, 2594-2597 (2012).

74. Duman, S., Cakmak, Y., Kolemen, S., Akkaya, E.U. & Dede, Y. Heavy Atom Free Singlet Oxygen Generation: Doubly Substituted Configurations Dominate S1 States of Bis-BODIPYs. *J. Org. Chem.* **77**, 4516-4527 (2012).

75. Kamkaew, A. et al. BODIPY dyes in photodynamic therapy. *Chem. Soc. Rev.* **42**, 77-88 (2013).

76. Anderson, H.J. & Lee, S.F. Pyrrole Chemistry .4. Preparation and Some Reactions of Brominated Pyrrole Derivatives. *Can. J. Chem.* **43**, 409-& (1965).

77. You, Y.J. et al. Water soluble, core-modified porphyrins. 3. Synthesis, photophysical properties, and in vitro studies of photosensitization, uptake, and localization with carboxylic acid-substituted derivatives. *J. Med. Chem.* **46**, 3734-3747 (2003).

78. Quartarolo, A.D., Russo, N. & Sicilia, E. Structures and electronic absorption spectra of a recently synthesised class of photodynamic therapy agents. *Chem-Eur. J.* **12**, 6797-6803 (2006).

79. Frisch, M.J.T., G. W.; Schlegel, H. B.; Scuseria, G. E.; Robb, M. A.; Cheeseman, J. R.; Scalmani, G.; Barone, V.; Mennucci, B.; Petersson, G. A.; Nakatsuji, H.; Caricato, M.; Li, X.; Hratchian, H. P.; Izmaylov, A. F.; Bloino, J.; Zheng, G.; Sonnenberg, J. L.; Hada, M.; Ehara, M.; Toyota, K.; Fukuda, R.; Hasegawa, J.; Ishida, M.; Nakajima, T.; Honda, Y.; Kitao, O.; Nakai, H.; Vreven, T.; Montgomery, Jr., J. A.; Peralta, J. E.; Ogliaro, F.; Bearpark, M.; Heyd, J. J.; Brothers, E.; Kudin, K. N.; Staroverov, V. N.; Kobayashi, R.; Normand, J.; Raghavachari, K.; Rendell, A.; Burant, J. C.; Iyengar, S. S.; Tomasi, J.; Cossi, M.; Rega, N.; Millam, N. J.; Klene, M.; Knox, J. E.; Cross, J. B.; Bakken, V.; Adamo, C.; Jaramillo, J.;

Gomperts, R.; Stratmann, R. E.; Yazyev, O.; Austin, A. J.; Cammi, R.; Pomelli, C.; Ochterski, J. W.; Martin, R. L.; Morokuma, K.; Zakrzewski, V. G.; Voth, G. A.; Salvador, P.; Dannenberg, J. J.; Dapprich, S.; Daniels, A. D.; Farkas, Ö.; Foresman, J. B.; Ortiz, J. V.; Cioslowski, J.; Fox, D. J. Gaussian 2009).

80. Rosen, B.M. et al. Predicting the Structure of Supramolecular Dendrimers via the Analysis of Libraries of AB(3) and Constitutional Isomeric AB(2) Biphenylpropyl Ether Self-Assembling Dendrons. *J Am. Chem. Soc.* **131**, 17500-17521 (2009).

81. Shi, F., Waldo, J.P., Chen, Y. & Larock, R.C. Benzyne click chemistry: Synthesis of benzotriazoles from benzynes and azides. *Org. Lett.* **10**, 2409-2412 (2008).

82. Becke, A.D. Density-Functional Thermochemistry .3. The Role of Exact Exchange. *J. Chem. Phys.* **98**, 5648-5652 (1993).

83. Lee, C.T., Yang, W.T. & Parr, R.G. Development of the Colle-Salvetti Correlation-Energy Formula into a Functional of the Electron-Density. *Phys. Rev. B.* **37**, 785-789 (1988).

84. Negishe, E. (ed.) Handbook of Organopalladium Chemistry for Organic Synthesis, Vol. 1. (Wiley, New York; 2002).

85. Johansson Seechurn, C.C.C., Kitching, M.O., Colacot, T.J. & Snieckus, V. Palladium-Catalyzed Cross-Coupling: A Historical Contextual Perspective to the 2010 Nobel Prize. *Angew.Chem. Int. Edit.* **51**, 5062-5085 (2012).

86. Littke, A.F. & Fu, G.C. Palladium-catalyzed coupling reactions of aryl chlorides. *Angew. Chem. Int. Edit.* **41**, 4176-4211 (2002).

87. Lakshmi, V. & Ravikanth, M. Synthesis of Sterically Crowded Polyarylated Boron-Dipyrromethenes. *J. Org. Chem.* **76**, 8466-8471 (2011).

88. Qdot 705 (Invitrogen Co.) in methanol exhibit a broad fluorescence spectrum (fwhm: 74 nm, 1140 cm^{-1}) with a peak at 705 nm. (see http://probes.invitrogen.com/media/publications/600.pdf)

89. Mitsunaga, M. et al. Cancer cell-selective in vivo near infrared photoimmunotherapy targeting specific membrane molecules. *Nature Med.***17**, 1685-1691 (2011).

90. Waldmann, T.A. Immunotherapy: past, present and future. *Nat. Med.* **9**, 269-277 (2003).

91. Reichert, J.M., Rosensweig, C.J., Faden, L.B. & Dewitz, M.C. Monoclonal antibody successes in the clinic. *Nat. Biotechnol.* **23**, 1073-1078 (2005).

92. Srinivasan, S. & Schuster, G.B. A Conjoined Thienopyrrole Oligomer Formed by Using DNA as a Molecular Guide. *Org. Lett.* **10**, 3657-3660 (2008).

93. Byrne, A.T. et al. Vascular-targeted photodynamic therapy with BF2-chelated Tetraaryl-Azadipyrromethene agents: a multi-modality molecular imaging approach to therapeutic assessment. *Brit. J. Cancer* **101**, 1565-1573 (2009).

94. O'Connor, A.E., Gallagher, W.M. & Byrne, A.T. Porphyrin and nonporphyrin photosensitizers in oncology: preclinical and clinical advances in photodynamic therapy. *Photochem. Photobiol.* **85**, 1053-1074 (2009).

95. Boyle, R.W. & Dolphin, D. Structure and biodistribution relationships of photodynamic sensitizers. *Photochem. Photobiol.* **64**, 469-485 (1996).

96. Wagner, C.E. et al. Modeling, Synthesis and Biological Evaluation of Potential Retinoid X Receptor (RXR) Selective Agonists: Novel Analogues of 4-[1-(3,5,5,8,8-Pentamethyl-5,6,7,8-tetrahydro-2-naphthyl)ethynyl]benzoic Acid (Bexarotene). *J. Med. Chem.* **52**, 5950-5966 (2009).

97. Gorman, A. et al. In vitro demonstration of the heavy-atom effect for photodynamic therapy. *J. Am. Chem. Soc.* **126**, 10619-10631 (2004).

Appendix 1

General Methods

Photophysical Properties

Molar Extinction Coefficient. To measure the extinction coefficient, about 1 mg of compounds **8-12** was dissolved in chloroform (50 ml). Serial dilutions were performed to yield different dye concentrations in the region of 10^{-7} – 10^{-6} M from the stock solution. The absorbance and absorption spectra measurements were taken using the Optics (CHEMUSB4-UV-Fiber) spectrophotometer. A graph of absorbance (A) versus concentration (C) was plotted and the extinction coefficient was determined from Beer–Lambert law.

Determination of Fluorescence Quantum Yield. The fluorescence emission spectra of **39-43** using KFL-4 as a standard were recorded at 25^{o}C. Dilute solutions of all dyes (5 µM) were prepared to compare their fluorescence emission spectra after the excitation at 710 nm. The quantum yields were calculated following standard protocol.[60, 97] Five serial dilutions were made with chloroform as a solvent, the absorbance (A) of these solutions were less than 0.1. The integrated fluorescence intensity (F) at each concentration was recorded after the excitation at 710 nm. A graph of F versus A was plotted to generate the gradient (G). The quantum yield was calculated using the equation:

$$\phi x = \phi std\left(\frac{Gx}{Gstd}\right)\left(\frac{\eta x^2}{\eta std^2}\right)$$

Where the subscripts std and x denote standard and test respectively, ϕ is the fluorescence quantum yield, G the gradient from the plot of integrated fluorescence intensity vs. absorbance and η the refractive index of the solvent. The quantum yield of KFL-4 was 0.56 in chloroform.

Detection of singlet oxygen by DPBF oxidation. A singlet oxygen generation experiment was set up, using a water filter and a 60 W halogen lamp at 0.5 mW/cm^2. Sample solutions were prepared in small test tubes containing a magnetic stir bar. The tubes contained 90 µM DPBF and 5 µM dye solution in THF (2 ml). The dyes used were **KFL-4**, **CMP**, and dyes **39-43.** The solutions were stirred in the dark for two minutes and the absorbance measured in a quartz cuvette on Spectra Max2 spectrophotometer (Molecular Devices). Stirring of the solutions continued under light irradiation for 18 min and the absorbance was measured at interval of 2 min.

Appendix 2

^{1}H-NMR Spectra of Compounds

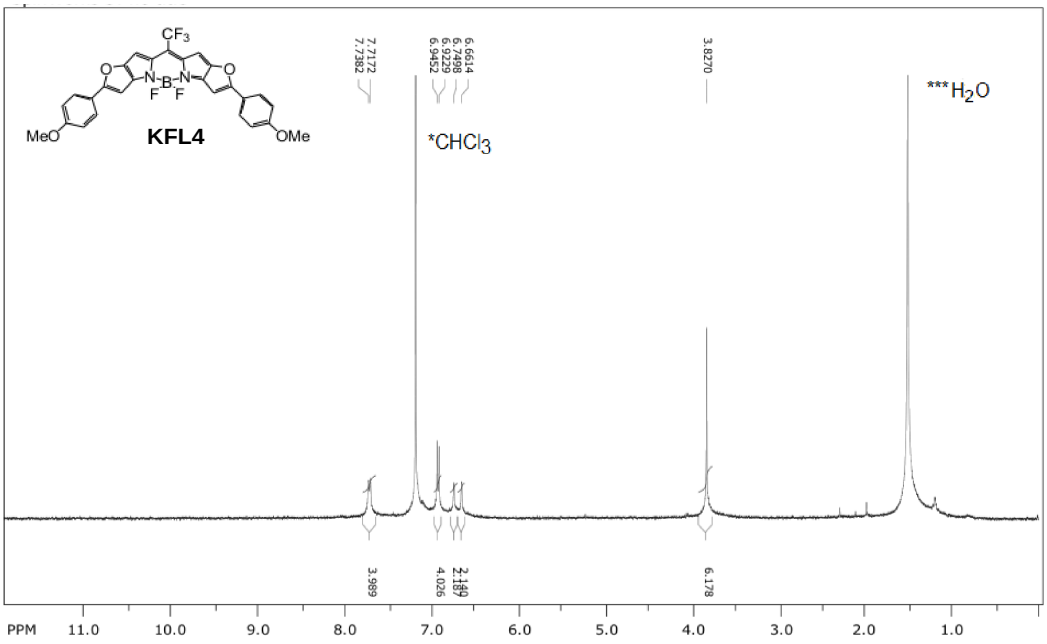

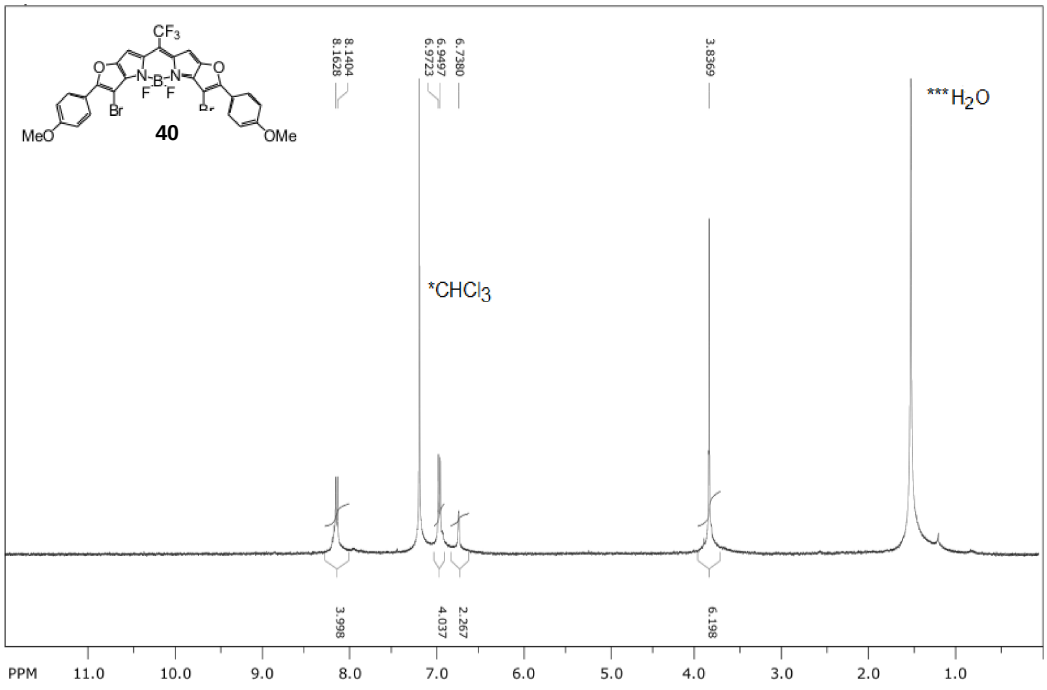

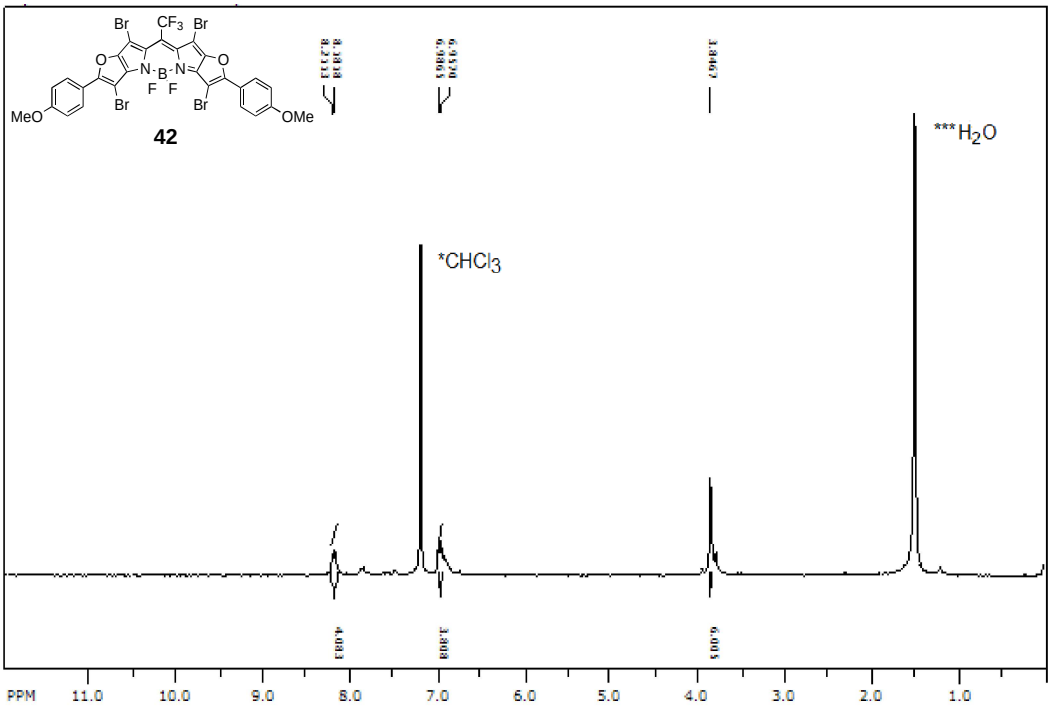
Br
CF3
Br
O
N
B
N
O
F F
Br
Br
MeO
OMe
42
8.2113
6.9865
3.8467
***H2O
*CHCl3
4.083
3.808
6.003
PPM
11.0
10.0
9.0
8.0
7.0
6.0
5.0
4.0
3.0
2.0
1.0

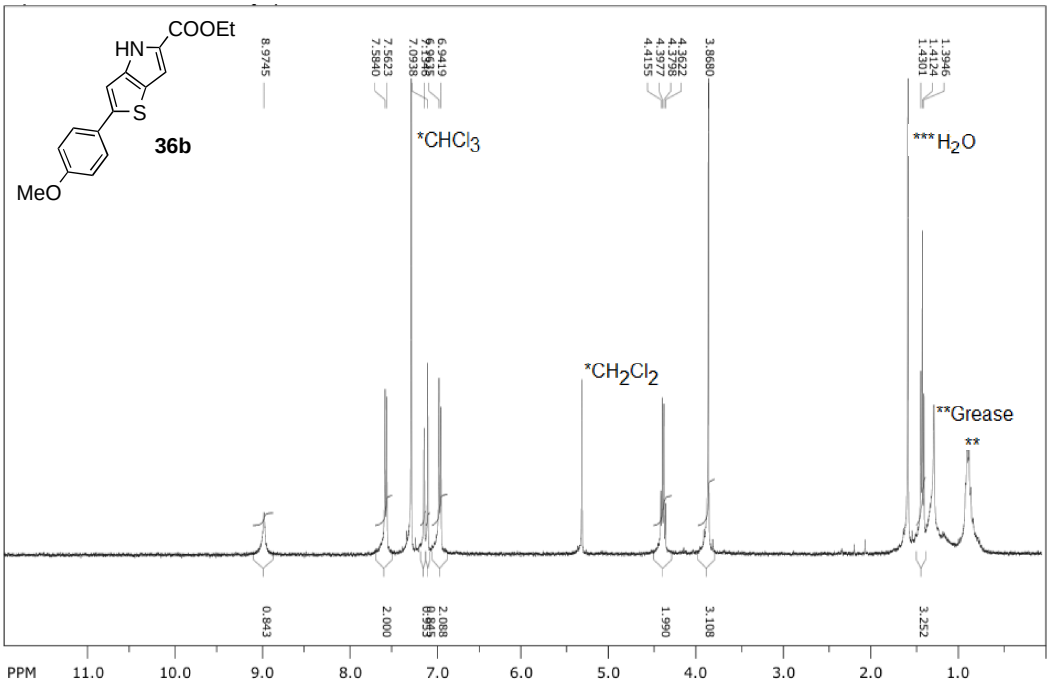
COOEt
HN
S
MeO
36b
8.9745
7.5923
7.5840
7.0938
6.9419
4.3622
4.3598
4.3977
4.4155
3.8680
1.3946
1.4124
1.4301
*CHCl3
***H2O
*CH2Cl2
**Grease
**
0.843
2.000
2.088
1.990
3.108
3.252
PPM
11.0
10.0
9.0
8.0
7.0
6.0
5.0
4.0
3.0
2.0
1.0

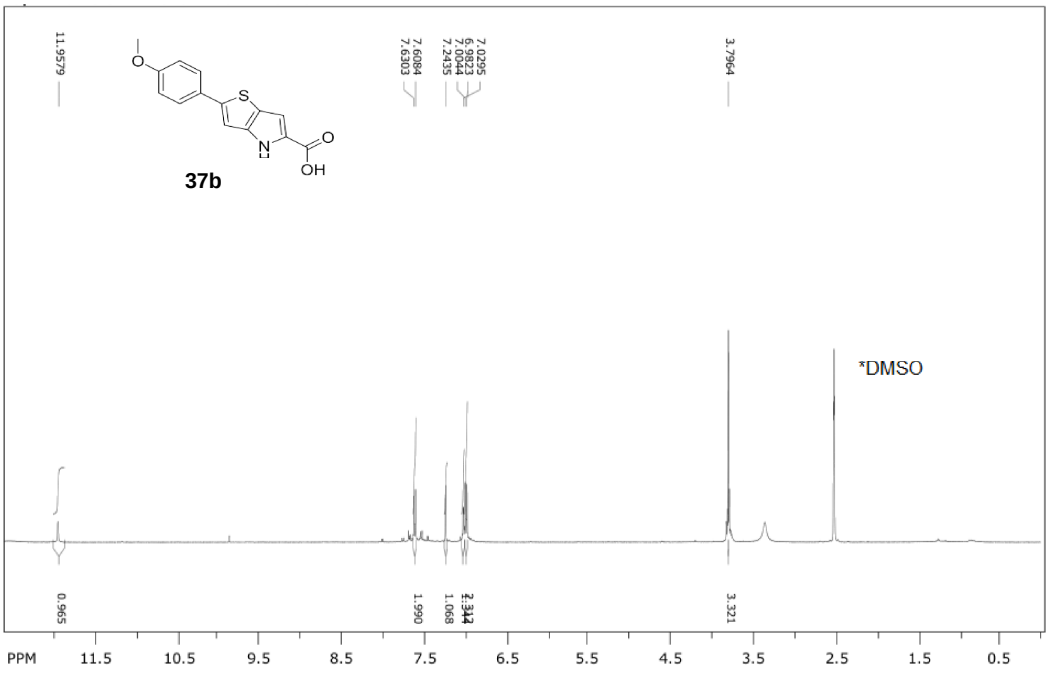
11.9579
7.6084
7.6303
7.0295
7.0644
7.2435
3.7964
37b
*DMSO
0.965
1.990
1.068
3.321
PPM
11.5
10.5
9.5
8.5
7.5
6.5
5.5
4.5
3.5
2.5
1.5
0.5

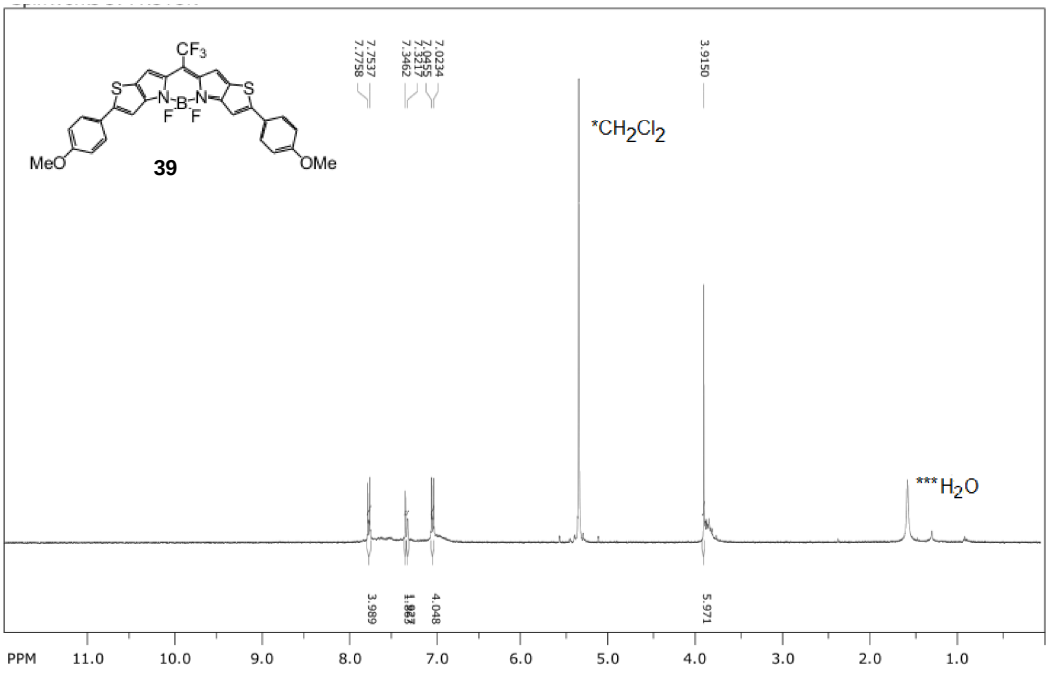
7.7537
7.7758
7.3462
7.0234
3.9150
39
*CH2Cl2
***H2O
3.989
4.048
5.971
PPM
11.0
10.0
9.0
8.0
7.0
6.0
5.0
4.0
3.0
2.0
1.0

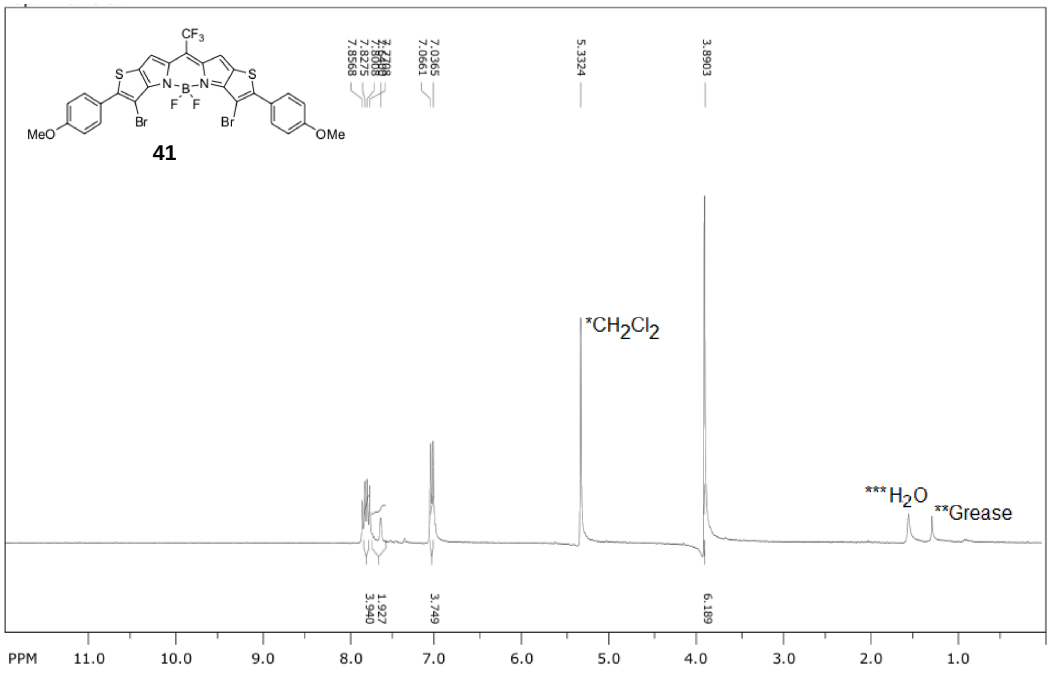
41
7.8568
7.8275
7.0365
7.0661
5.3324
3.8903
*CH2Cl2
***H2O
**Grease
1.927
3.940
3.749
6.189
PPM
11.0
10.0
9.0
8.0
7.0
6.0
5.0
4.0
3.0
2.0
1.0

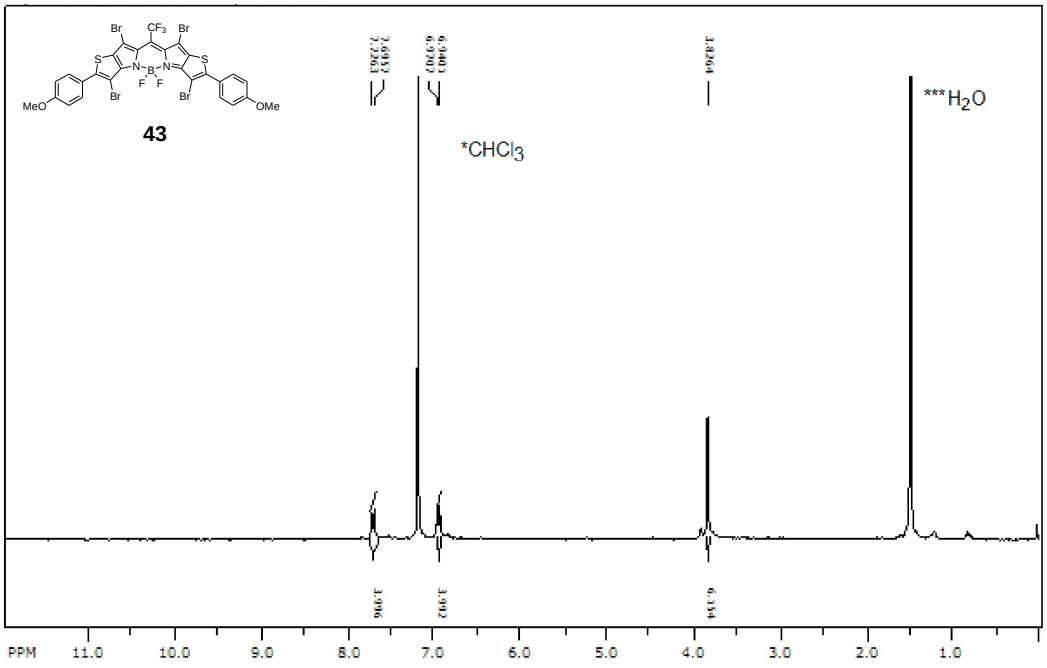
43
7.7263
6.9401
6.9307
3.8264
*CHCl3
***H2O
3.996
3.992
6.194
PPM
11.0
10.0
9.0
8.0
7.0
6.0
5.0
4.0
3.0
2.0
1.0

1D NOESY and ROESY NMR

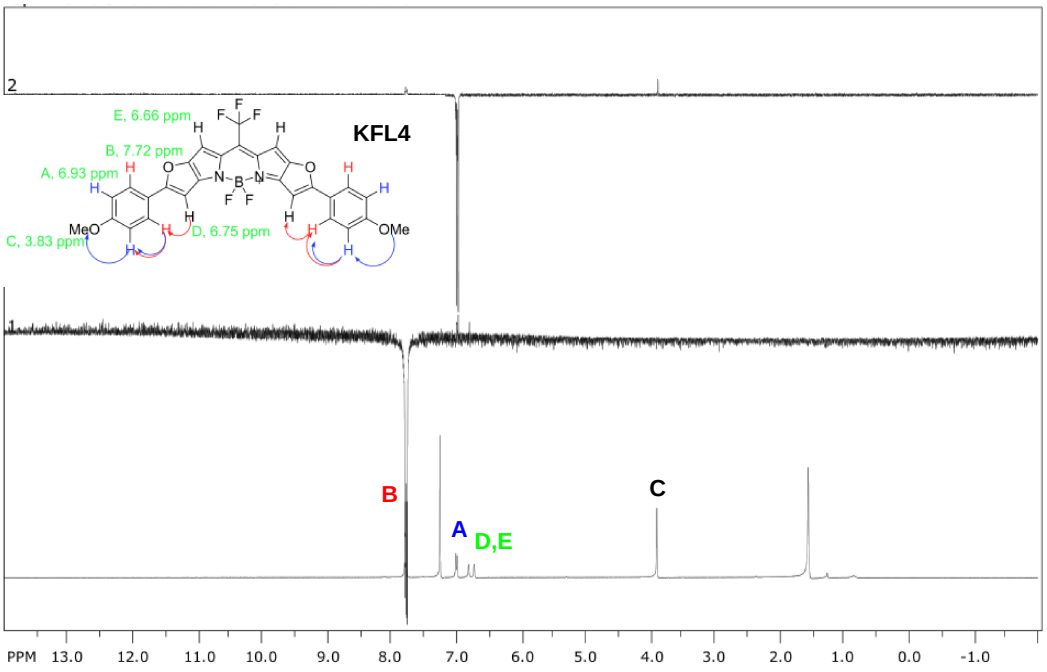

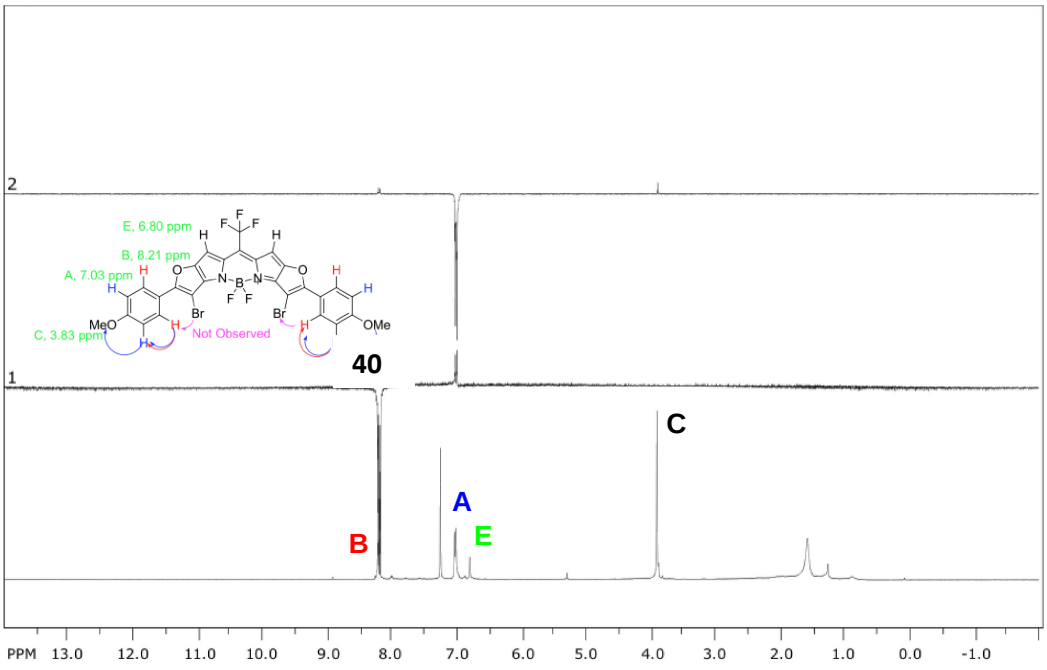

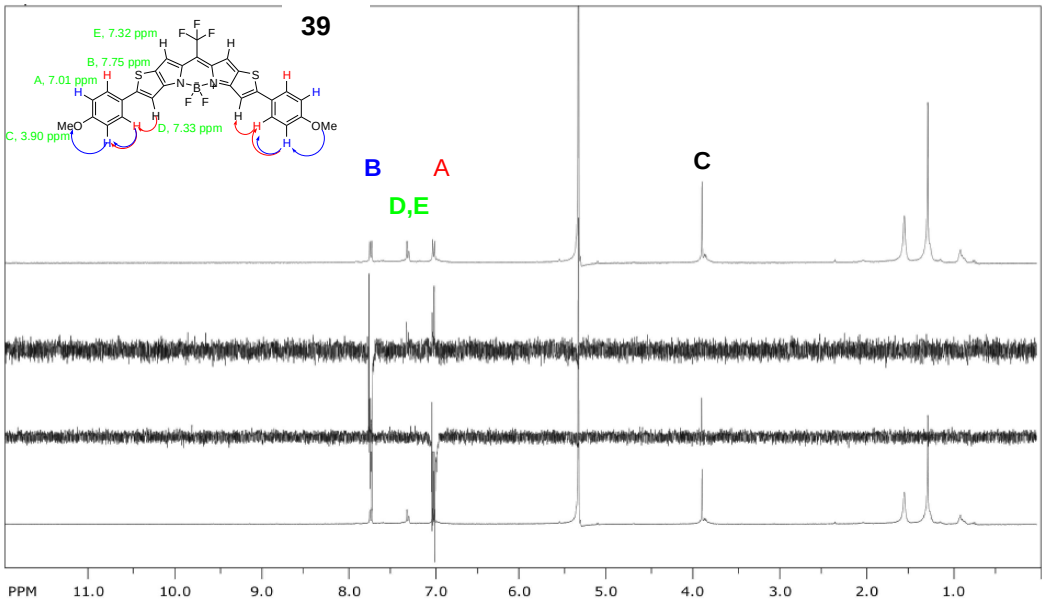
39
E, 7.32 ppm
B, 7.75 ppm
A, 7.01 ppm
C, 3.90 ppm
D, 7.33 ppm
MeO
OMe
B
A
D,E
C
PPM
11.0
10.0
9.0
8.0
7.0
6.0
5.0
4.0
3.0
2.0
1.0

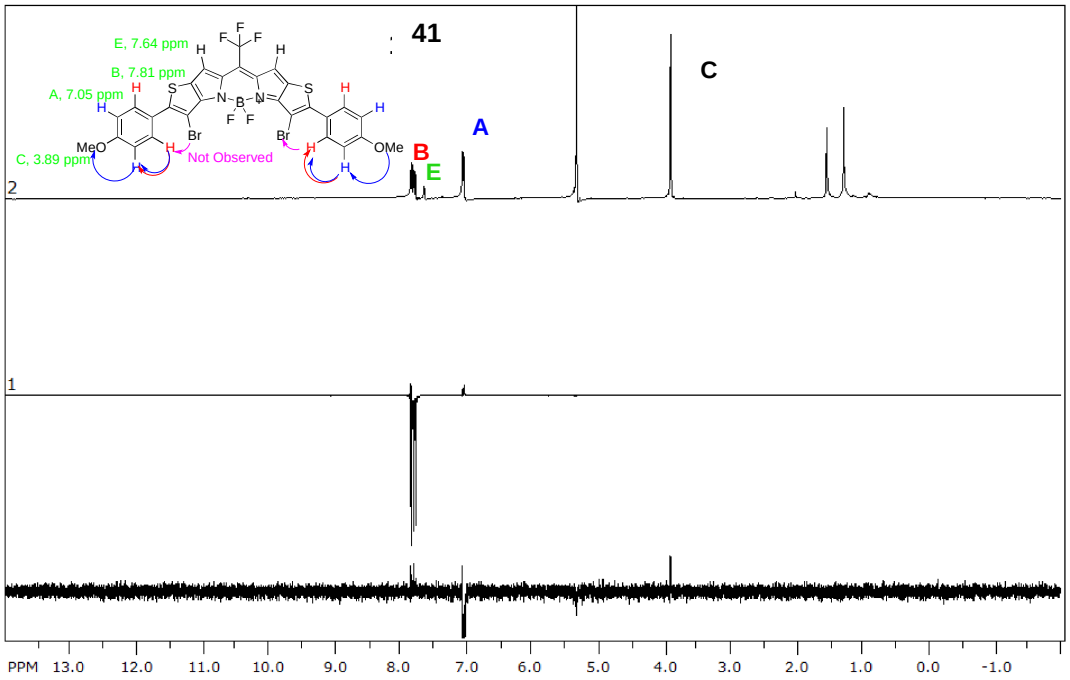
41
E, 7.64 ppm
B, 7.81 ppm
A, 7.05 ppm
C, 3.89 ppm
Not Observed
MeO
OMe
Br
C
A
B
E
2
1
PPM
13.0
12.0
11.0
10.0
9.0
8.0
7.0
6.0
5.0
4.0
3.0
2.0
1.0
0.0
-1.0

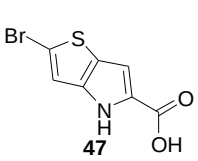
Br
S
N
H
O
OH

47

TMS
*DMSO
14
13
12
11
10
9
8
7
6
5
4
3
2
1
-0
-1
ppm

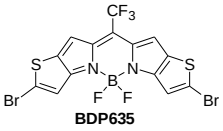
CF3
S
N
B
N
S
F
F
Br
Br

BDP635

7.0694
7.3149
*CHCl3
1.941
2.000
PPM
11.0
10.0
9.0
8.0
7.0
6.0
5.0
4.0
3.0
2.0
1.0

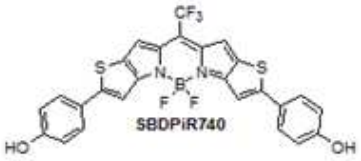

SBDPiR740

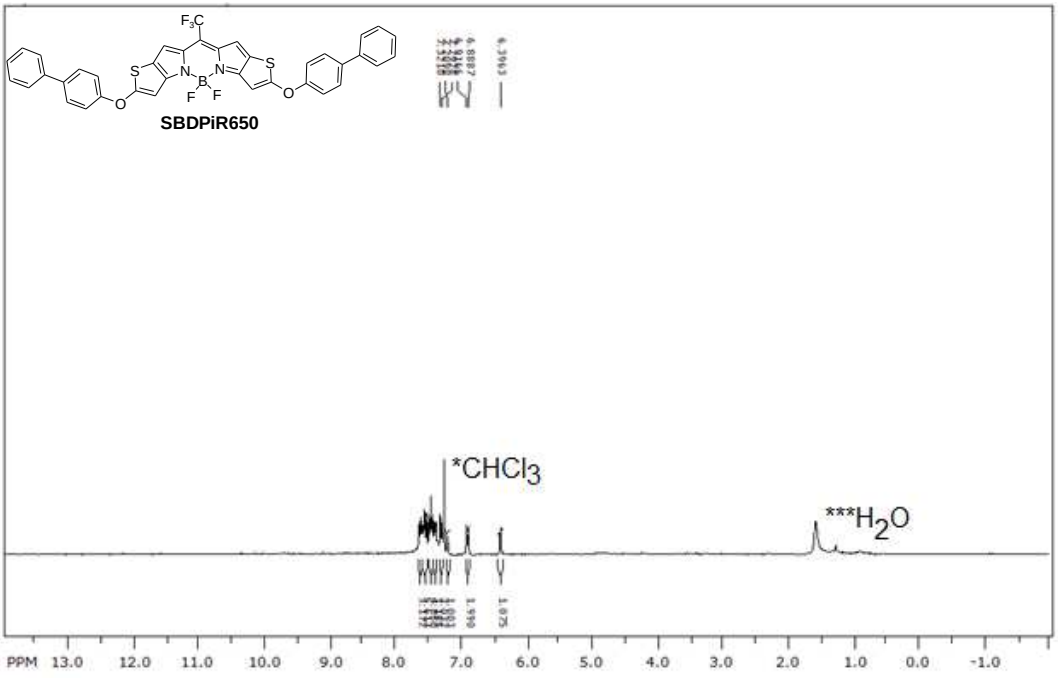

SBDPiR650

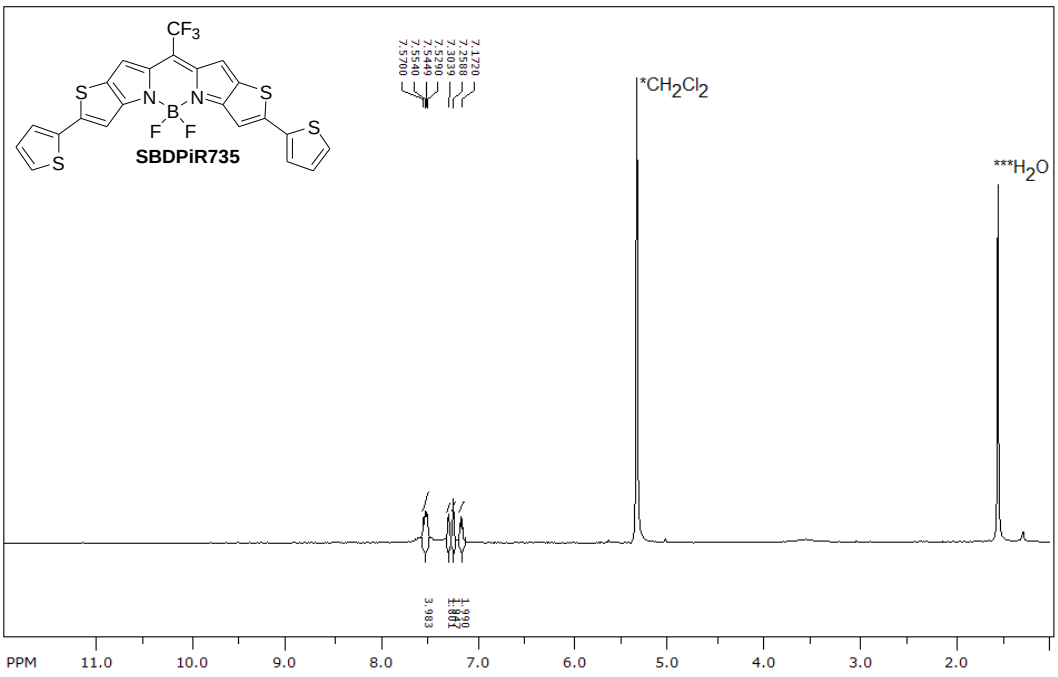
CF3
S
N
B
F
F
S
S
S
SBDPiR735
7.1720
7.2588
7.3039
7.5249
7.5340
7.5700
*CH2Cl2
***H2O
3.983
1.000
1.801
PPM
11.0
10.0
9.0
8.0
7.0
6.0
5.0
4.0
3.0
2.0

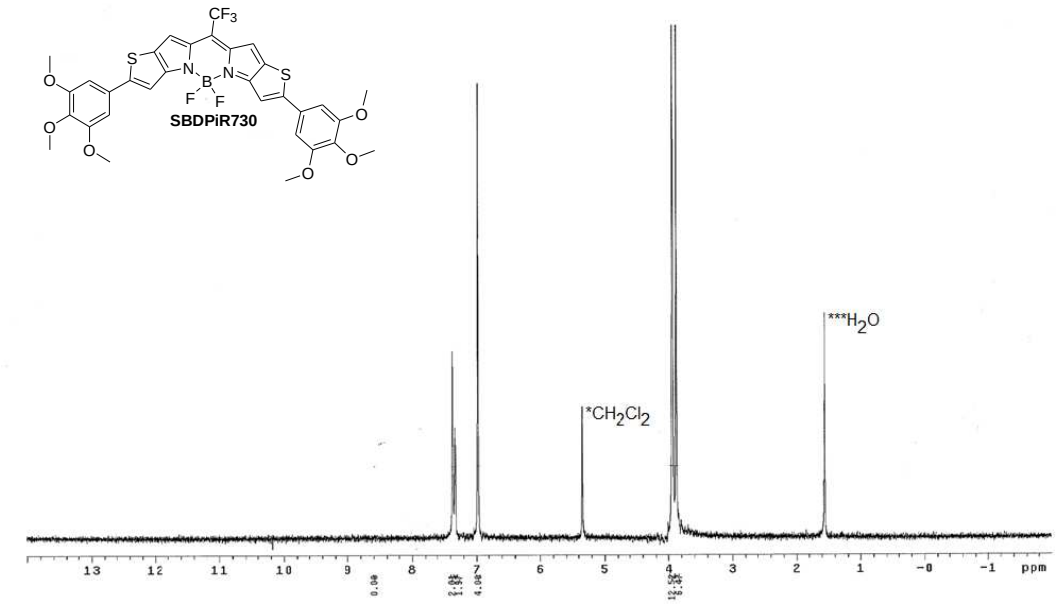
CF3
S
N
B
F
F
S
S
O
O
O
O
O
O
SBDPiR730
*CH2Cl2
***H2O
13
12
11
10
9
8
7
6
5
4
3
2
1
-0
-1
ppm

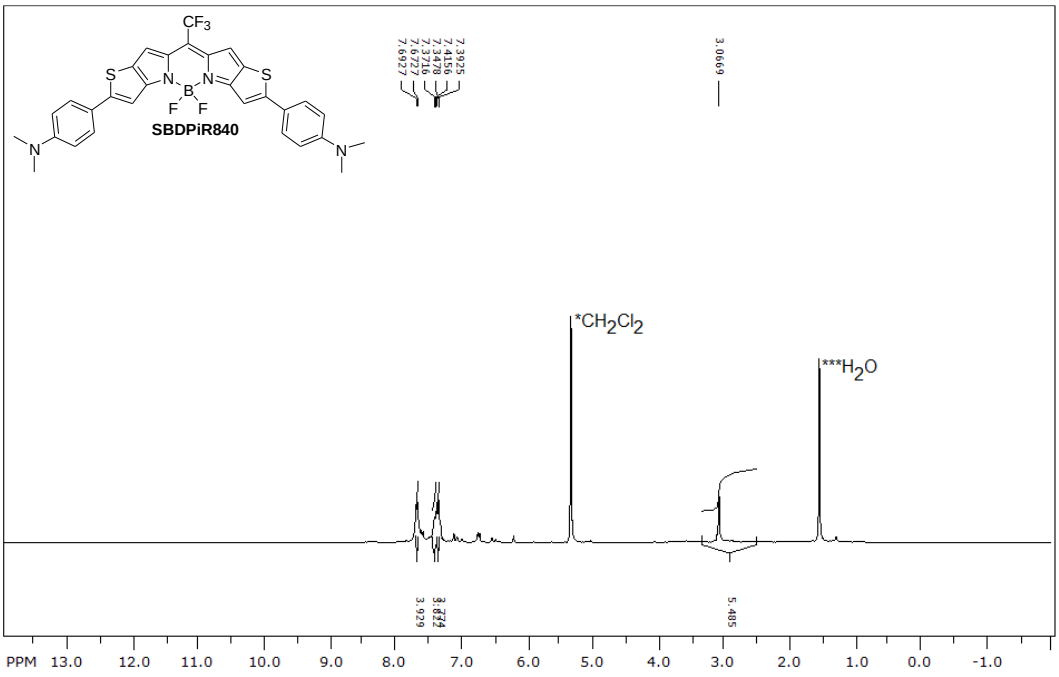
SBDPiR840
*CH2Cl2
***H2O
PPM 13.0 12.0 11.0 10.0 9.0 8.0 7.0 6.0 5.0 4.0 3.0 2.0 1.0 0.0 -1.0

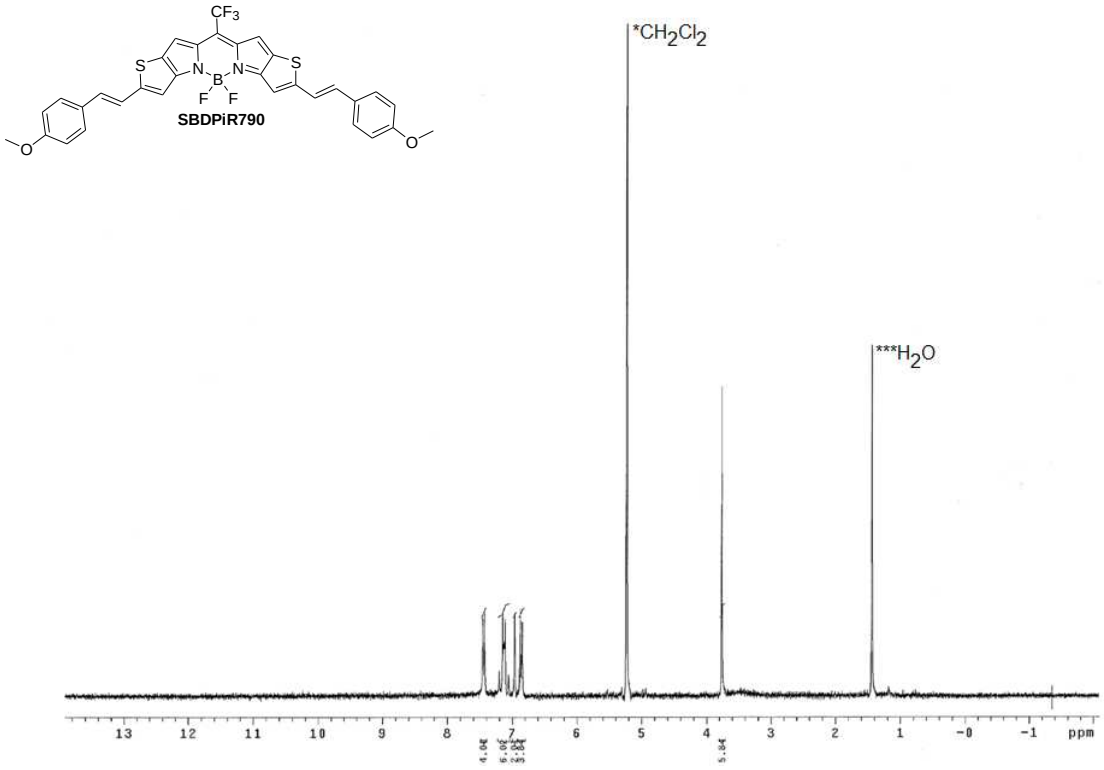
SBDPiR790
*CH2Cl2
***H2O
ppm

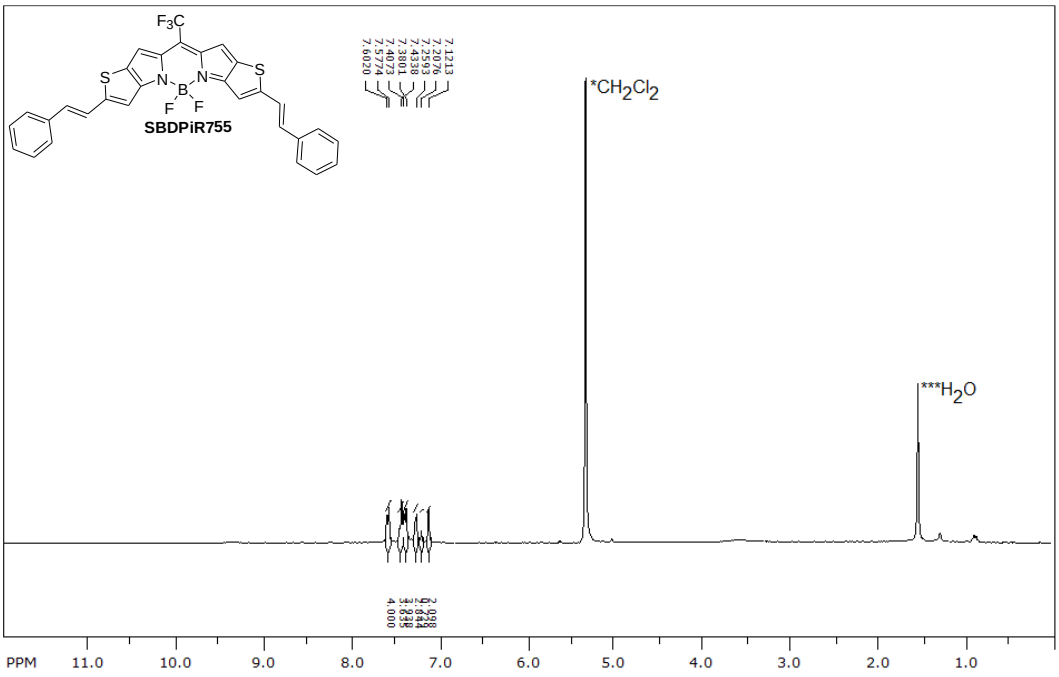
F3C
S
N
B
F
F
N
S
SBDPiR755
7.1213
7.2076
7.4133
7.4073
7.3801
7.5774
7.6020
*CH2Cl2
***H2O
2.098
4.000
PPM
11.0
10.0
9.0
8.0
7.0
6.0
5.0
4.0
3.0
2.0
1.0

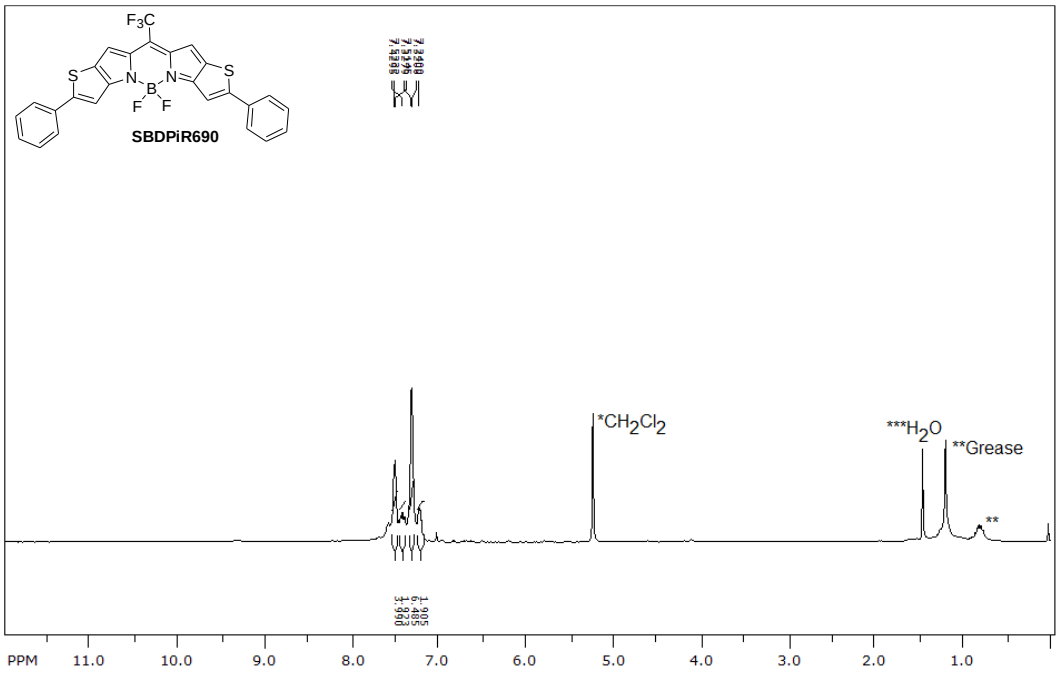
F3C
S
N
B
F
F
N
S
SBDPiR690
*CH2Cl2
***H2O
**Grease
**
1.995
1.923
3.990
PPM
11.0
10.0
9.0
8.0
7.0
6.0
5.0
4.0
3.0
2.0
1.0

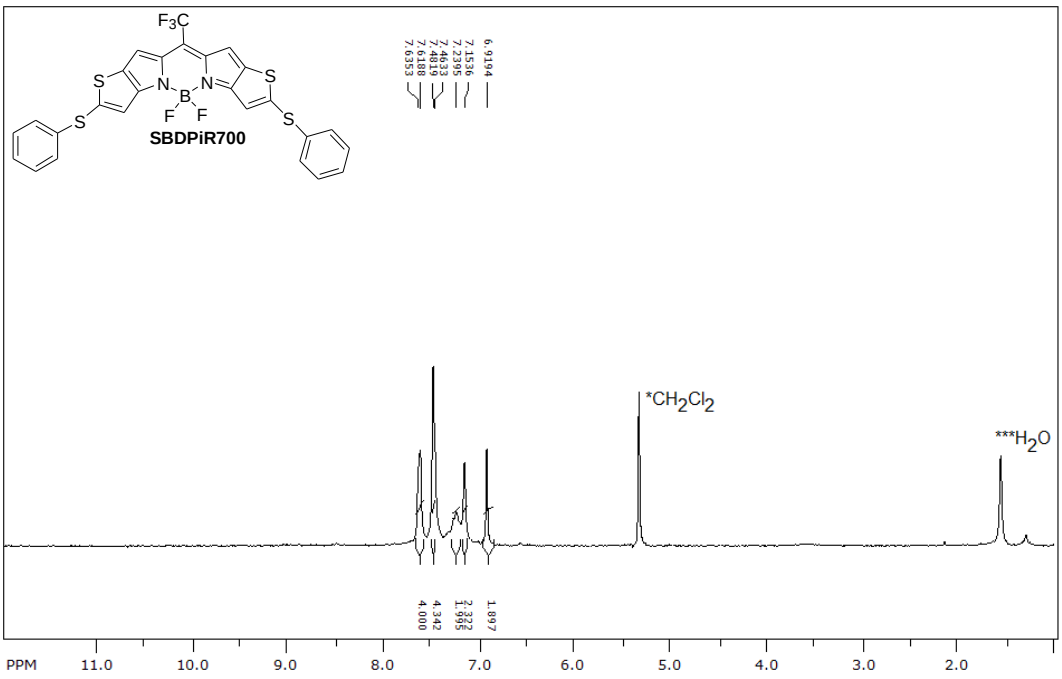
SBDPiR700
*CH2Cl2
***H2O
PPM

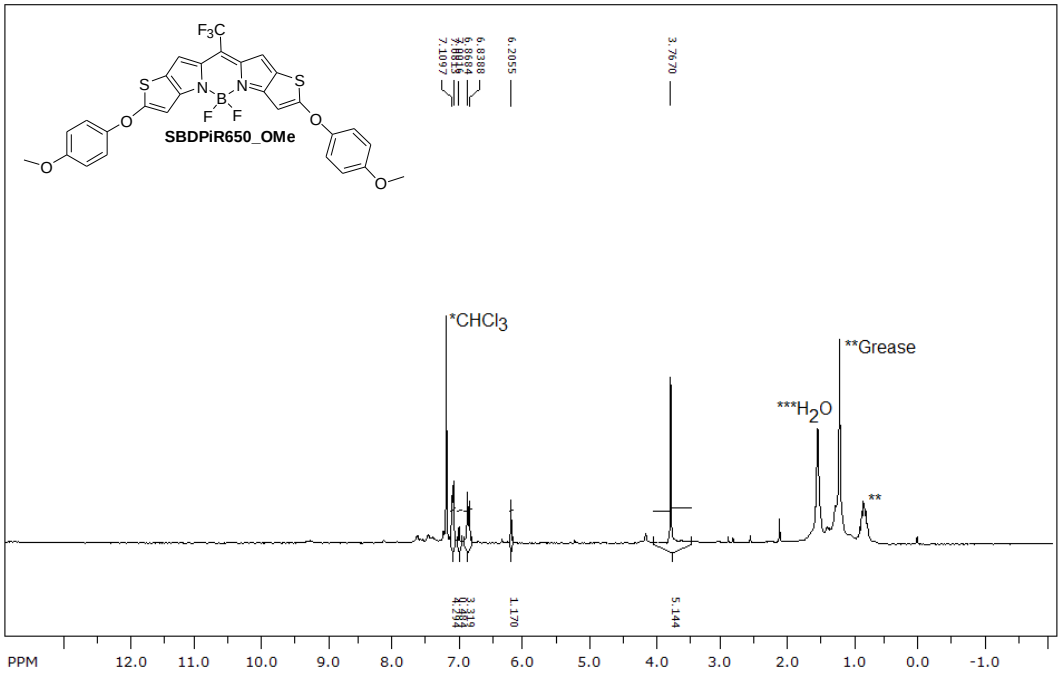
SBDPiR650_OMe
*CHCl3
**Grease
***H2O
**
PPM

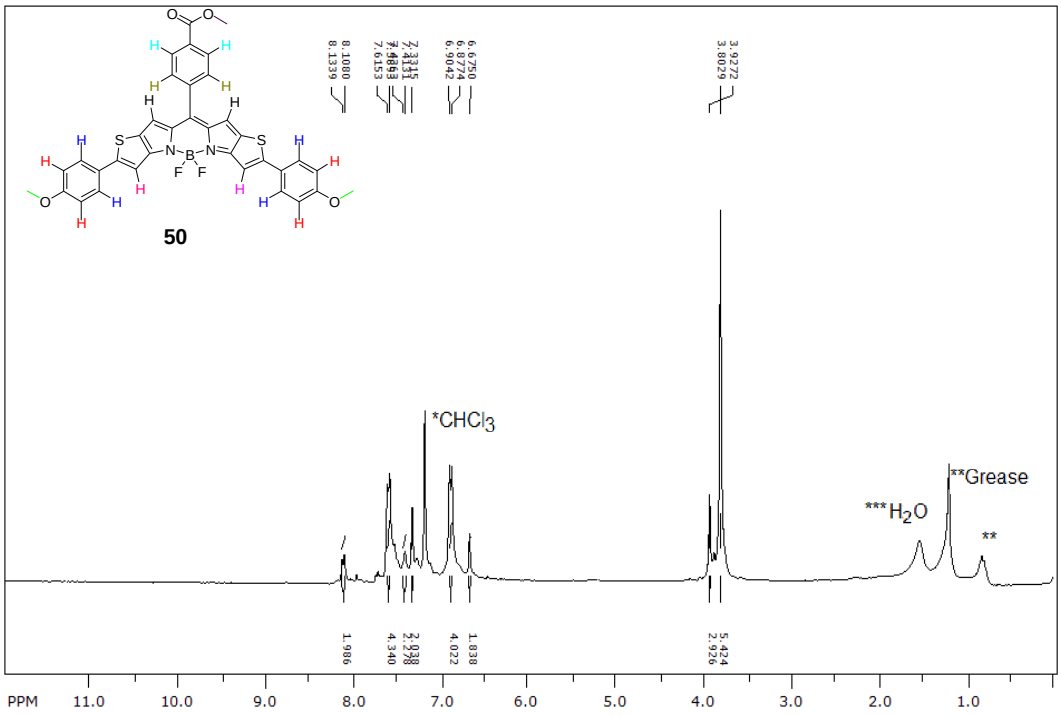
50
*CHCl3
***H2O
**Grease
**
PPM 11.0 10.0 9.0 8.0 7.0 6.0 5.0 4.0 3.0 2.0 1.0

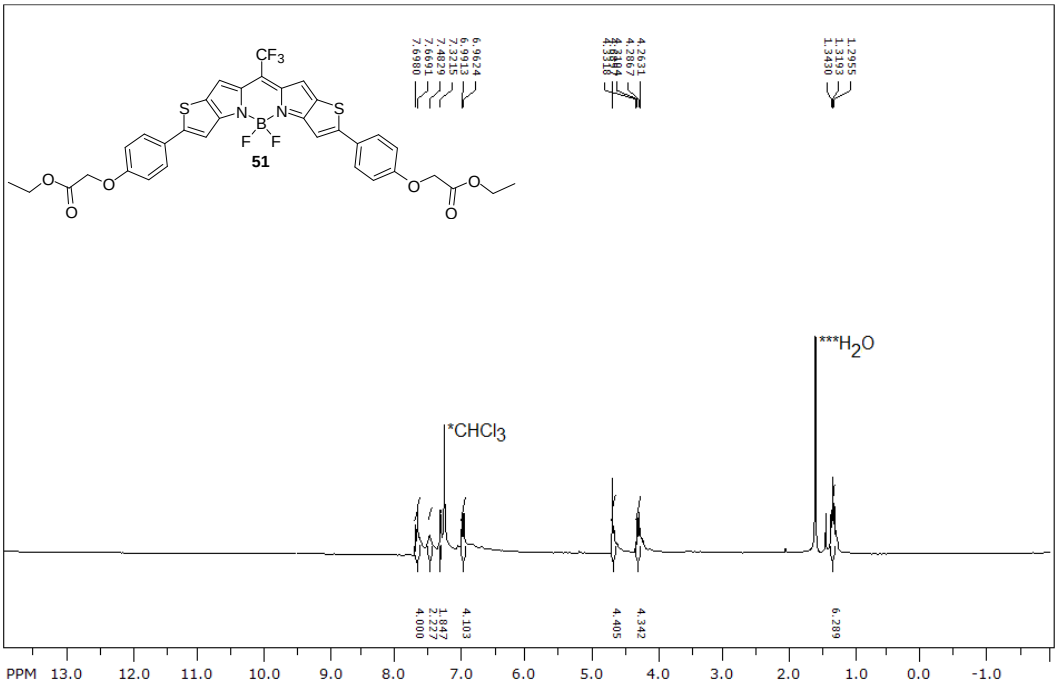
51
*CHCl3
***H2O
PPM 13.0 12.0 11.0 10.0 9.0 8.0 7.0 6.0 5.0 4.0 3.0 2.0 1.0 0.0 -1.0

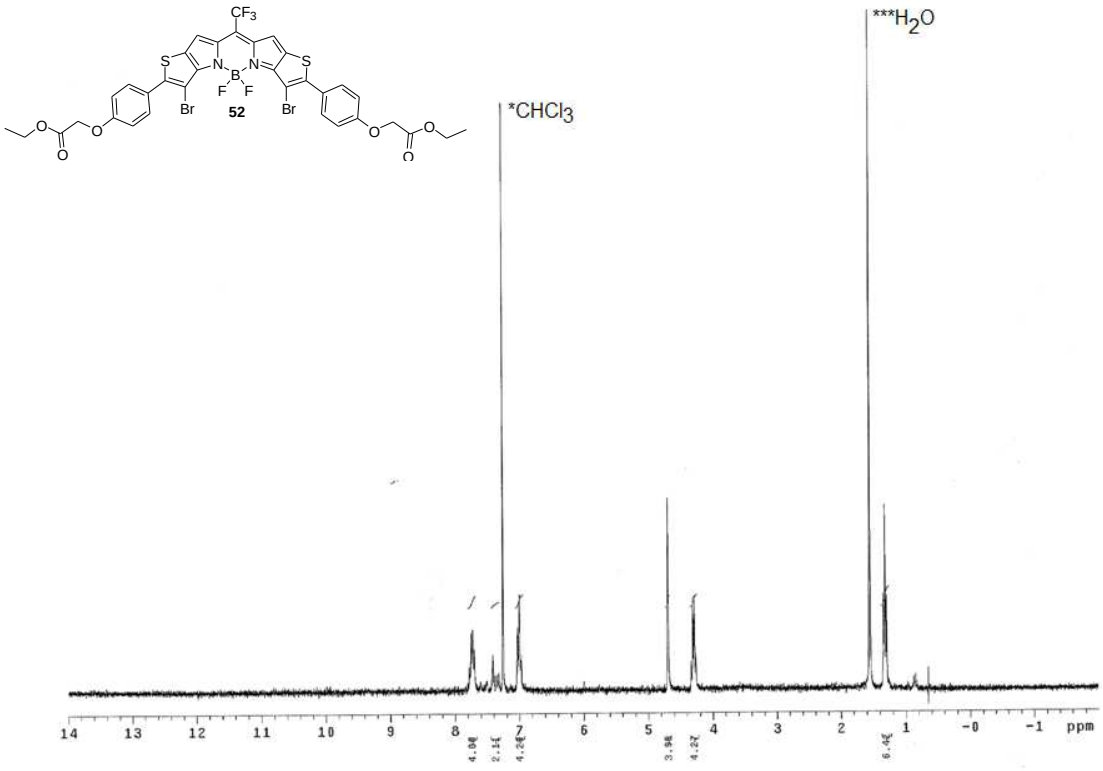
CF3
S
N
B
F
F
N
S
Br
Br
52
O
O
O
O
O
O
*CHCl3
***H2O
14
13
12
11
10
9
8
7
6
5
4
3
2
1
-0
-1
ppm

Appendix 3

Crystallographic Data

BDP635 single crystals were grown by slow evaporation from dichloromethane to obtain black plates. X- ray crystal structure was determined by Douglas R. Powell at the University of Oklahoma and thanks to the University of Oklahoma and the National Science Foundation (grant CHE-0130835) for funds to purchase the X-ray instrument and computers.

Comment

The displacement ellipsoids were drawn at the 50% probability level.

Experimental

A black plate-shaped crystal of dimensions 0.44 x 0.41 x 0.08 mm was selected for structural analysis. Intensity data for this compound were collected using a diffractometer with a Bruker APEX ccd area detector (1) and graphite-monochromated Mo Kα radiation (λ = 0.71073 Å). The sample was cooled to 100(2) K. Cell parameters were determined from a non-linear least squares fit of 8858 peaks in the range 2.59 < θ < 28.27°. A total of 17716 data were measured in the range 1.94 < θ < 28.30° using ϕ and ω oscillation frames. The data were corrected for absorption by the empirical method (2) giving minimum and maximum transmission factors of 0.2032 and 0.6757. The data were merged to form a set of 4021 independent data with R(int) = 0.0404 and a coverage of 100.0 %.

The monoclinic space group $P2_1/c$ was determined by systematic absences and statistical tests and verified by subsequent refinement. The structure was solved by direct methods and refined by full-matrix least-squares methods on F^2 (3). The positions of hydrogens bonded to carbons were initially determined by geometry and refined by a riding model. Non-hydrogen atoms were refined with anisotropic displacement parameters. Hydrogen atom displacement parameters were set to 1.2 times the isotropic equivalent displacement parameters of the bonded atoms. A total of 235 parameters were refined against 4021 data to give wR(F^2) = 0.0712 and S = 1.003 for weights of w = 1/[σ^2 (F^2) + (0.0360 P)^2 + 1.5000 P], where P = [F_o^2 + 2F_c^2] / 3. The final R(F) was 0.0279 for the 3498 observed, [$F > 4\sigma(F)$], data. The largest shift/s.u. was 0.001 in the final refinement cycle. The final difference map had maxima and minima of 0.573 and -0.445 e/Å^3, respectively.

Empirical formula	C_{14} H_4 B Br_2 F_5 N_2 S_2	
Formula weight	529.94	
Crystal system	monoclinic	
Space group	$P2_1/c$	
Unit cell dimensions	a = 7.3337(3) Å	α= 90°
	b = 15.7558(7) Å	β= 101.567(2)°
	c = 14.3108(6) Å	γ= 90°
Volume	1620.01(12) $Å^3$	
Z, Z'	4, 1	
Density (calculated)	2.173 Mg/m^3	
Wavelength	0.71073 Å	
Temperature	100(2) K	
F(000)	1016	
Absorption coefficient	5.316 mm^{-1}	
Absorption correction	Semi-empirical from equivalents	
Max. and min. transmission	0.6757 and 0.2032	
Theta range for data collection	1.94 to 28.30°	
Reflections collected	17716	
Independent reflections	4021 [R(int) = 0.0404]	
Data / restraints / parameters	4021 / 0 / 235	
$wR(F^2$ all data)	$wR2$ = 0.0712	
$R(F$ obsd data)	$R1$ = 0.0279	
Goodness-of-fit on F^2	1.003	
Observed data [I > 2σ(I)]	3498	
Largest and mean shift / s.u.	0.001and 0.000	
Largest diff. peak and hole	0.573 and -0.445 e/$Å^3$	

$wR2 = \{ \Sigma [w(F_o^2 - F_c^2)^2] / \Sigma [w(F_o^2)^2] \}^{1/2}$

$R1 = \Sigma ||F_o| - |F_c|| / \Sigma |F_o|$